FABRICATION AND CHARACTERIZATION OF CORRUGATED
MICROFILTRATION MEMBRANES

A THESIS SUBMITTED TO
THE GRADUATE SCHOOL OF NATURAL AND APPLIED SCIENCES
OF
MIDDLE EAST TECHNICAL UNIVERSITY

BY

YİĞİT GENÇAL

IN PARTIAL FULFILLMENT OF THE REQUIREMENTS
FOR
THE DEGREE OF MASTER OF SCIENCE
IN
CHEMICAL ENGINEERING

SEPTEMBER 2014

Approval of the thesis:

FABRICATION AND CHARACTERIZATION OF CORRUGATED MICROFILTRATION MEMBRANES

submitted by **YİĞİT GENÇAL** in partial fulfillment of the requirements for the degree of **Master of Science in Chemical Engineering Department, Middle East Technical University** by,

Prof. Dr. Canan Özgen   _____
Dean, Graduate School of **Natural and Applied Sciences**

Prof. Dr. Halil Kalıpçılar   _____
Head of Department, **Chemical Engineering**

Asst. Dr. Zeynep Çulfaz Emecen   _____
Supervisor, **Chemical Engineering Dept., METU**

Examining Committee Members:

Prof. Dr. Halil Kalıpçılar   _____
Chemical Engineering Dept., METU

Asst. Prof. Dr. Zeynep Çulfaz Emecen   _____
Chemical Engineering Dept., METU

Prof. Dr. Levent Yılmaz   _____
Chemical Engineering Dept., METU

Asst. Prof. Dr. Erhan Bat   _____
Chemical Engineering Dept., METU

Asst. Prof. Dr. Berna Topuz   _____
Chemical Engineering Dept., Ankara University

Date: 05.09.2014

I hereby declare that all information in this document has been obtained and presented in accordance with academic rules and ethical conduct. I also declare that, as required by these rules and conduct, I have fully cited and referenced all material and results that are not original to this work.

Name, Last name : Yiğit Gençal

Signature :

ABSTRACT

FABRICATION AND CHARACTERIZATION OF CORRUGATED
MICROFILTRATION MEMBRANES

Gençal, Yiğit

M.Sc., Department of Chemical Engineering

Supervisor : Asst. Prof. Dr. Zeynep Çulfaz Emecen

September 2014, 121 pages

In this study, the effect of corrugations on the membrane fouling performances of polyethersulfone (PES) membranes was investigated. Membranes were prepared by non-solvent induced phase inversion method and they were characterized by scanning electron microscopy (SEM), pure water permeance (PWP) and fouling during Baker's yeast (*saccharomyces cerevisiae*) filtration.

Since, it is nearly impossible to create the skin-layer on the mold side of the membrane a symmetric morphology was sought. In order to achieve this, firstly, modifications were done on the phase separation conditions and casting solution recipe to get symmetric membrane morphology on flat membranes which were easier to fabricate. When 10 wt% PES, 60 wt% PEG 400, 5 wt% H_2O and 25 wt% NMP solution was pre-coagulated in humid air for 10 minutes and fully coagulated in water, a symmetric morphology with connected pores of the average size 1.3 µm and no observable skin layer was obtained.

The chosen recipe was applied on corrugated mold with 50µm corrugation depth and width successfully. Moreover, in addition to 10 minutes humid air exposure, 5 minutes humid air also gave usable membranes with smaller pores (nearly 1µm) on the mold side and larger ones on the solution, non-solvent interface (nearly 1.8µm). The membranes with 15 minutes humid air exposure and same concentration also gave symmetric morphologies with 1.2µm average pore size. However, increase in humid air exposure increased shrinkage for the membranes.

Even if the area enhancement was eliminated there has still been a nearly twofold increase in pure water permeabilities of corrugated membranes compared to flat ones. The difference between fouling performances of corrugated and flat membranes was negligibly small.

Key words: Membrane, microfiltration, membrane fouling, concentration polarization, corrugated membrane.

ÖZ

OLUKLU YÜZEYLERE SAHİP MİKROFİLTRASYON MEMBRANLARININ HAZIRLANMASI VE KARAKTERİZASYONU

Gençal, Yiğit

Yüksek Lisans, Kimya Mühendisliği Bölümü

Tez Yöneticisi: Asst. Prof. Dr. Zeynep Çulfaz Emecen

Eylül 2014, 121 sayfa

Bu çalışmada, membran üzerindeki olukların polietersülfon (PES) membranlarının kirlenme performanslarına etkisi araştırılmıştır. Membranlar çözmeyen ile faz değişimi metoduyla hazırlanmıştır ve taramalı elektron mikroskobu (SEM), saf su geçirgenliği (PWP) ve ekmek mayası (*saccharomyces cerevisiae*) filtrasyonu boyunca kirlenmesiyle karakterize edilmiştir.

Kabuk tabakasını membranın kalıba bakan yüzeyinde oluşturmak neredeyse olanaksız olduğundan, membranlarda simetrik morfoloji aranmıştır. Simetrik membran morfolojisini elde edebilmek için ilk olarak, üretimi daha kolay olan düz membranların, faz değişimi şartlarında ve dökme çözeltisi reçetesinde değişiklikler yapılmış, birbirine bağlı ve ortalama boyutu 1.3 µm olan gözenekli, simetrik morfoloji kütlece 10 % PES, 60 % PEG 400, 5 % H_2O and 25 % NMP içeren çözelti, koagülasyondan önce 10 dakika nemli havaya maruz bırakıldığında ve suda tamamen koagüle edildiğinde elde edilmiştir.

50 µm oluk derinliği ve genişliği olan oluklu kalıp üzerine seçilen recete başarıyla uygulanmıştır. Ek olarak, 10 dakika nemli havanın yerine 5 dakika nemli hava da

kalıp tarafında daha küçük gözenekler (neredeyse 1µm) ve çözelti – çözemeyen arayüzeyinde daha büyük gözenekler (neredeyse 1.8µm) oluşturarak filtrasyon işlemi için kullanılabilir membranlar üretmiştir. Aynı çözelti konsantrasyonuyla 15 dakika nemli havaya maruz bırakılan membranda ortalama gözenek boyutu 1.2 µm olan simetrik morfoloji gözlemlenmiş fakat nemli havaya maruz bırakılma süresi arttırmak membranlarda büzüşmeyi arttırmıştır.

Alan artışı ortadan kaldırıldığında bile ultra saf su geçirgenliği oluklu membranlarda düz olanların neredeyse iki katı olarak hesaplanmıştır. Düz ve oluklu membranların kirlenme performansları arasındaki farkın ihmal edilebilecek kadar küçük olduğu görülmüştür.

Anahtar Kelimeler: Membran, mikrofiltrasyon, membran kirlenmesi, konsantrasyon kutuplaşması, oluklu membran

To My Dearest Family,

ACKNOWLEDGMENTS

TABLE OF CONTENTS

LIST OF TABLES

TABLES

LIST OF FIGURES

FIGURES

xvii

NOMENCLATURE

MF : Microfiltration

NIPS : Non-solvent Induced Phase Separation

CFV : Cross-flow Velocity

Cw : Concentration at the wall

Cb : Bulk concentration

J : Permeate flux

δ : Concentration polarization layer thickness

Rmem : Retention of the membrane

D : Diffusivity of rejected component

TMP : Trans-membrane pressure,

μ : Viscosity of permeate stream and,

R_{tot} : Total resistance to flow

Rm : Membrane intrinsic resistance.

Rg : Resistance due to gel layer

Rcp : Resistance due to concentration polarization

Rp : Resistance due to pore blocking

Ra : Resistance due to adsorption phenomena

RFR : Relative flux reduction

Q : Volumetric flow rate read from rotameter and

A : Area perpendicular to flow in membrane module.

Re : Reynolds number

ρ : Density of the feed stream

d_H : Hydraulic diameter and

P : Wetted perimeter

PWP : Pure water permeance

TMP : Trans-membrane pressure difference

dR/dt : Fouling rate

Rff : Final fouling resistance R

Rfi : Initial fouling resistance

ΔP_m : Measured pressure difference

ΔP_o : Offset pressure difference when permeate flux is 0

D_{AB} : Binary diffusion coefficient

k : Mass transfer coefficient

CHAPTER 1

INTRODUCTION

1.1 Membrane Separation

Membrane is a semi-permeable barrier which is used in many different areas such as, pharmaceutical industry, sterilization and clarification of beverages and drinking water production. The purpose of membrane filtration processes is leaving rejected components at the retentate side while some components of a mixture permeate the membrane freely. The stream that passes through membrane is called permeate and the rejected stream is called retentate.
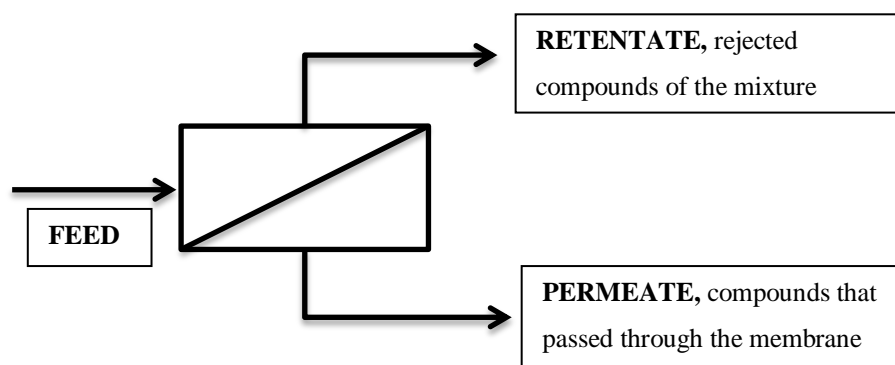
Figure 1. 1 Schematic representation of a membrane filtration process.

There are four membrane filtration processes according to the particle size range that can be filtered which are reverse osmosis (pores are 10^{-4} and 10^{-3} µm in size), nanofiltration (pores are 10^{-3} and 10^{-2} µm in size), ultrafiltration (pores are 10^{-2} and 10^{-1} µm in size) and microfiltration(pores are 10^{-1} and 10^{1} µm in size).

Microfiltration is the processes that use porous membranes to separate suspended particles with the diameter larger than 0.1 µm [1]. Membranes can be isotropic and anisotropic with respect to their morphologies. Isotropic (symmetric) membranes have the same structure from top layer of the membrane to bottom layer. Commercially, almost all microfiltration (MF) membranes have this structure.

On the other hand, anisotropic (asymmetric) membranes consist of different layers and structures on their morphology. Generally, anisotropic membranes have a skin layer on one side and a support layer under the skin. The skin layer is relatively dense, thin layer which performs separation while the support layer is much thicker and porous than the skin layer which provides mechanical strength to the membrane.
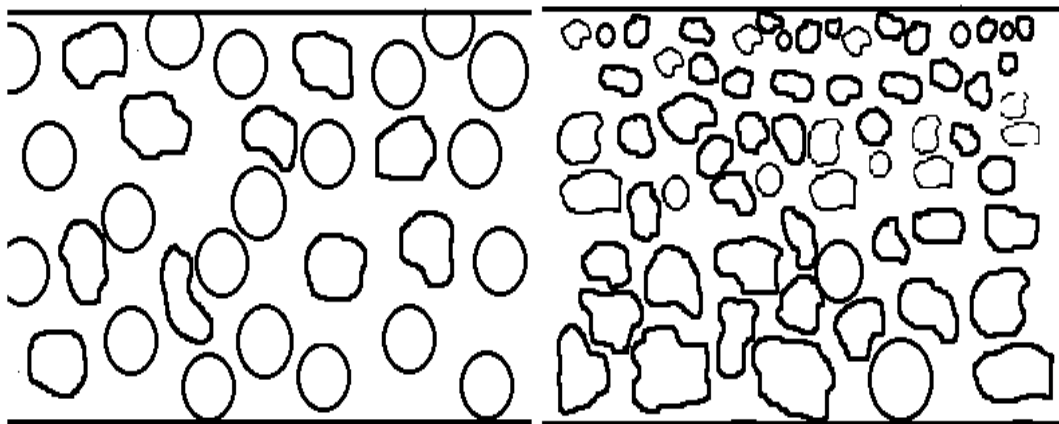
Figure 1. 2 Symmetric and asymmetric porous membrane morphologies.

1.1.1 Phase Separation Methodology

Phase separation process is the most widely used method for preparation of porous polymeric membranes [2]. There are three types of phase separation processes which are;

1.Non-Solvent Induced Phase Separation (NIPS): There are two types of NIPS method which are non-solvent precipitation and non-solvent vapor absorption.

-Non-Solvent Precipitation: The cast polymer solution is immersed in a non-solvent (generally water) bath. Absorption of non-solvent and loss of solvent cause the film to rapidly precipitate from the top to bottom.

-Non-Solvent Vapor Absorption: The cast polymer solution is placed in a non-solvent atmosphere. Non-solvent vapor absorption causes the film to precipitate.

2.Thermal Gelation: Polymer solution is cast hot. Cooling causes precipitation.

3.Solvent Evaporation: A mixture of solvents is used to form the polymer casting solution. Evaporation of one of the solvents after casting changes the concentration and causes precipitation. [1]

Non-solvent induced phase separation is the process of changing one phase casting solution into two different phases by a non-solvent addition. These two separate phases are a solid, polymer rich phase which creates the matrix of membrane and a liquid, polymer poor phase which creates membrane pores [2]. In the phase separation process casting solution composition moves to the final membrane composition by losing solvent and taking non-solvent. In the Figure 1.3, a typical phase separation process can be seen. The corners of the triangle represent pure components; polymer, solvent and non-solvent and the points within the triangle represents a mixture composition of these three components. As said above mixture starts at one phase region and by losing solvent and gaining non-solvent mixture is separated into two different phases; one is polymer rich phase which forms the

matrix of the membrane and the other is polymer lean phase which creates pores in membrane morphology.

The phase separation process goes through a series of steps. Firstly, solvent exchanges with non-solvent and after solution enters two phase region precipitation occurs. During the precipitation process, solution enters the two phase region after passing binodal boundary. Slow precipitation processes, generally make average pore sizes larger because there is more time for separation of two phases via nucleation and growth. Passing binodal boundary makes casting solution to enter metastable region. This metastable region is very small for low molecular weight polymers and can be very large for high molecular weight polymers. By further decreasing in solvent concentration, solution enters an unstable, two phase region. In this region solution spontaneously separates into two phases [1, 3].
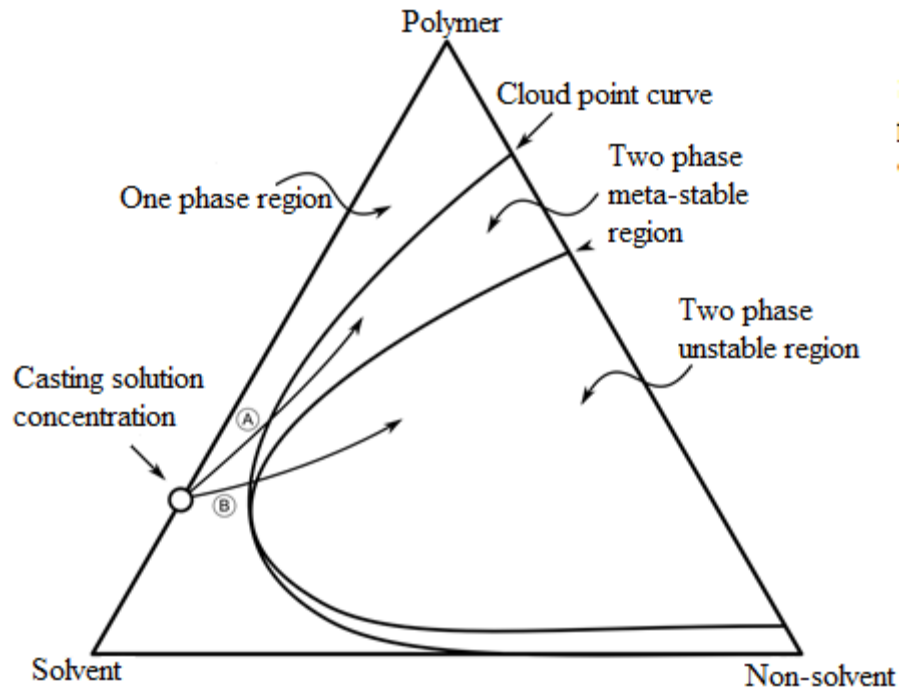
Figure 1. 3 The changes in polymer solution concentrations during phase separation in ternary phase diagram.

1.2 Factors Reducing Membrane Performance

Concentration polarization, which occurs in the boundary layer adjacent to membrane wall, and membrane fouling are the biggest problems that reduce the membrane performance by increasing a membrane's resistance to flow either by decreasing permeate flux or increasing filtration pressure. The difference between membrane fouling and concentration polarization is; concentration polarization leads to a loose, highly concentrated layer which reduces concentration of permeating component near the surface. Membrane fouling is the deposition of rejected components on the membrane surface or in the pores. Although both phenomena cannot be totally prevented, adjusting operating conditions such as cross flow

velocity (CFV), operating pressure or flux and feed concentration can control fouling and concentration polarization's extent [4].

1.2.1 Membrane Fouling

Fouling is the accumulation of dispersed particles on the membrane surface or within the membrane. For pressure driven membrane processes such as reverse osmosis, nanofiltration, ultrafiltration and microfiltration membrane fouling is an important drawback for industrial usage.

1.2.2 Concentration Polarization

In the membrane filtration process, components of the feed permeate selectively through the membrane [5]. The rest of the feed components are left on the feed side of the membrane. The build-up of these rejected materials on the surface of the membrane makes permeating components concentration less near the membrane wall. This phenomenon is called concentration polarization. Since concentration polarization reduces concentration difference of permeating component between sides of the membrane it also lowers flux and selectivity. In addition, because concentration polarization increases the resistance to filtration, filtration becomes more costly. In the figure below concentration gradient near the membrane wall because of concentration polarization can be seen.

$$Back\ Diffusion = D\frac{dC}{dx}$$

Membrane

C_w

J_v

Bulk feed C_b

Permeate C_P

Concentration polarization layer

thickness $= \delta$

C

x
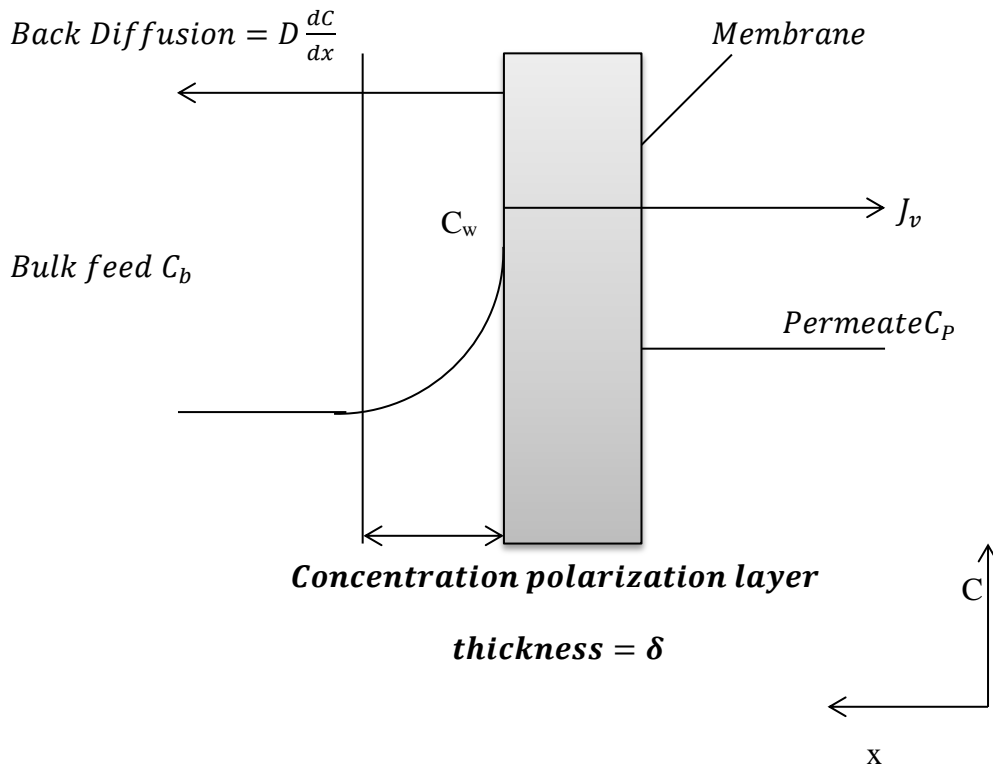
Figure 1. 4 Concentration polarization phenomena

The effect of concentration polarization in a filtration process can be understood by the value of concentration polarization modulus;

$$\frac{C_w}{C_b} = \frac{exp\left\{\frac{J\delta}{D}\right\}}{exp\left\{\frac{J\delta}{D}\right\} - Rmem\left[exp\left\{\frac{J\delta}{D}\right\} - 1\right]}$$

If retention is 100%;

$$\frac{C_w}{C_b} = exp\left\{\frac{J\delta}{D}\right\}$$

In equation above Cw/Cb is concentration polarization modulus where Cw is concentration at the wall, Cb is bulk concentration, J is the permeate flux, δ is concentration polarization layer thickness, Rmem is retention of the membrane and D is the diffusivity of rejected component. If concentration polarization equals to

unity, that means there is no concentration polarization (CP) and concentration at the wall equals to concentration of bulk (Cw = Cb).

1.2.3 Mitigation of Fouling and Concentration Polarization

In order to mitigate fouling surface modification is a common approach and since most of the membrane forming polymers and foulants are hydrophobic, such modifications are generally trying to make these surfaces more hydrophilic [6]. Hydrophilic surfaces have strong interactions with water molecules which may act as a buffer for hydrophobic foulants.

Reduction in concentration polarization in a membrane filtration processes is generally achieved by modifications of the hydrodynamics on the membrane surface. The purpose of these modifications is to increase back transport from the membrane surface which can be done by creating vortices or flow instabilities. In order to make flow instabilities and vortices on the membrane surface, turbulence promoters (such as corrugations) on the membrane wall, pulsating flow or two phase flow (liquid flow with air bubbles) can be implemented. In addition, by increasing Reynolds Number (Re) flow can be changed into turbulent flow which is more costly than the former methods mentioned. Decreasing permeate flux also reduces the effect of concentration polarization however at the expense of slower filtration.

In this study, polyether sulfone (PES) membranes were prepared with and without corrugations on the surface via combined vapor and liquid induced phase inversion method. In the cross-flow filtration system, at two different cross-flow velocities 0.1 and 0.2 m/s and different permeate fluxes, pure water permeabilities and fouling performances of flat and corrugated membranes were compared. The method suggested in this study is a novel and simple method for fabrication of corrugated membranes.

CHAPTER 2

LITERATURE SURVEY

2.1 Membrane Fouling

Membrane fouling is the major problem in membrane filtration processes which means losing permeance because of the accumulation of rejected compounds on the membrane surface or inside the membrane pores. This accumulation may change the effective pore size distribution and make additional resistance to flow through the membrane which causes reduction in the permeate flux or increase in trans-membrane pressure.

Darcy's Law can be used to describe the overall characteristics of flux reduction;

$$J = \frac{TMP}{\mu(R_{tot})}$$

Where,

TMP is trans-membrane pressure,

μ is the viscosity of permeate stream and,

R_{tot} is the total resistance to flow.

There are various types of fouling resistances in pressure driven membrane separation processes which can be seen in Fig. 2.1. In the ideal case, without any

fouling only Rm should be involved which is the membrane intrinsic resistance. However, since membrane retains some of the rejected materials on its surface a gel layer will be formed near membrane wall which exerts a resistance to mass transfer, Rg. Increase in concentration of retained materials also creates a resistance to mass transfer by decreasing concentration difference between feed and permeate side, Rcp. Moreover, some solutes can penetrate and block membrane pores and leading pore blocking resistance, Rp. Final resistance is Ra which is the resistance due to adsorption phenomena [7].
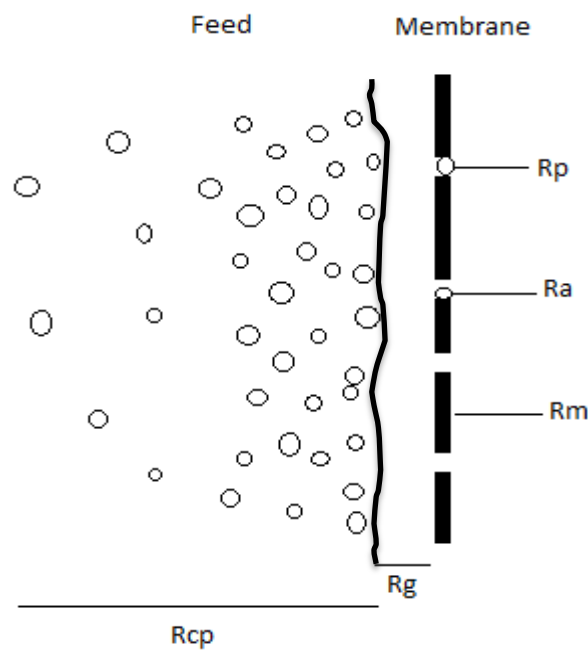
Figure 2. 1 Various resistances of membrane filtration processes.

So, R_{tot} equals to summation of these resistances.

$$R_{tot} = R_m + R_g + R_{cp} + R_p + R_a$$

There are two different filtration methods which are dead-end and cross-flow modes. Operation mode is chosen according to optimization between productivity and cost of the operation. Generally, for operations that have tendency to be fouled heavily cross-flow filtration is the economically more feasible choice. However, operations with low fouling potential works with dead-end filtration method in which the retained particles are continuously accumulated on the membrane surface. In order to prevent excessive performance reduction, periodic back washes can be necessary which removes the deposited particles from membrane surface.

In order to observe the effect of fouling, monitoring trans-membrane pressure at constant permeate flux and flux decline in constant trans-membrane pressure can be used. During constant flux experiments, fouling causes increase in TMP while it decreases the permeate flux for constant TMP experiments. A common method is to incrementally increase the flux for a fixed duration each is called flux step. Until critical flux for each increment a stable TMP is observed. Beyond the critical flux TMP will increase for the same flux step [8]. Howell et al. defined critical flux as the flux below which there is no deposition of particles on the membrane surface [9]. Another important term is the threshold flux. According to Stoller et al. the threshold flux is the flux that separates a low fouling region, which has almost constant fouling rate, from high fouling region, where flux dependent high fouling rates can be observed [10].

D.J. Miller et al. compared membrane fouling at constant flux and constant trans-membrane pressure on ultrafiltration membranes used to filter oil water emulsions. In constant flux experiments, below the threshold flux mild increase in TMP was observed while above threshold flux this change in TMP was rapid. In constant TMP experiments regardless of whether the initial flux is above or below threshold flux all experiments have similar flux decline behaviour. Constant TMP in comparison to constant flux experiments gave nearly same resistances within experimental error for fluxes below threshold flux. However, above the threshold flux the constant TMP resistance initially increased sharply and reached a steady state because flux fell

rapidly to below threshold while constant flux resistances continues to increase sharply after TMP resistance reached the steady state value [11].

2.2 Fouling Mitigation in Membrane Separation Processes

There are two different approaches for fouling mitigation in membrane filtration processes. One of them is modifying the surface of the membrane in order to prevent adsorption of particles and solutes. In many cases, hydrophilic surfaces are more resistant to fouling, so a common methodology for modifying membrane surface is addition of hydrophilic polymers into casting solution before phase separation. The other method is changing the flow hydrodynamics in order to increase back transport and decrease concentration polarization by creating flow instabilities. This can be achieved by turbulent, pulsating, two phase flow or turbulence promoters. The method which will be focused on in this work is making patterns (turbulence promoters) on the membrane surface and decreasing fouling by creating eddies near these patterns.

2.2.1 Membranes with Hydrophilic Additives

Blending hydrophilic additives is the simplest method to modify polymeric membranes. Directly blending hydrophilic polymers, such as PVP and PEG, increases membrane hydrophilicity and antifouling property [112]. Since smaller molecular weight additives have relatively higher diffusivity than higher molecular weight ones, they can diffuse out during the immersion along with the solvent. Higher molecular weight additives have much lower diffusion rates than solvent and take more time to reach the surface which causes enough time for polymer molecules to aggregate on top of the solution and form a denser top layer with smaller pores. As a result, it can be said that, PEG with high molecular weight acted as both pore former and pore size reducer. However, PEG with low molecular weight such as 400 kDa generally acts as a weak non-solvent for the polymer which reduces the solvent power in the solution [13].

12

Susanto et al. worked on PES ultrafiltration membranes which were prepared by non-solvent induced phase separation method with different macromolecular additives, polyvinylpyrrolidone (PVP), poly(ethylene glycol) (PEG) (MW-10.000 g/mol) and poly(ethylene oxide)-b-poly(propylene oxide)-b-poly(ethylene oxide) (Pluronic). Their effects on membrane structure and performance and their stabilities in the polymer matrix were compared. The membrane with addition of Pluronic showed the highest hydraulic permeability among all macromolecular additives. Although, PES-PEG blend membrane had the highest surface hydrophilicity from contact angle measurements, stability in the polymer matrix was low. After BSA adsorption experiments it was seen that PES-PEG 10k and PES-Pluronic membranes had the lowest relative flux reduction values and ultrafiltration experiments showed that PES-Pluronic membranes had much higher permeate flux than other membranes with or without additives and after filtration 70% of initial water flux can be recovered by just external cleaning with water [14].

Pagidi et al. worked on polysulfone (PSF) ultrafiltration membranes synthesized by non-solvent induced phase separation method. The additives they used were polyvinylpyrrolidone (PVP), polyetherimide (PEI), polyethylene glycol (PEG) (Mw-600Da) and polyethersulfone (PES). It was seen that resistance to fouling had increased by the addition of PEG and PVP. In this work oil and water mixture was filtered. Since the hydrophilic characteristics of PEG and PVP tend to weaken the hydrophobic interactions between oil droplets and membrane surface, membranes with PEG and PVP had higher flux recovery and lower flux decay than pure Psf membrane [15].

Another research of Susanto et al. was about polyethersulfone microfiltration membranes prepared by vapor induced phase separation with non-solvent induced phase separation method. Pluronic and TEG (triethylene glycol) were used as hydrophilic additive and weak non-solvent, respectively. From contact angle measruements it was seen that, hydrophilicity increased with increasing concentration of Pluronic in casting solution. On the other hand, increasing humid air exposure time decreased hydrophilicity. Another observation was that, high

performance membranes can be prepared with high non-solvent (TEG) content and relatively long exposure in humid air. Even though prevention of fouling totally is impossible, the membranes with Pluronic additive were more resistant to fouling [16].

Mendez et al. used PEG with different molecular weights (400, 1000, 10000 gmol) as additive for ultrafiltration membranes. From infrared analysis they found that after 24h of water immersion there are nearly no PEG staying on the surface of the membrane. However, due to increased hydrophilicity, addition of PEG increased pure water permeability and decreased relative flux reduction in spite of decreased pore sizes. The reduction in pore size and number were increased with molecular weight of PEG additive. The flux and permeabilities increased when middle size PEG (1000 g/mol) added to the solution but decreased again with very high molecular weight PEG (10000 g/mol) addition. For PEG 10kDa, it was concluded that these reductions were too strong to be balanced with hydrophilicity.

Relative Flux Reduction, RFR (%) $= \left(\frac{J_i - J_f}{J_i}\right) . 100$

J_i is the initial water flux of the membrane while J_f is water flux after BSA filtration. $J_i - J_f$ term gives the reduction in the water flux after BSA filtration which means flux reduction after fouling. Dividing this term by initial permeate flux gives the relative value of flux reduction to initial flux. Higher relative flux reduction value means lower resistance to fouling. It was seen that membranes with PEG additive have RFR values below 20% and membranes without additive have around 50% RFR. This situation supports the idea of PEG addition to polymer solution increases resistance to fouling [17].

Membrane surface coating with hydrophilic additives is another option that can reduce fouling. Miller et al. modified polysulfone ultrafiltration membranes with polydopamine and polydopamine-g-poly(ethylene glycol) hydrophilic coatings. In the literature it was observed that, such coatings increase the overall mass transfer resistance which reduces permeability [18,19]. Soybean oil emulsion was filtered with six different permeate fluxes for fouling studies. Threshold fluxes were

estimated by using flux stepped procedure. At the fluxes below threshold unmodified membranes gave the lowest trans-membrane pressure. The reason behind higher trans-membrane pressures in coated membrane for fluxes below threshold was attributed to the increased overall mass transfer resistance with coating. On the contrary, at fluxes higher than threshold, modified membranes again had higher trans-membrane pressure initially but rapid fouling of unmodified membranes resulted in greater pressure than coated membranes at the later stages of the filtration [6].

From these researches it can be concluded that, hydrophilic polymer additives increases pure water flux values although in some situations they reduce pore sizes. Hydrophilicity of membrane attracts water molecules and makes a layer of water molecules on the membrane surface which prevents interaction between hydrophobic membrane surface and colloids or solutes [14,15,17].

2.2.2 Corrugated (Patterned) Membranes

Turbulence promoters reduce the level of concentration polarization on the membrane surface. Making corrugations on membrane wall as turbulence promoters was used in this work which create eddies and increase mass transfer away from the membrane [4].
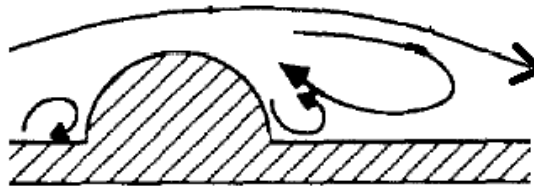
Figure 2. 2 Corrugation as turbulence promoter

Racz et al. made hyperfiltration experiments on membranes with corrugations which were prepared by pressing cellulose acetate membranes into a corrugated PVC plate. Corrugations on the membrane were half cylinders with 1.5 mm diameter and distances between corrugations were 15, 23,40,80 mm. It was found that corrugations with mutual distances of 23 and 40 mm improve mass transfer when compared with a flat membrane. According to this work, corrugated membranes with mutual distances 15 and 80 mm have higher pressure drops than flat ones while corrugated membranes with 23 and 40 mm mutual distances have less for the same mass transfer coefficient. However, these membranes also have increased mass transfer when compared with flat ones. In order to find which one is more energy efficient, a k, mass transfer coefficient versus energy consumption graph was prepared. From this graph, it was concluded that, corrugations with 40 mm mutual distance between them are the best choices for both energy consumption and mass transfer increment [5].

Racz et al. also worked on corrugated polysulfone membranes for ultrafiltration experiments and found that corrugations increase flux by up to 150% depending on mutual distances between corrugations. Three different mutual distances again 23, 40 and 80 mm were tried. Mutual distance of 40 mm gave the highest flux increase at 0.67 m/sec cross flow velocity. In addition, again the most effective membrane for energy consumption was the corrugated one which had 40 mm between its corrugations and in ultrafiltration processes all corrugated membranes have lower pressure drop values than flat one [20].

K.Scott et al. worked on corrugated PVDF (Polyvinylidene Fluoride) and PTFE (Polytetrafluoroethylene) membranes in order to observe the effect of crossflow velocity, channel height, trans-membrane pressure and the angle between flow and corrugations. The corrugations on the membrane surface were made by mechanical pressing between metal dies at 120°C and they were in triangular shape with 2 mm wide and 1 mm high. It was concluded that in all cases increased cross-flow velocity significantly improves permeate flux and for membranes with corrugations the effect of CFV was higher than flat membranes. The reasons behind this were attributed to increasing mass transfer away from the membrane with increased feed velocity and increased shear effects on membrane surface. In addition, it was observed that, decreasing channel height increases permeate flux by increasing shear rate again. Flow angle was defined as the angle between flow and the direction of corrugations and the most flux enhancement was seen when corrugations were perpendicular to flow direction with 160% increased flux in comparison with flat ones. This enhancement is due to the combined effects of turbulence and increased effective membrane area. Three different flow angles were used in these experiments which were parallel, 45° and 90° and flux increases 30, 100 and 160% in comparison with flat membrane respectively. Increased trans membrane pressure firstly increased the permeate flux until 0.8 bar. Between 0.8 and 1.5 bars flux decreased because of increased build-up of concentration polarization or blocked membrane pores by water droplets. After 1.5 bar it was seen that because both water and oil droplets permeate, flux was increased again [4].

In 2012, Won et al. made two different shapes of corrugation on PVDF membranes and compared prism, pyramid patterned and flat membranes according to their characteristics and mitigation of biofouling. In this work, a modified precipitation immersion method was used in order not to create a dense layer on the opposite side of the membrane. In this method, polymer solution is cast on patterned PDMS replica mold, then immediately after casting a non-woven fabric is placed on the solution and immersed into the coagulation bath for precipitation. By using this method immediate soldification of solvent nonsolvent interface was prevented. Firstly, in order to compare the modified precipitation method with conventional immersion

and conventional air drying method, prism patterned membrane morphologies were examined. They found modified method is the most effective one with porous morphology and without a dense layer on the opposite side of corrugations. Regardless of the pattern type, corrugated membranes had 20% increased water flux in comparison to the flat membranes. The heights of the corrugations were; for pyramid patterned 8.2-9.6 μm and for prism patterned 9.3-9.9 μm. After 4 hours of cross-flow filtration of activated sludge fouling in prism patterned membranes was much less than flat membranes. For further investigation membranes were also operated in MBR and it was seen that trans-membrane pressure increased much more in flat membranes [21].

In 2013 Maruf et al. worked on polysulfone ultrafiltration membranes and used nano-imprint lithography on silicon molds in order to make corrugations with 834 nm periodicity and 200 nm depth. Patterned membranes were made by pressing imprinted silicon molds on originally flat membranes at 120 °C and 4 MPa for 180 seconds. Although corrugation on the mold depth is 200 nm, the height of the corrugations of membrane was between 100 and 120 nm. Imprinted membranes had higher membrane area but still had lower water flux. It was concluded that NIL process should have made pores smaller or decreased the number of pores. All imprinted membranes had higher critical flux values than flat ones. In their critical flux measurements, it was seen that critical flux increases with particle size in the suspension for flat membranes and imprinted membranes have 42% higher flux for 0.25 μm, 46% higher flux for 0.5 μm and 19% higher flux for 1 μm silica particles in the suspension than pristine membranes. Moreover, they worked on different flow angles to observe deposition of 0.5 μm silica particles after 2h of filtration on the membrane surface and they found that by increasing the angle between flow direction and corrugations, deposition of particles become less. The least deposition on the membrane surface was observed when flow direction was perpendicular to the corrugations [22].

Another research with prism patterned membranes was done by Lee et al. Patterned membranes were prepared by modified phase inversion processes which have been

used in Won et al. research for the first time. After making patterned PDMS mold by soft lithographic method, polymer solution was cast on these molds and immediately after casting the fabric was placed on top of the casting solution before immersing into precipitation bath. Prisms on the membrane surface had 400 µm width and 200 µm height. The flat membranes were made with same method for comparison. Both membranes had same thickness and corrugated membrane's pore size was slightly larger (about 0.06 µm) then flat membrane's pores. As expected pure water flux of patterned membrane was higher also. From both experimental and CFD studies it was observed that the deposition of microbials were reduced on the patterned surface and a vortex was anticipated via CFD simulation at the upper part of the valley between corrugations which lead to higher fouling below that region, which was stagnant [23].

Gohari et al. compared the effect of angle between flow direction and corrugations and observed that when the feed flow direction is perpendicular to corrugations BSA fouling can be mitigated. However, when the feed flow direction is parallel to corrugations, fouled membranes could be washed more effectively [24].

Won et al. examined the relationship between pattern height and membrane performance and parameters affecting pattern fidelity on PVDF membranes. Patterned master mold was prepared by photo lithography from a photo resistant polymer and a PDMS replica of master mold was taken. Casting solution was poured onto the PDMS replica and immersed into the coagulation bath. In the filtration process, the cross flow velocity was 0.3 m/s and the Reynolds number was 1000. PVDF membranes with different molecular weights had different morphologies. The lowest molecular weight of PVDF (180 kDa) showed finger-like structure while higher molecular weights (275, 430 kDa) made sponge-like membrane structure. This observation implies that increasing molecular weight of the polymer increases the viscosity of the solution which restricts the exchange between solvent and non-solvent. This restriction reduces the phase separation rate and prevents macrovoid formation. The fidelity of the membrane was calculated with dimensions of pattern in

a patterned membrane divided by same dimension of pattern in replica mold. For example;

$$Width\ Fidelity = \frac{Width\ of\ pattern\ in\ a\ patterned\ membrane}{Width\ of\ pattern\ in\ a\ replica\ mold}$$

From these formulas, it was found that, area fidelity was decreased with increasing polymer molecular weight. PVDF with the lowest molecular weight which was 180 kDa had 0.90 and with the highest molecular weight had 0.20 area fidelity. Width fidelity was not changed much but height fidelity changed as much as area fidelity. Height fidelity also increased from 0.25 to 0.90 when molecular weight decreased from 430 kDa to 180 kDa.It was concluded that, in slow phase separation processes caused by high molecular weight, coagulation progresses through nucleation and growth and nucleation started at the solvent non-solvent interface, and since the polymer diffuses up to grow nuclei, polymer concentration at the bottom of the pattern decreased which resulted in a lower height fidelity. On the other hand, fast phase separation progresses through spinodal decomposition and polymer did not have time to diffuse up before coagulation which meant greater fidelity for the membrane patterns. Fidelity was reduced in slow nucleation and growth process because of decreased amount of PVDF in the triangle. Polymer concentration effect on the membrane area fidelity was also examined with 15% and 10% PVDF concentrations in the solution. For 10% polymer concentration and high molecular weight (430 kDa), area fidelity was 0.20. However, same molecular weight with 15% polymer concentration had 0.91 area fidelity which implies that although the diffusion of the polymer takes place from bottom of the solution to solvent, non-solvent interface, there are still enough PVDF in the triangles to form patterns with high fidelity. Another important variable for pattern fidelity was found to be the interaction between replica mold and polymer solution. Since attraction between mold and polymer solution makes solution spread out non-uniformly, pattern fidelity

will be also affected. In order to observe this interaction effect, polymer solution was cast on different replica molds such as PDMS, PDMS with hydrophilized surface, PS (polystyrene) and PUA (polyurethaneacrylate). After works of adhesion were calculated from contact angle measurements it was seen that replica mold with the lowest work of adhesion value which, was PDMS, had the greatest fidelity and PUA had the highest work of adhesion value and unobservable patterns. After pattern fidelity observations, the relationship between fidelity and membrane performance was investigated. Since high area fidelity means higher surface area, patterns with increased fidelity had more water flux and because of high shear stress, biofouling tendency was lower for higher height fidelity [25].

Table 2. 1 Summary of corrugation dimensions and methodology of membrane preparation in literature.

Researcher	Corrugation Width	Corrugation Height	Distance between Corrugations	Preparation Methodology
Racz et al. (89)	1.5 mm	1.5 mm	15,23,40,80 mm	pressing into a corrugated PVC plate
Racz et al. (89)	1.5 mm	1.5 mm	23, 40 and 80 mm	pressing into a corrugated PVC plate

Table 2. 1(cont'd) Summary of corrugation dimensions and methodology of membrane preparation in literature.

Scott et al. (2000)	2 mm	1 mm		mechanical pressing between metal dies at 120°C
Won et al. (2012)		For pyramid patterned; 8.2-9.6 μm For prism patterned; 9.3-9.9 μm		modified precipitation immersion method
Maruf et al. (2013)	834 nm	100-120 nm	834 nm	pressing imprinted silicon molds on originally flat membranes at 120 °C and 4 MPa for 180 seconds
Lee et al. (2013)	400 μm	200 μm		modified precipitation immersion method
Won et al. (2014)	39-45 μm	4-18 μm		Precipitation immersion method

From Table 2.1 the change in corrugation dimension by the time can be seen. It is obvious that corrugation dimensions became much smaller in time until today. Patterns dimensions have been in millimeters in the work of Racz et al. which was published in 1989. However, using lithography in replica molds changed this situation to micrometers and nanometers. Moreover, although in the past the only choice for making patterns on the desired surface of the membrane was pressing a flat sheet membrane to some patterned surface, while recently patterns can be made during immersion precipitation method on the corrugated molds with modifications in order not to have a skin layer on non-corrugated side [5,20].

In this work, patterned membranes were prepared by simple non-solvent phase inversion method on a corrugated mold. No pressure or temperature treatment was used in order to create patterns. However, since in non-modified phase separation method skin layer will be formed on solution, non-solvent interface, symmetric morphology on membranes was sought. The method developed is a new and simple approach for preparation of microfiltration patterned membranes.

The fouling behavior of the corrugated and flat membranes was compared via filtration of 1g/L Baker's yeast (*Saccharomyces cerevisiae*) suspension during constant flux, flux stepped experiments.

CHAPTER 3

EXPERIMENTAL METHODS

3.1 Materials

PES (Ultrason E6020P) was provided from BASF. Because of its mechanical strength, thermal and chemical stability and excellent film forming properties polyethersulfone (PES) has been used very commonly for the fabrication of microfiltration and ultrafiltration membranes [3]. N-methyl pyrrolidone (NMP, %99) was used as non-solvent and PEG 400 and PEG 6k were used as additives which were purchased from Sigma-Aldrich. Ultrapure water was used as non-solvent in the solution and tap water was the coagulant. Before use, PES was kept in an oven at 80 ^{o}C for one night and PEG 6k was kept in a vacuum oven at room temperature.

3.2 Membrane Preparation

3.2.1 Solution Preparation

Casting solution has significant effect on membrane morphology and performance. In this work 7 different polymer solutions were used. Solutions were stirred at room temperature except for the one with 30% PEG 6k and 8% ultrapure water. This solution needed higher temperatures and in order not to cause any deformation, it was stirred at 50 ^{o}C. While stirring the temperature was controlled via a thermometer. After stirring, solutions were filtered with a 25 mesh (0.707mm) screen.

Table 3. 1 Polymer solution concentrations.

PES	PEG400	PEG6k	UP Water	NMP
10	-	-	-	90
10	30	-	-	60
10	60	-	-	30
10	-	30	-	60
10	60	-	5	25
10	-	30	8	52
10	30	-	8	52

3.2.2 Flat Membranes

As it can be seen in Table 3.1 flat membranes were fabricated with 10% PES and different concentrations of PEG 400, PEG 6k, NMP and ultrapure water. A stainless steel casting bar was used to cast the solution uniformly with the thickness of 250 µm on a stainless steel flat mold.

$$R - r = 250 \mu m$$
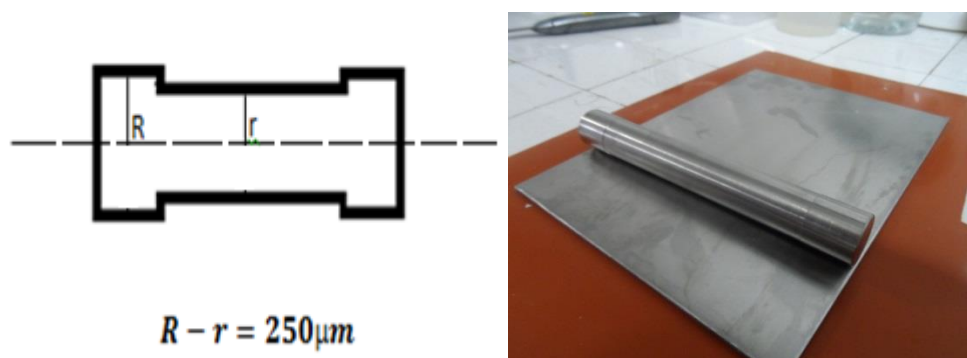
Figure 3. 1 Stainless steel casting bar and flat mold used in fabrication of flat membranes.

After pouring polymer solution onto stainless steel mold and casting with 250 µm thickness, mold was put into pre-coagulation media or directly into tap water bath. After 1 hour, water in the bath was changed in order to cleaning the membrane remove the solvent more effectively. Membranes stayed in water bath overnight and then took into ethanol bath. Before drying, ethanol bath was applied for one hour in order to reduce the Laplace pressure in the pores and to prevent their collapse during drying. After that, membranes were taken and dried.

3.2.3 Corrugated Membranes

Fabrication of the corrugated membranes was nearly same with the flat membranes. However, these membranes were not cast on flat stainless steel mold. The mold used in fabrication of corrugated membranes was made of a silicon wafer and the corrugations on it were made via deep reactive-ion etching (DRIE) method by METU-BIOMEMS center.
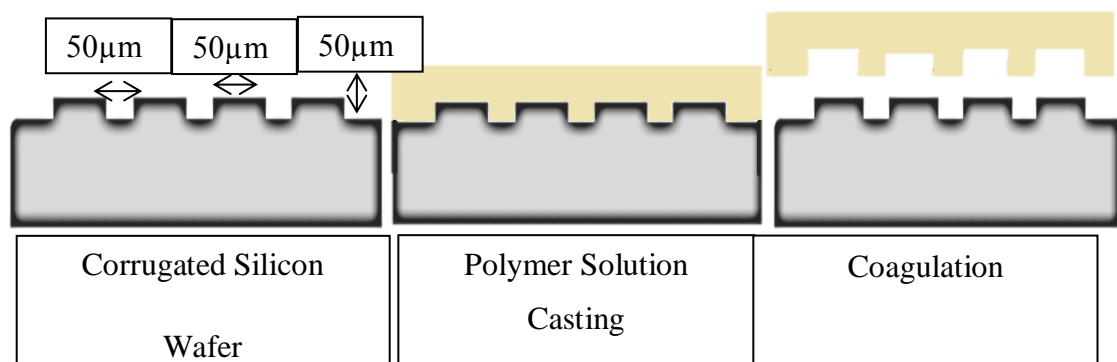
Figure 3. 2 Procedure for fabrication of corrugated membranes.

27

Solutions were poured onto silicon wafer and cast via Sheen 1117/100 micrometer adjustable film applicator with 200 μm thickness. After casting, corrugated membranes procedure was the same with flat membranes. They were subjected to pre-coagulation media or immersed directly into water bath.

3.2.4 Pre-Coagulation Media

In this work two different pre-coagulation treatments were used which were humid air exposure and NMP/water bath immersion. In order to provide humid air exposure, air was pumped by an aquarium pump into a gas washing bottle with filter disc which had ultrapure water in it. Filter disc makes air bubbles which help to increase relative humidity of the air. The gas wash bottle was in water bath which was at 50 $^{\circ}$C. Exit stream of this bottle was connected to a box in which cast solution was put. By doing this a relative humidity of 75±10% was achieved during the fabrication of membranes. Relative humidity values were measured by a hygrometer. Humid air exposure set-up can be seen in Figure 3.3.
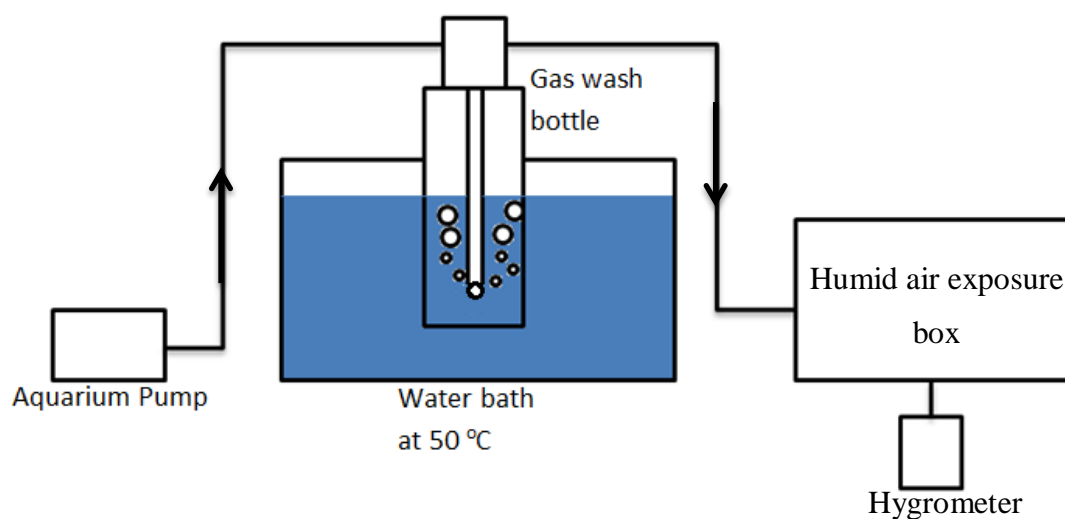
Figure 3. 3 Humid air exposure set-up

28

NMP/water (75 wt% NMP, 25 wt% water) bath was another option of pre-coagulation treatment in this work.

3.3 Membrane Characterization

In this work membrane characterization achieved by scanning electron microscopy (SEM) images, pure water permeance experiments and 0.1 g/L saccharomyces cerevisiae suspension filtrations. Both pure water and fouling experiments were performed with perpendicular flow to corrugations and in the same cross-flow filtration set-up which can be seen in Figure 3.4.
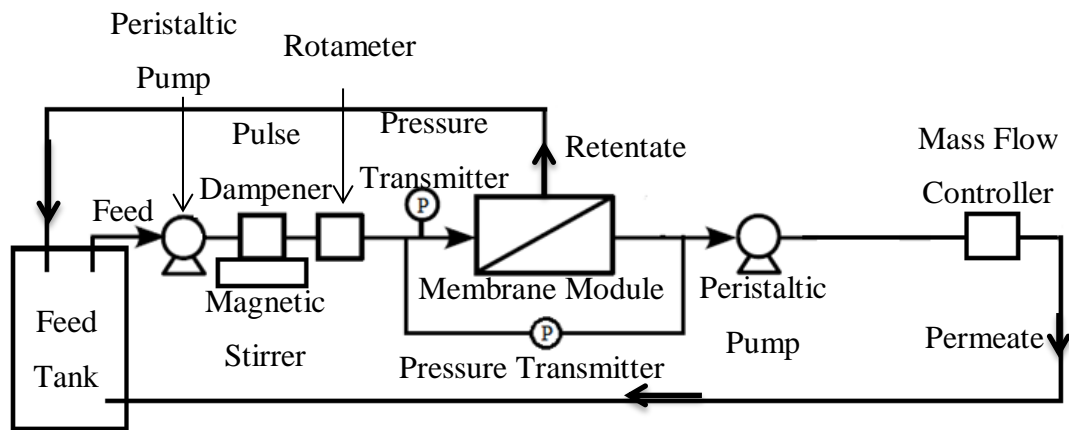
Figure 3. 4 Cross-flow filtration set-up.

In cross-flow filtration set-up, feed solution (ultrapure water or yeast solution) was pumped with cross-flow velocities 0.1 and 0.2 m/s via peristaltic pump. Since the rotameter was measuring the volumetric flow rate, cross flow velocity was calculated from following equation.

$$CFV = \frac{Q}{A}$$

Where,

Q is the volumetric flow rate read from rotameter and A is the area perpendicular to flow in membrane module. After cross-flow velocity was calculated, Reynolds number (Re) was computed.

$$Re = \frac{\rho v d_H}{\mu}$$

In this equation, ρ is the density of the feed stream, v is the cross flow velocity, d_H is the hydraulic diameter and μ is the feed viscosity. P and μ were taken as those of water. Hydraulic diameter was calculated as,

$$d_H = \frac{4A}{P}$$

A is the area perpendicular to flow and P is the wetted perimeter.

During the experiments, feed flux was controlled from the rotameter next to the pump. The pressure transmitters measured absolute feed pressure and pressure difference between feed and permeate streams which equals to trans-membrane pressure. Transmitters measured pressure in each seconds and logged the data on a computer. Permeate stream was connected to another peristaltic pump which can be managed by mass flow controller so that permeate flux could be fixed and also logged on a computer and change in pressure data was observed.

3.3.1 Membrane Pore Size and Effective Thickness Measurements

Membrane average pore size and thicknesses were measured from SEM images via ImageJ software. (App. B) In Figure 3.5, measurement of flat membrane thickness can be seen.
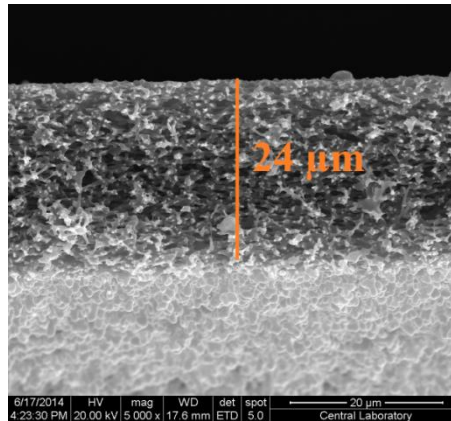
Figure 3. 5 SEM image of flat membrane with 10 minutes humid air exposure

On the other hand, the effective thickness of corrugated membrane was calculated differently. Effective thicknesses of the corrugated membranes were calculated from dividing cross sectional area to width of that area.
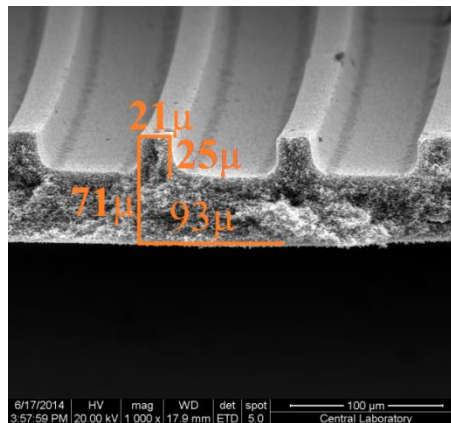
Figure 3. 6 SEM image of corrugated membrane with 10 minutes humid air exposure

$$Thickness = \frac{Cross - sectional\ area}{Width}$$

3.3.2 Pure Water Permeance Measurements

In pure water permeance experiments, ultrapure water (18.2 $\mu\Omega$.cm) was permeated with constant flux steps. Permeate fluxes were 20, 40 and 60 L/h.m^2. While calculating the permeate fluxes, the area enhancement due to corrugations were taken into consideration.

For each flux, permeation was done for 900 seconds and average of the 900 data taken was used. The pure water permeance of membranes at each flux was calculated from;

$$PWP = \frac{J}{TMP}$$

Where,

PWP is the pure water permeance, L/h.m^2.bar

J is the permeate flux, L/h.m^2

TMP is the trans-membrane pressure difference, bar

For each membrane and each cross-flow velocity, these experiments were done for two times. Average of measurements with error margins are given at the result part.

The permeability values were also calculated which equals to multiplication of permeance and effective membrane thicknesses.

$$Permeability = Permeance \times Effective\ Thickness$$

Moreover, the resistance of membrane was calculated with pressure data from the pure water permeabilities via Darcy's Law;

$$J = \frac{TMP}{\mu \times R_m}$$

Where, J is the permeate flux, TMP is the trans-membrane pressure, μ is the permeate stream viscosity and R_m is intrinsic membrane resistance.

3.3.3 Yeast Suspension Filtration Measurements

1 gram of saccharomyces cerevisiae (Dr. Oetker) particles was suspended in 1 liter of ultrapure water, without washing the yeast. During the experiment, stirring proceeded in order to have a homogeneous dispersion of yeast colloids in the suspension. Yeast suspension filtrations were done after pure water permeations so before filtration, membrane module was ejected from the set-up and the water in the set-up was poured by the help of peristaltic pumps. After that, yeast suspension was recirculated until no observable air bubble was existed. Then, membrane module was placed again and filtration started.

Yeast filtrations done with again 20,40 and 60 L/h.m^2 normalized permeate fluxes and each constant flux step lasted for 1800 seconds. After setting the cross-flow velocity from feed pump, two different softwares were used in these filtrations which were Dali08 and FlowPlot (Bronkhorst). FlowPlot gave the opportunity of remote control and observation of permeate fluxes while Dali08 showed the pressure values coming from transmitters. From pressure difference values between feed and permeate streams total resistances were calculated from Darcy's Law;

$$J = \frac{TMP}{\mu \times R_{tot}}$$

R_{tot} is the total resistance to flow and by substracting clean membrane resistances from total resistance values, fouling resistances were also calculated.

$$R_f = R_{tot} - R_m$$

After calculating fouling resistances, the fouling rates (dR/dt) for each flux were calculated as follows,

$$\frac{dR}{dt} = \frac{R_{ff} - R_{fi}}{\Delta t}$$

Rff means final fouling resistance, Rfi indicates initial fouling resistance and Δt was the time.

3.3.4 Membrane Morphology Observations

The morphologies of the membranes were observed by scanning electron microscopy (SEM) analysis (FEI Quanta-400 F) in METU central laboratory. For both corrugated and flat membranes, membrane thickness and for corrugated membranes dimensions of corrugations and distance between two corrugations were determined. Moreover, macrovoid and pore sizes, porosity and connectivity between pores were monitored which are all important for membrane performances.

The flat membrane cross section SEM images that were shown in this work had the mold sides on the bottom and the interface between non-solvent and polymer solution side on the top. However, in the corrugated membrane SEM images the mold sides were on the top as it can be seen in the Figure 3.7.
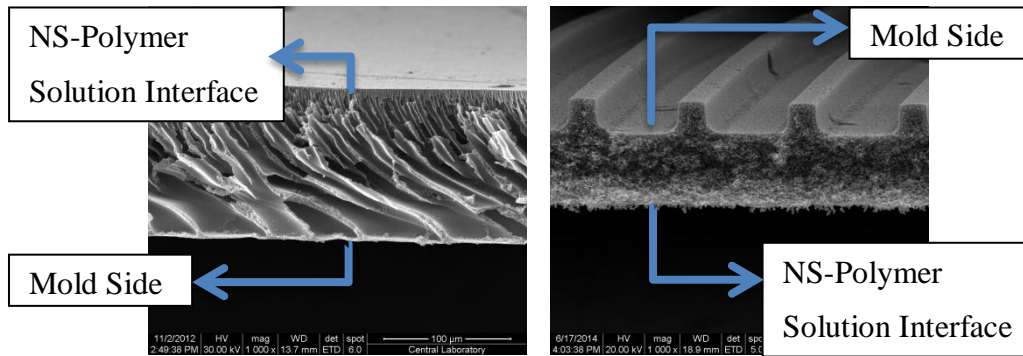
Figure 3. 7 Sides of the membranes in SEM images. a)Flat membrane b)Corrugated membrane

The SEM samples were prepared by breaking membranes in liquid nitrogen and placed vertically on a carbon tape for cross sectional view and horizontally for surface vew. In order to catch clear images samples were dried in a vacuum oven at room temperature for 24 hours. Before taking images, samples were coated with palladium/gold particles in order to have conductive layer. Images were taken with different magnifications from 250x to 200000x.

CHAPTER 4

RESULTS AND DISCUSSION

4.1 Membrane Morphology

In non-solvent induced phase separation processes, in the coagulation medium solvent diffuses out of the polymer solution and non-solvent diffuses in. During the coagulation process, increasing concentration of non-solvent makes casting solution move from one phase region to two phase, unstable region. After solution reaches binodal boundary, phase separation proceeds via nucleation and growth. The time solution spends in this meta-stable region determines the size of pores and structure. If polymer solution rapidly goes into unstable region after one phase region spinodal decomposition takes place and makes interconnected, bicontinuous structures. Since coagulation starts at the interface between solution and non-solvent, a finely porous skin layer is formed on top which acts as a barrier for further diffusion. This skin layer makes coagulation slower and provides more time for nuclei to grow below it. As a result, an asymmetric membrane with a relatively dense skin layer and a support layer which has larger pores below that skin layer is formed. In the Figure 4.1, an example of asymmetric membrane morphology is shown.
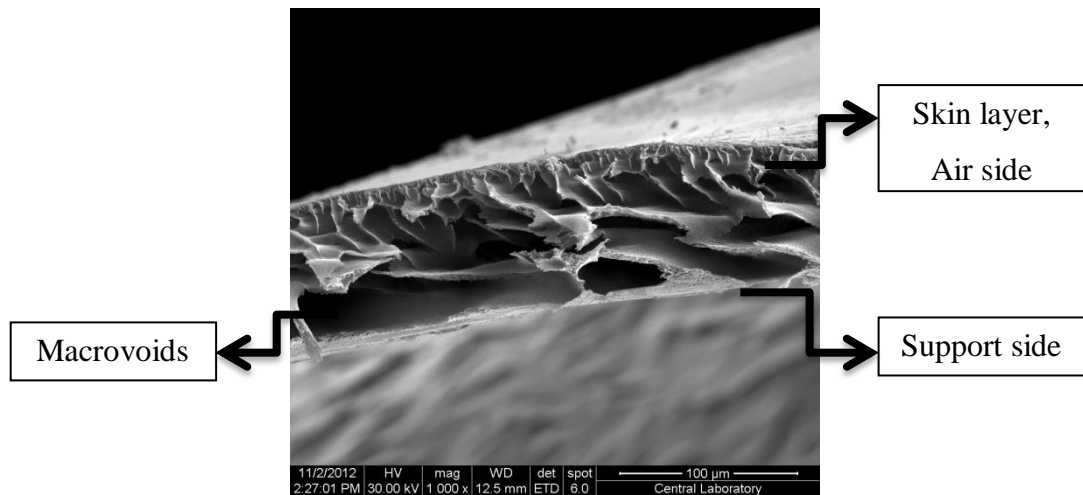
Figure 4. 1 Membrane made from 10% PES solution and directly coagulated in water bath.

The surface with skin layer is the selective layer which should be on the same side with corrugations that will face the feed solution, in order to affect the flow. However, since the interface between solution and non-solvent is on the opposite side of corrugations it is very tricky and in most cases not possible to form skin layer or start phase separation at the mold side so in our research a symmetric morphology without a skin layer was sought. In Figure 4.2 SEM image of a symmetric membrane can be seen. Symmetric morphology can generally be achieved when there is sufficient time for nucleation and growth. In order to slow down the phase separation and increase the time spent in metastable region to grow nuclei, some modifications were done on both precipitation conditions and casting solution.
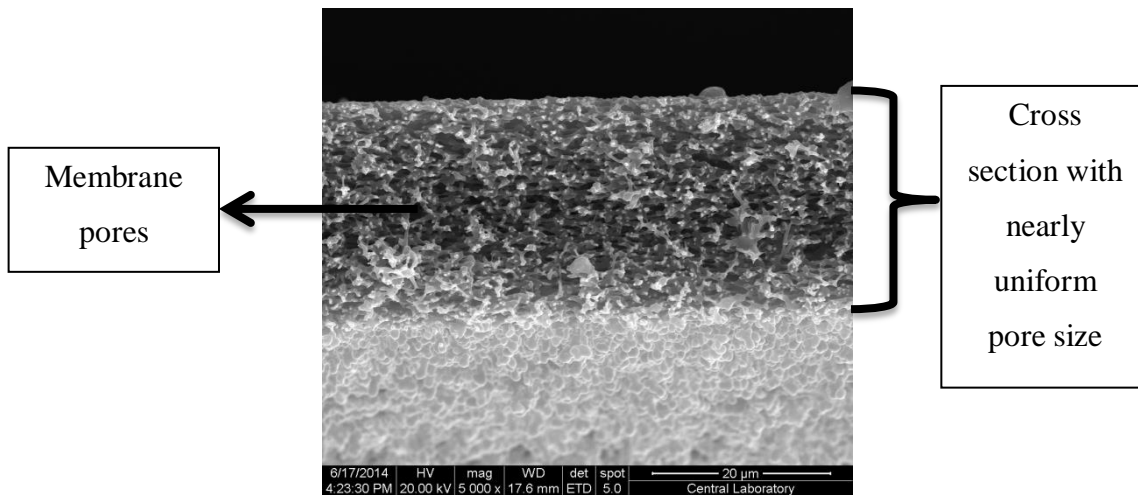
Figure 4. 2 PES (10% w/w) membrane with water (5% w/w) and PEG 400 (60% w/w) addition and exposed to humid air for 10 minutes.

Since corrugated membranes will be compared with flat ones and flat membranes are easier to prepare, modifications were used for flat membranes first and after desired morphology was achieved, they were tried on corrugated molds.

Before starting the effect of modifications on membrane morphologies, in Table 4.1 the effective thickness which is very important to calculate permeabilities of all membranes prepared in this work can be seen.

Table 4. 1 The thickness values of all membranes

Membrane Properties		Membrane Thickness
Polymer Solution	Coagulation Procedure	(μm)
10% PES 90% NMP	Directly Coagulated In Water at Room Temperature	85
10% PES 90% NMP	3 min Humid Air, Coagulated In Water at Room Temperature	110
10% PES 30% PEG 400 60% NMP	Directly Coagulated In Water at Room Temperature	117
10% PES 30% PEG 400 60% NMP	3 min Humid Air, Coagulated In Water at Room Temperature	139
10% PES 30% PEG 400 60% NMP	15 min Humid Air, Coagulated In Water at Room Temperature	107
10% PES 30% PEG 400 60% NMP	Coagulated In Water at 40 ^{o}C	85
10% PES 30% PEG 400 60% NMP	3 min Humid Air, Coagulated In Water at 40 ^{o}C	99

Table 4. 1(cont'd) The thickness values of all membranes

10% PES 30% PEG 400 60% NMP	10 min Humid Air, Coagulated In Water at 40 $^{\circ}$C	67
10% PES 30% PEG 400 60% NMP	15 min Humid Air, Coagulated In Water at 40 $^{\circ}$C	16
10% PES 30% PEG 400 60% NMP	20 min Humid Air, Coagulated In Water at 40 $^{\circ}$C	13
10% PES 60% PEG 400 30% NMP	3 min Humid Air, Coagulated In Water at Room Temperature	184
10% PES 60% PEG 400 30% NMP	10 min Humid Air, Coagulated In Water at Room Temperature	106
10% PES 60% PEG 400 30% NMP	15 min Humid Air, Coagulated In Water at Room Temperature	31
10% PES 30% PEG 400 60% NMP	Coagulated In Water at 70 $^{\circ}$C	73
10% PES 30% PEG 400 60% NMP	3 min Humid Air, Coagulated In Water at 70 $^{\circ}$C	78

Table 4. 1(cont'd) The thickness values of all membranes

10% PES 30% PEG 400 60% NMP	10 min Humid Air, Coagulated In Water at 70 ^{o}C	53
10% PES 30% PEG 400 60% NMP	15min Humid Air, Coagulated In Water at 70 ^{o}C	84
10% PES 60% PEG 400 5% Water 25% NMP	10 min Humid Air, Coagulated In Water at Room Temperature	24
10% PES 60% PEG 400 5% Water 25% NMP	15 min Humid Air, Coagulated In Water at Room Temperature	55
10%PES 30% PEG 400 60% NMP	10 min Humid Air, Coagulated In Water at Room Temperature	89
10%PES 30% PEG 400 60% NMP	20 min Humid Air, Coagulated In Water at Room Temperature	20
10% PES 30% PEG 400 60% NMP	20 min Humid Air, Coagulated In Water at 70 ^{o}C	74

Table 4. 1(cont'd) The thickness values of all membranes

10% PES 30% PEG 400 8% Water 52% NMP	10 min Humid Air, Coagulated In Water at Room Temperature	30
10% PES 30% PEG 6k 8 % Water 52% NMP	10 min Humid Air, Coagulated In Water at Room Temperature	36
10% PES 30% PEG 400 5% Water 55% NMP	10 min Humid Air, Coagulated In Water at Room Temperature	24
10% PES 30% PEG 400 8% Water 52% NMP	2 min NMP/Water Bath, Coagulated In Water at Room Temperature	41
10% PES 30% PEG 400 8% Water 52% NMP	2 min NMP/Water Bath, Coagulated In Water at Room Temperature	29
10% PES 60% PEG 400 5% Water 25% NMP	2 min NMP/Water Bath, Coagulated In Water at Room Temperature	149
10% PES 60% PEG 400 25% NMP	3 min Humid Air, Coagulated In Water at Room Temperature	181

Table 4. 1(cont'd) The thickness values of all membranes

10% PES 30% PEG 400 8% Water 52% NMP	10 min Humid Air, Coagulated In Water at Room Temperature	42
10% PES 60% PEG 400 5% Water 25% NMP (Corrugated)	15 min Humid Air, Coagulated In Water at Room Temperature	63*
10% PES 60% PEG 400 5% Water 25% NMP (Corrugated)	2 min NMP/Water Bath, Coagulated In Water at Room Temperature	99*
10% PES 30% PEG 400 60% NMP	3 min Humid Air, Coagulated In Water at Room Temperature	145
10% PES 30% PEG 6k 60% NMP	10 min Humid Air, Coagulated In Water at Room Temperature	65
10% PES 60% PEG 400, 5% Water 25% NMP (Corrugated)	5 min Humid Air, Coagulated In Water at Room Temperature	146*
10% PES 60% PEG 400, 5% Water 25% NMP (Corrugated)	10 min Humid Air, Coagulated In Water at Room Temperature	51*

*Effective thickness is reported for corrugated membranes as explained is section 3.3.1.

4.2 Modifications on Phase Separation Conditions

4.2.1 Effect of Humid Air Exposure

Liquid induced phase separation method creates relatively dense, selective skin layer at the interface of solution and non-solvent [2]. In order to mitigate the formation of this skin layer, a combination of vapor induced and liquid induced phase separation methodology was used. Casting solutions with different polymers and concentrations were exposed to humid air for 3, 10, 15 and 20 minutes before immersing into the water.

The reason behind asymmetric morphology is different phase inversion rates at different membrane parts. In liquid induced phase inversion method, because of rapid exchange of solvent and non-solvent, a relatively dense skin layer forms on the film surface while interior of the film is still far away from binodal point. However since the diffusion of water vapor will not cause a rapid exchange, entire membrane may precipitate at nearly same time which is expected to make membrane more symmetric [26].
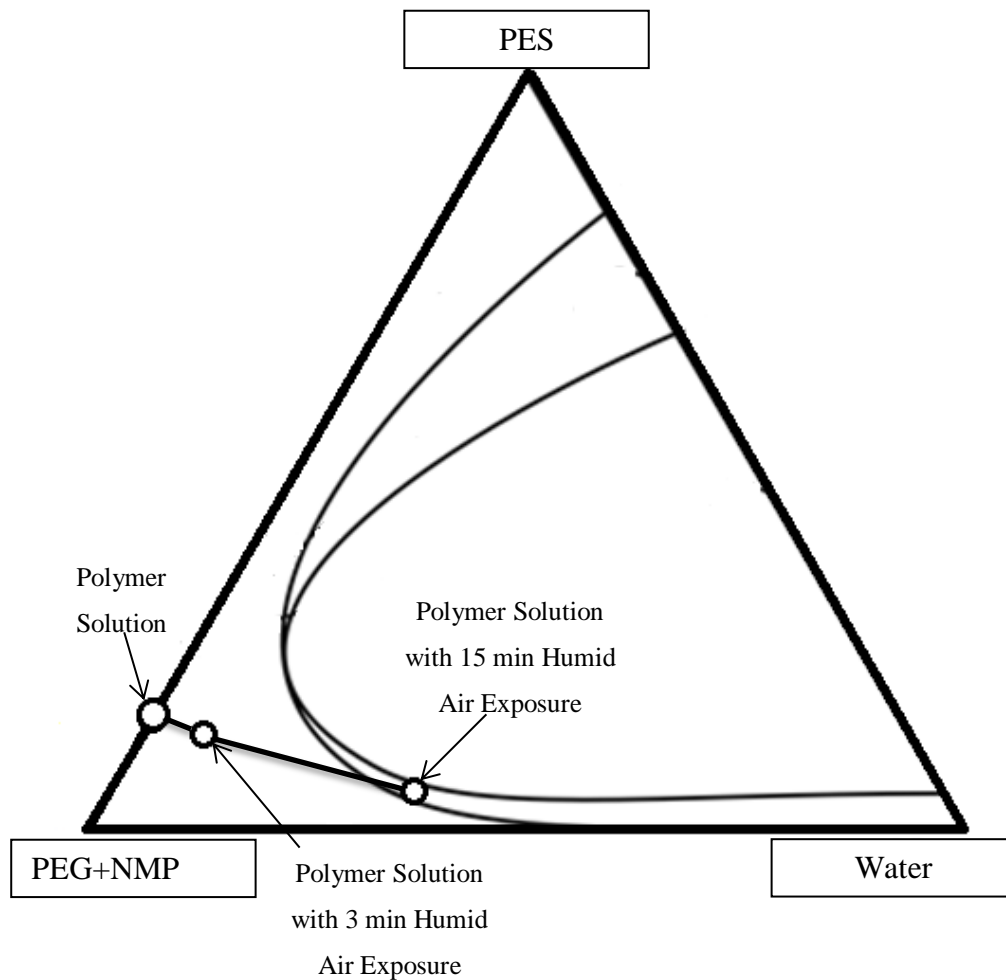
Figure 3. 8 Estimated locations of polymer solutions with or without humid air
exposure before coagulation in ternary phase diagram.

In ternary phase diagram, predicted locations and behaviours of phase separation of
pure polymer solution without precoagulation and the same solution with 3 and 15
minutes of humid air exposure as precoagulation treatments can be seen in the Figure
3.8.

The solution without any precogulation treatment will show a similar beginning
location and progress with the one in Figure 1.3. On the other hand, after 3 minutes
of humid air exposure it is expected that some water molecules will diffuse into the
solution and the concentrations of NMP, PEG and PES will decrease since there will

be no diffusion out. Humid air exposure for 3 minutes was not enough to make the polymer solution pass binodal curve. However, 15 minutes humid air exposure made polymer solution cloudy for almost all membranes which is a sign of precipitation, so the location of polymer solution which was exposed to humid air for 15 minutes should have passed the binodal curve. Solutions with water addition were also expected to be closer than the ones without water to binodal curve in the phase separation diagram, which is probably the reason why less humid air exposure is needed to reach the symmetric morphology.
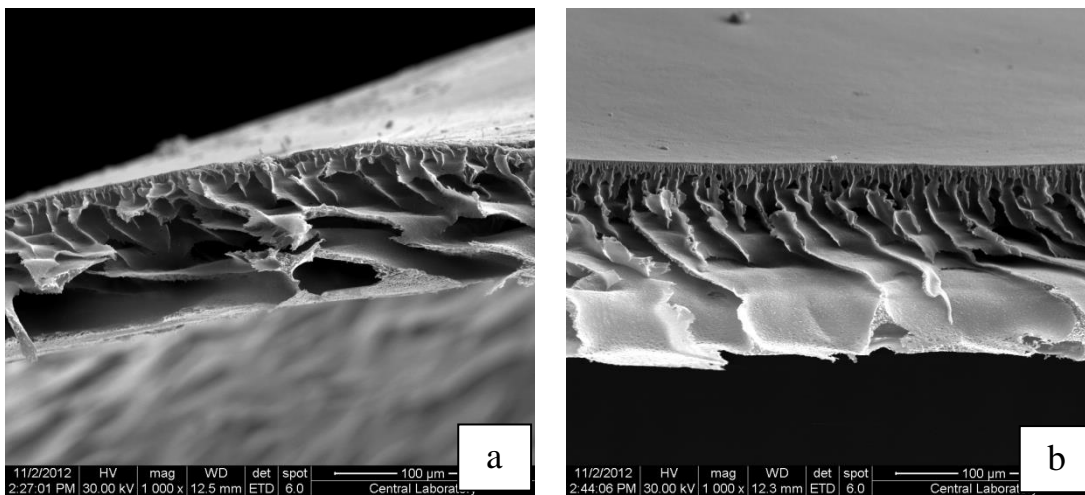
Figure 4. 3 Effect of humid air exposure for pure PES membranes a) No exposure b) 3 minutes exposure
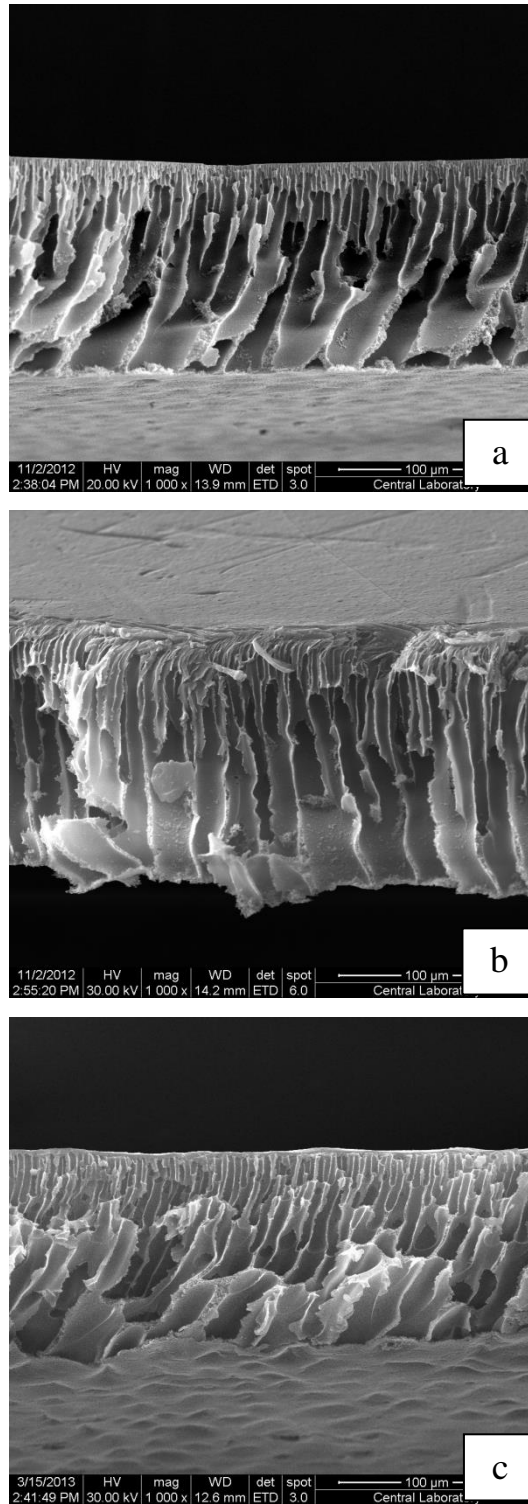
Figure 4. 4 Effect of humid air exposure for membranes with 30% PEG 400 addition
a) No exposure b) 3 minutes exposure c) 15 minutes exposure
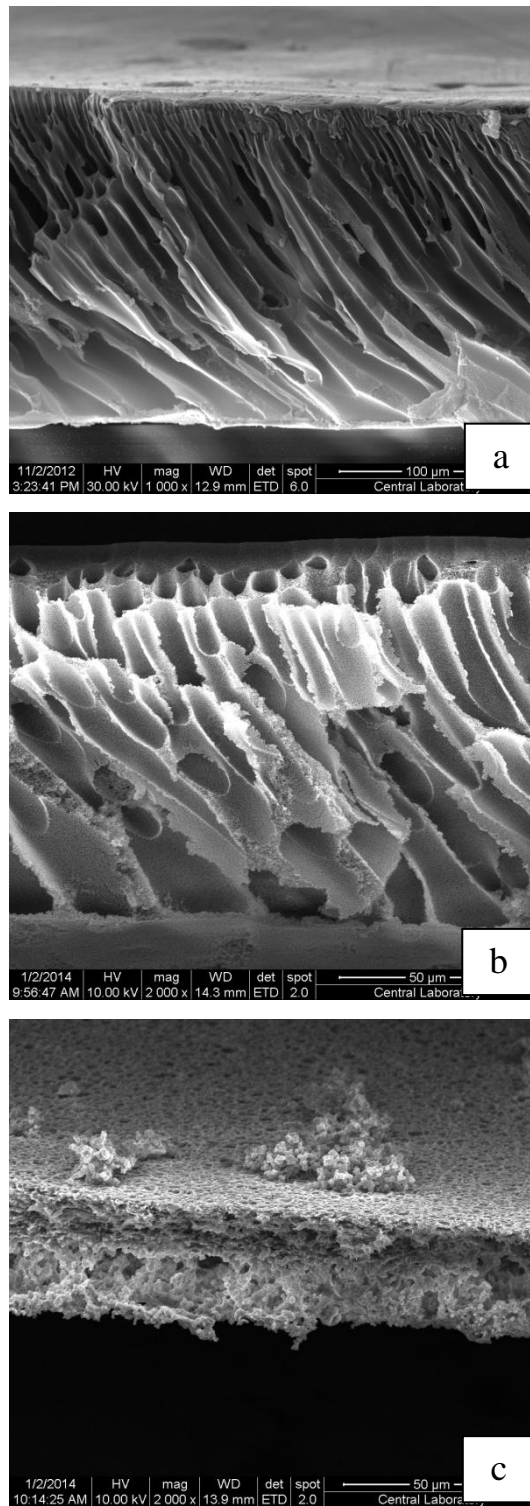
Figure 4. 5 Effect of humid air exposure for membranes with 60% PEG 400 addition. a) 3 minutes exposure b) 10 minutes exposure c) 15 minutes exposure
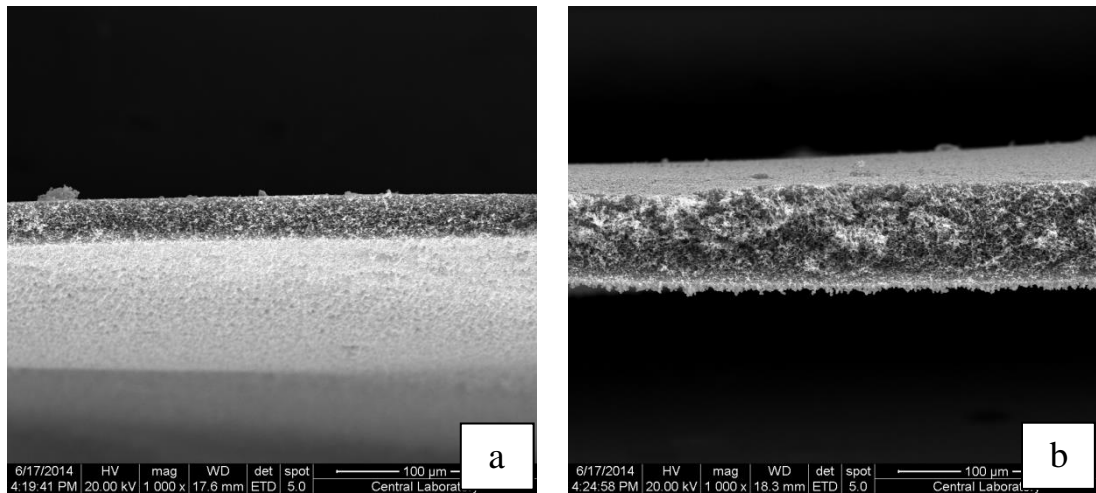
Figure 4. 6 Effect of humid air exposure for membranes with 60% PEG 400 and 5% water addition. a) 10 minutes exposure b) 15 minutes exposure

First of all, 3 minutes of humid air exposure did not change morphology for neither pure PES membrane nor membranes with PEG400 and water additives. Further increase in humid air exposure time still gave asymmetric structure for 30% PEG 400 added membrane. Asymmetric morphology changed into symmetric one when 60% PEG 400 added solution was exposed to humid air for 15 minutes as pre coagulation treatment. Moreover, for casting solution with 60% PEG 400 and 5% water, 10 minutes humid air exposure was enough to get a symmetric morphology. Another effect of humid air exposure was reduction in membrane thickness. Membrane thickness decreased by increasing humid air exposure.
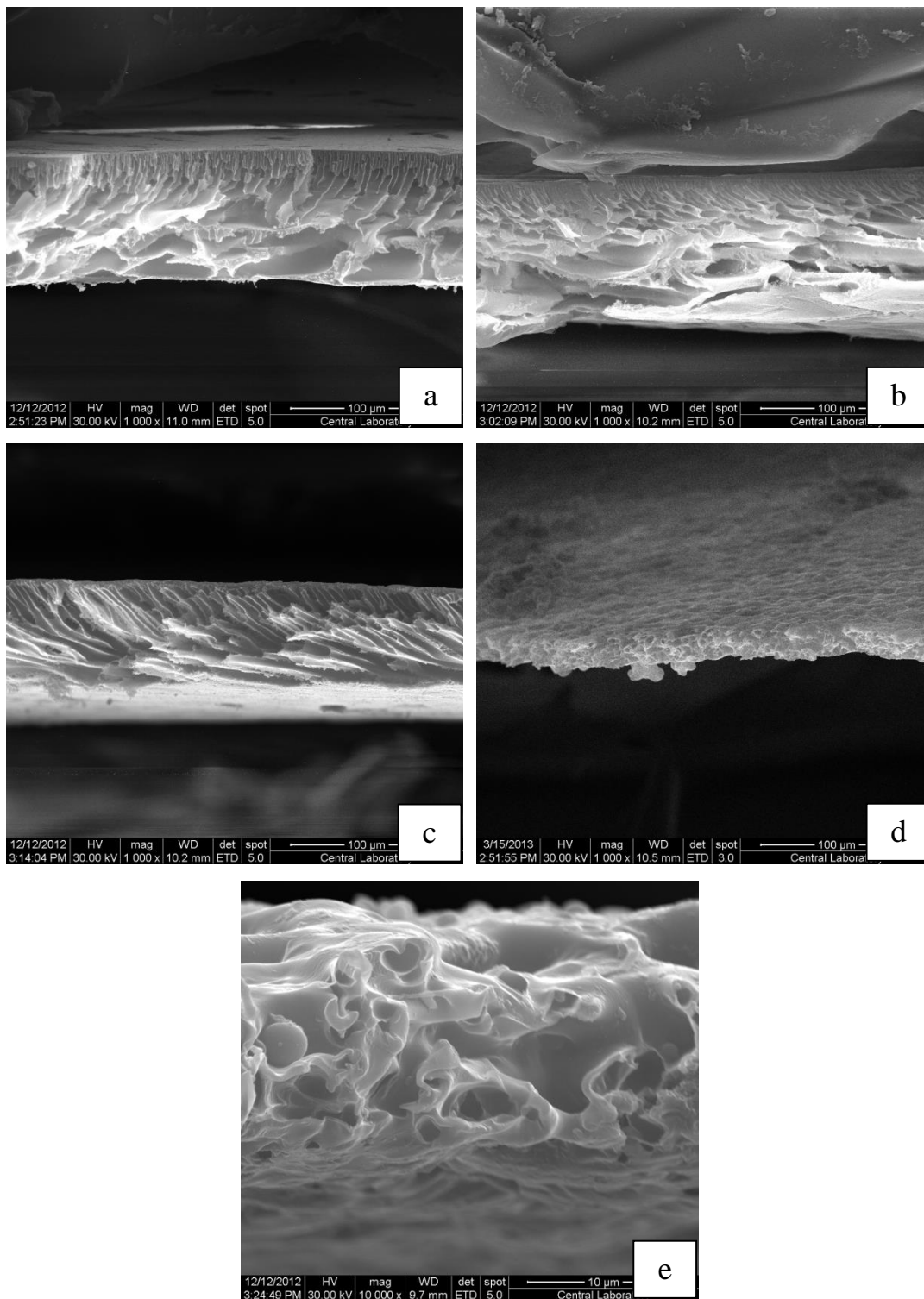
Figure 4. 7 Effect of humid air exposure for membranes with 30% PEG 400 addition and coagulated at 40 °C. a) No pre-coagulation b) 3 minutes exposure c) 10 minutes exposure d) 15 minutes exposure e) 20 minutes exposure
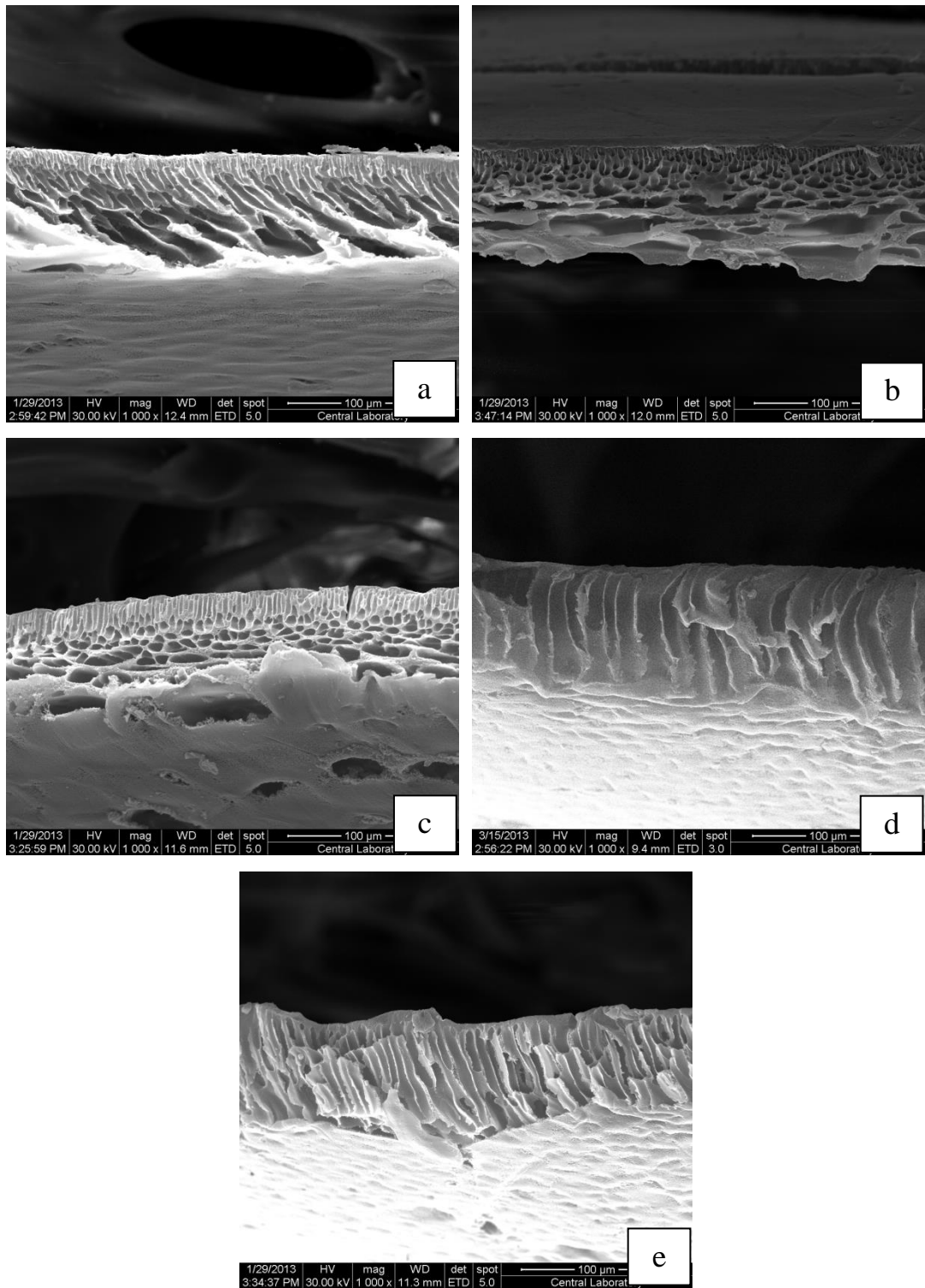
Figure 4. 8 Effect of humid air exposure for membranes with 30% PEG 400 addition and coagulated at 70 ^{o}C. a) No pre-coagulation b) 3 minutes exposure c) 10 minutes exposure d) 15 minutes exposure e) 20 minutes exposure

In the Figures 4.7 and 4.8, membranes with 30% PEG 400 added to their dope solutions were prepared with 40 ^{o}C and 70 ^{o}C coagulation bath and different humid air exposure times. Further exposure of humid air after 10 minutes also prevented formation of skin layer at coagulation temperature of 40 ^{o}C. Too much exposure of humid air changed membrane morphology totally. Membrane with 20 min humid air exposure and coagulated at 40 ^{o}C water has a different and impractical morphology for microfiltration with too big, unconnected pores. The closest structure to desired one was the membrane exposed to humid air for 15 minutes and coagulated at 40 ^{o}C. However it was too thin and still had quite large pores of 5 μm size.

4.2.2 Effect of Coagulation Bath Temperature

After humid air exposure effect, membrane morphology changes were observed with different coagulation bath temperatures which were room temperature, 40 ^{o}C and 70 ^{o}C. Since PEG 400 addition as weak non-solvent affected the morphology positively for a symmetric membrane, experiments started from casting solution with PEG 400 addition. In order to see both humid air and coagulation bath temperature at the same time, membranes coagulated at different temperatures after exposed to humid air for 3, 10, 15 and 20 minutes.
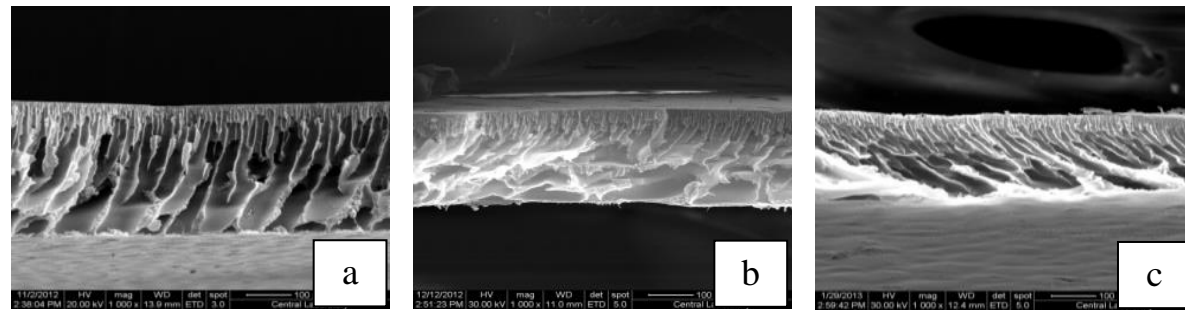
Figure 4. 9 Effect of coagulation bath temperature for membranes with 30% PEG 400 addition. a) Room temperature b) 40 ^{o}C c) 70 ^{o}C
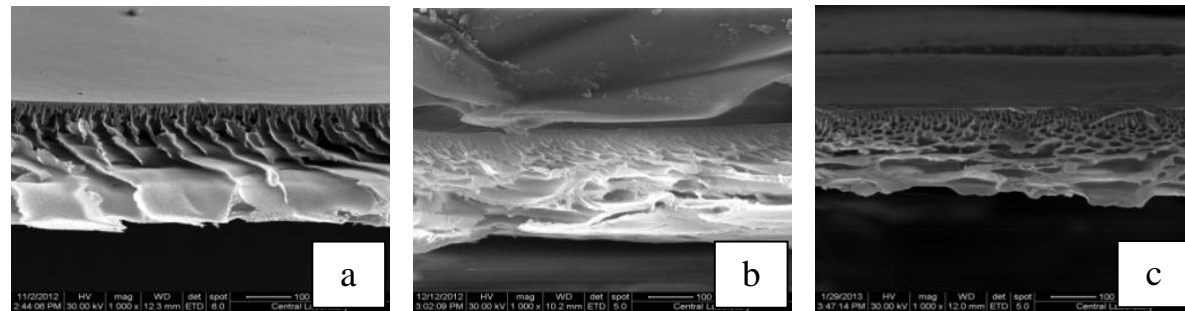
Figure 4. 10 Effect of coagulation bath temperature for membranes with 30% PEG 400 addition and 3 minutes humid air exposure. a) Room temperature b) 40 ^{o}C c) 70 ^{o}C
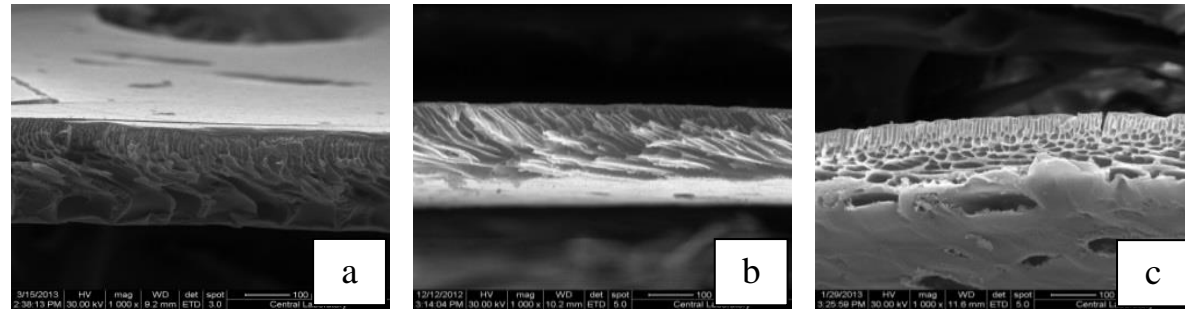
Figure 4. 11 Effect of coagulation bath temperature for membranes with 30% PEG 400 addition and 10 minutes humid air exposure. a) Room temperature b) 40 ^{o}C c) 70 ^{o}C
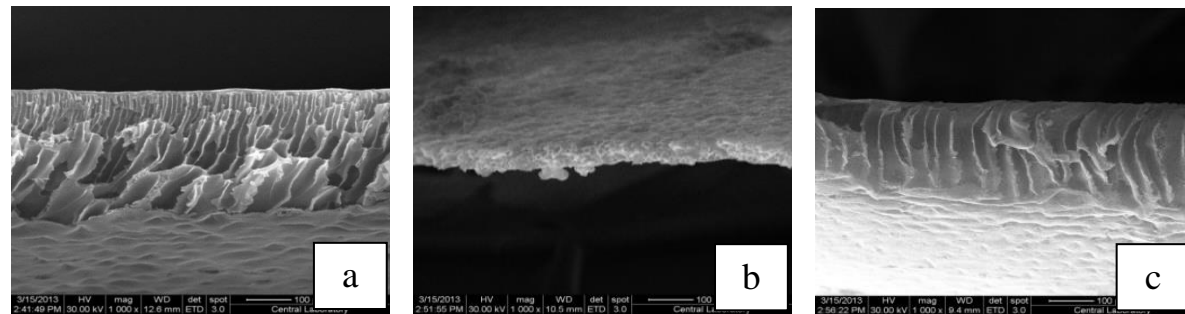
Figure 4. 12 Effect of coagulation bath temperature for membranes with 30% PEG 400 addition and 15 minutes humid air exposure. a) Room temperature b) 40 ^{o}C c) 70 ^{o}C
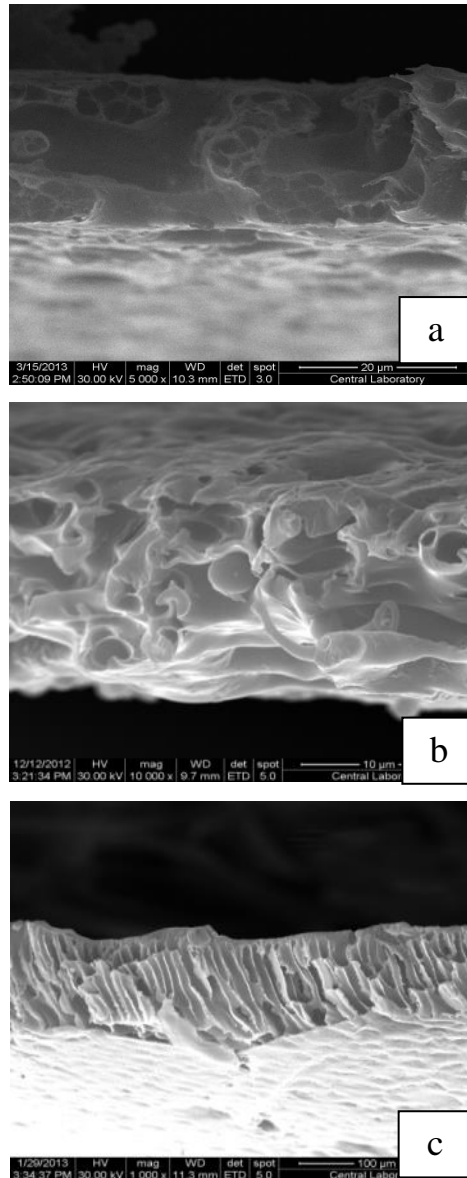
Figure 4. 13 Effect of coagulation bath temperature for membranes with 30% PEG
400 addition and 20 minutes humid air exposure. a) Room temperature
b) 40 ^{o}C c) 70 ^{o}C

The effect of coagulant temperature is considered to affect membrane formation via two ways;

- Speeding up phase inversion due to reduced solution viscosity and increased diffusivity

- Altering the phase diagram

Membranes without any pre-coagulation treatment showed nearly no difference on morphology when coagulation temperature was changed. Only observable change was decreasing in membrane thickness with increasing coagulant temperature. Thickness change was still observable for 3 and 10 minutes humid air exposed membranes and it can also be seen that, increasing coagulant temperature to 70 $^{\circ}$C changed macro voids shape from fingerlike to rounded. In addition, coagulation temperature did not prevent the formation of skin layer for membranes with no pre-coagulation step and exposed to humid air for 3 and 10 minutes.

Symmetric morphology of the membranes was seen for the membrane exposed to humid air for more than 15 minutes and coagulated at 40 $^{\circ}$C but not at 70 $^{\circ}$C. Moreover, although membranes exposed to humid air for 20 minutes seem symmetric with coagulants at room temperature and 40 $^{\circ}$C, they had large unconnected pores.

4.2.3 Effect of 75/25 (w/w) NMP/Water Bath Before Coagulation

In this work, a pre coagulation bath with 75/25 (w/w) NMP/water solution was also used and its effects on membrane morphology observed. The difference between 10 minutes humid air and 2 minutes NMP/water solution as pre coagulation treatments can be seen in the Figures 4.14-4.16.
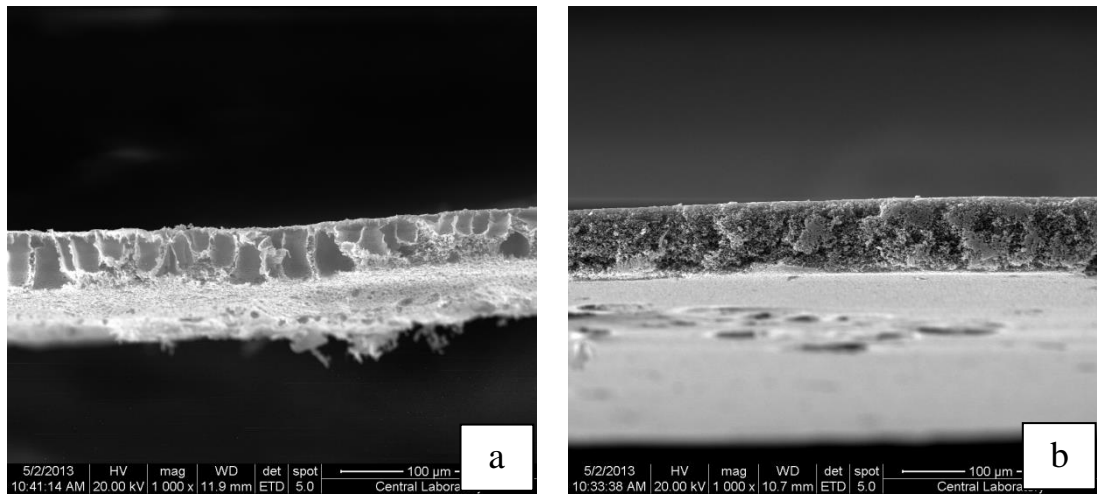
Figure 4. 14 Effect of different pre-coagulation treatments for membranes with 30% PEG 400 and 8% water addition. a) 10 minutes humid air exposure b) 2 minutes NMP/water bath
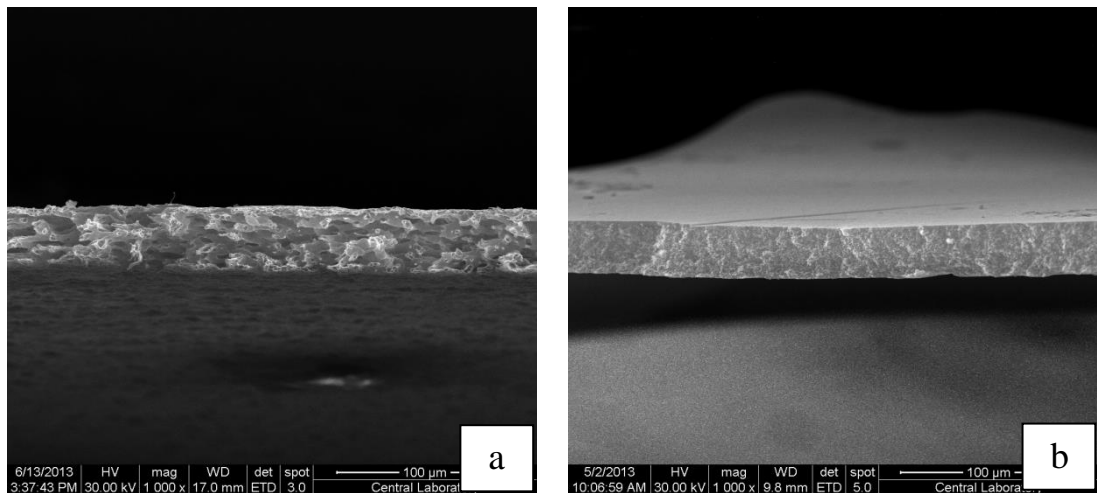
Figure 4. 15 Effect of different pre-coagulation treatments for membranes with 30% PEG 6k and 8% water addition. a) 10 minutes humid air exposure b) 2 minutes NMP/water bath
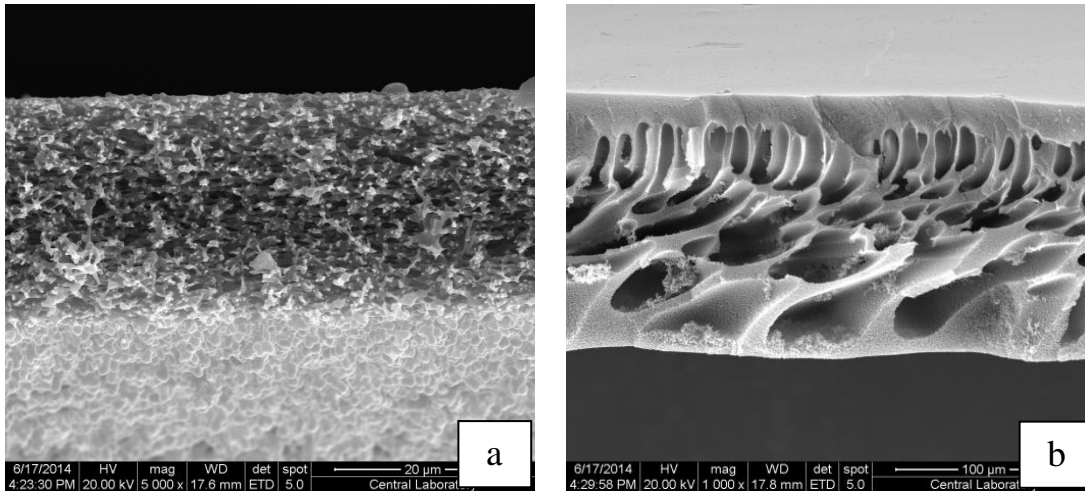
Figure 4. 16 Effect of different pre-coagulation treatments for membranes with 60% PEG 400 and 5% water addition. a) 10 minutes humid air exposure b) 2 minutes NMP/water bath

From Figure 4.14 it is seen that 10 minutes of humid air could not mitigate macro void formation with 10% PES, 30% PEG 400, 8% water and 52% NMP solution. However, neither humid air exposed nor NMP/water bath immersed membrane has an observable skin layer. Pore sizes on both sides of the membrane in Figure 4.14a were of similar sizes. For membranes with 30% PEG 6k and 8% water addition, both pretreatments resulted in elimination of macrovoids. The difference is membrane thickness and the pore size. The one with 10 minutes humid air exposure had an average pore size of nearly 3 µm and they were not connected very well to each other. Thickness of this membrane was 35 µm. On the other hand, membrane with NMP/water treatment was thinner (28 µm) and had smaller pores than 1 µm. Fig. 4.16 shows a comparison for humid air exposure and NMP/water bath for membranes with 60% PEG 400 and 5% water addition. Although, humid air gave a desired symmetric morphology, NMP/water bath still had thicker, asymmetric morphology with macrovoids and a skin layer. The reason behind this difference in behavior of humid air and NMP/water bath treatments with solution composition can

58

be due to the change of the beginning location of polymer solution composition in ternary phase diagram.

4.3 Modifications on Casting Solution

4.3.1 Effect of PEG 400 addition

The membrane cast from 10% PES and 90% NMP solution and without any pre-coagulation treatment immersed into water bath for coagulation had asymmetric morphology. In Figure 4.17 the effect of adding 30% PEG 400 to casting solution and directly immersing into coagulation medium is shown.
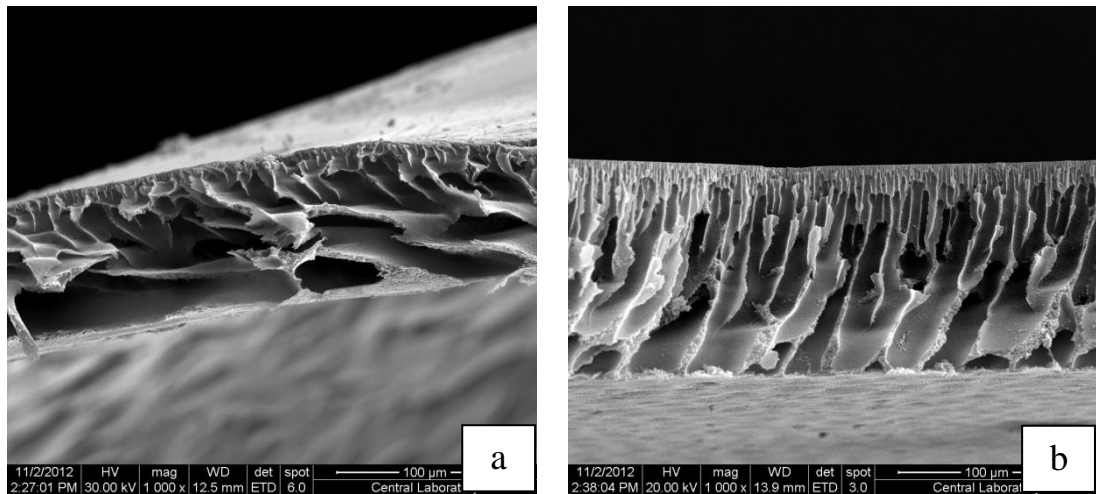
Figure 4. 17 Effect of PEG 400 addition on membranes without any pre coagulation treatment. a) Without PEG 400 addition b) 30% (w/w) PEG 400 is added.

From the Figure 4.17 it is observed that 30% PEG 400 addition did not alter the membrane morphology from asymmetric to symmetric. However, it can be said that PEG 400 partly supressed macrovoid formation and reduced the volume of macrovoids. Macrovoids are often seen in membranes with asymmetric morphology. Since supressing macrovoids can be a sign of approaching to symmetric morphology [7]., PEG addition was further investigated and we worked on membranes that have

60% (w/w) PEG 400 in their solution also. 60% PEG 400 was added to membranes that were exposed to humid air before coagulation which led to a morphology with thinner skin layer and narrower macrovoids in the literature [17].
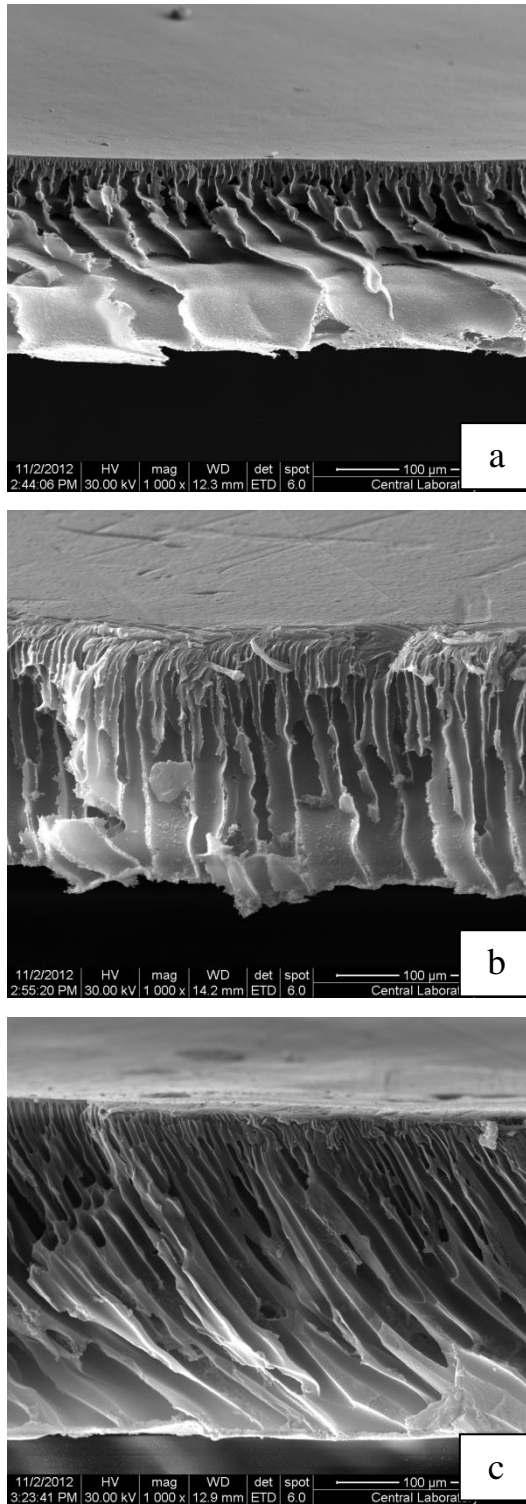
Figure 4. 18 Effect of further PEG 400 addition for 3 minutes humid air exposed
membranes. a) Pure PES membrane b) 30% PEG addition c) 60% PEG addition
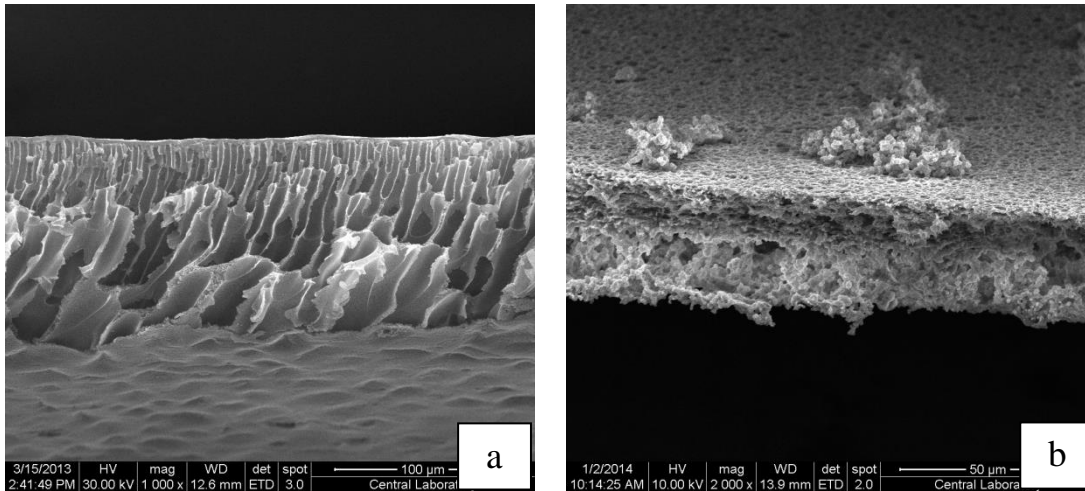
Figure 4. 19 Effect of further PEG 400 addition for 15 minutes humid air exposed membranes. a) 30% PEG addition b) 60% PEG addition

Membranes with humid air exposure for 3 minutes have lower macrovoid volumes with increasing PEG 400 concentration in the solution. However, they still have asymmetric morphologies. On the other hand, combination of 15 minutes humid air exposure and 60% (w/w) PEG 400 addition resulted in symmetric morphology without any observable macrovoids.

4.3.2 Effect of PEG's Molecular Weight

Addition of PEG into polymer solution increases viscosity and viscosity depends of molecular weight of PEG also. The higher the molecular weight of PEG, the higher the solution viscosity. Increase in solution viscosity means lower diffusivity of non-solvent in the casting solution. This situation hinders phase separation kinetics [27].
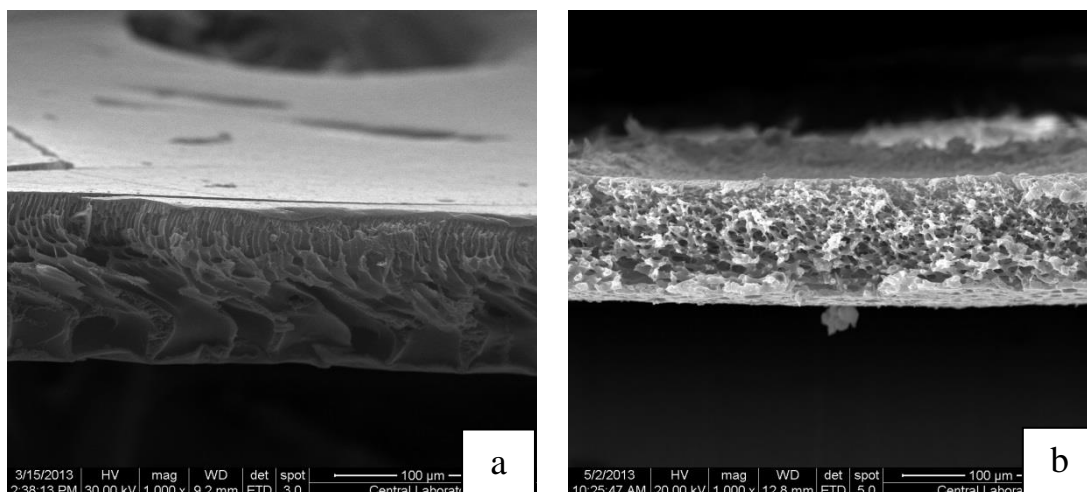
Figure 4. 20 Effect of PEG molecular weight for 10 minutes humid air exposed membranes. a) 30% PEG 400 addition b) 30% PEG 6k addition

From Figure 4.20 , it is seen that, PEG 6k added solution became symmetric with 10 minutes humid air exposure. However, PEG 400 added solution still gave an asymmetric morphology with macrovoids.

4.3.3 Effect of Water Addition

Nonsolvent addition into polymer solution also affects phase separation by make the starting solution nearer to binodal boundary. Starting phase separation from somewhere near binodal boundary typically increases the porosity and decreases the skin layer thickness [28]. In experiments, at most 8% (w/w) water was used in dope solution in order not to start precipitation before casting. Effect of water addition can be seen in Figure 4.21 for 30% and 60% (w/w) PEG 400 added solutions exposed to humid air for 10 minutes, 30% PEG 6k added exposed solutions to humid air for 10 minutes and 30% PEG 6k added solution immersed into 75% NMP / 25% Water (w/w) solution for 2 minutes membranes.

8 % H₂O → ... 5 % H₂O →
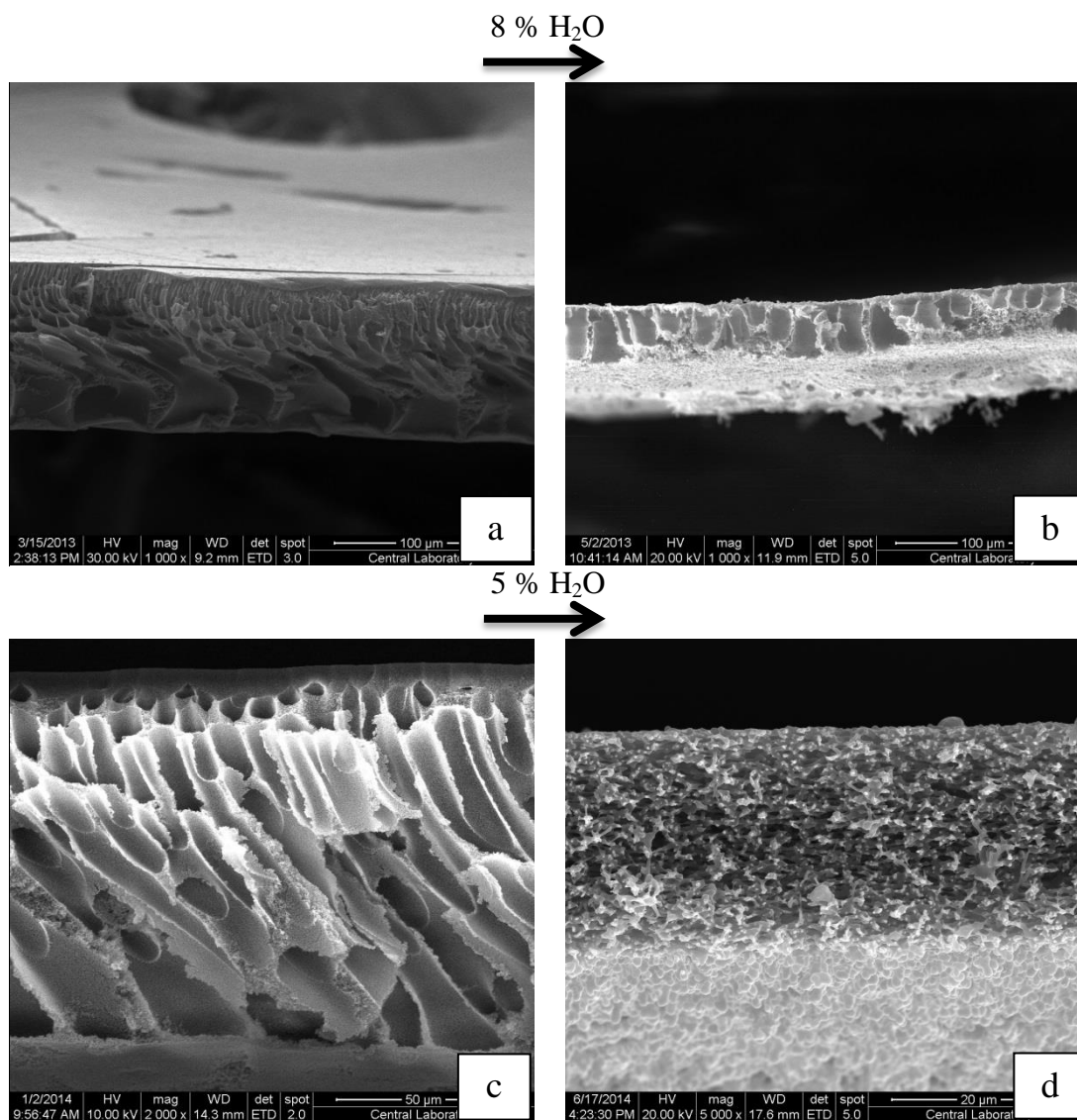
Figure 4. 21 Effect of water addition a) 30% PEG 400 addition, 10 minutes of humid air exposure b) 8% water, 30% PEG 400 addition, 10 minutes of humid air exposure c) 60% PEG 400 addition, 10 minutes of humid air exposure d) 5% water, 60% PEG 400 addition, 10 minutes of humid air exposure e) 30% PEG 6k addition, 10 minutes of humid air exposure f) 8% water, 30% PEG 6k addition, 10 minutes of humid air exposure g) 30% PEG 6k addition, 2 minutes of NMP/Water bath h) 8% water, 30% PEG 6k addition, 2 minutes of NMP/Water bath

8 % H$_2$O

8 % H$_2$O
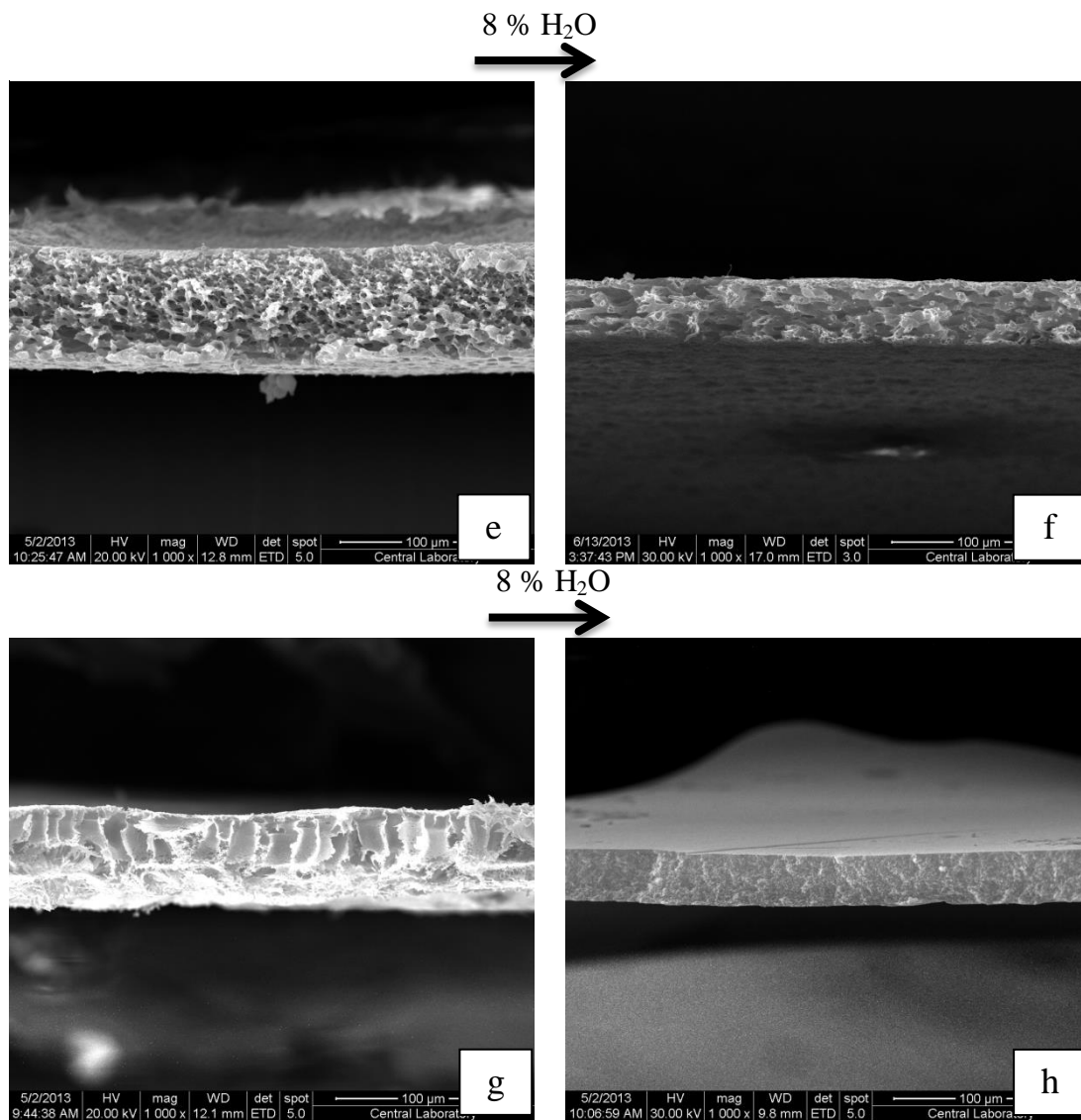
Figure 4. 21 (cont'd) Effect of water addition a) 30% PEG 400 addition, 10 minutes of humid air exposure b) 8% water, 30% PEG 400 addition, 10 minutes of humid air exposure c) 60% PEG 400 addition, 10 minutes of humid air exposure d) 5% water, 60% PEG 400 addition, 10 minutes of humid air exposure e) 30% PEG 6k addition, 10 minutes of humid air exposure f) 8% water, 30% PEG 6k addition, 10 minutes of humid air exposure g) 30% PEG 6k addition, 2 minutes of NMP/Water bath h) 8% water, 30% PEG 6k addition, 2 minutes of NMP/Water bath

Because of cloud point limitation at most 8% water could be added to solution and without any exception, addition of water to the dope solution made all membranes more symmetric and suppressed macro void formation significantly. The only membrane that still had macro voids in spite of water addition is the one with 30% PEG 400 addition and 10 minutes humid air exposed. The thickness of all membranes was reduced by addition of non-solvent into casting solution.

4.4 Membrane Selection

After modifying casting solution and precipitation conditions, several membranes with symmetric morphology were obtained. In the table below, the comparison of symmetric membranes is shown with respect to morphology, casting solution, preparation conditions and average pore diameters.

Table 4. 2 Comparison of the membranes with symmetric morphology.

Solution (w/w) %	PreCoagulation	Average Pore Diameter	Morphology
PES 10 PEG400 60 H$_2$O 5 NMP 25	Humid Air Exposure for 10 minutes	1.3±0.3 μm	
PES 10 PEG400 60 NMP 30	Humid Air Exposure for 15 minutes	1.2±0.4 μm	
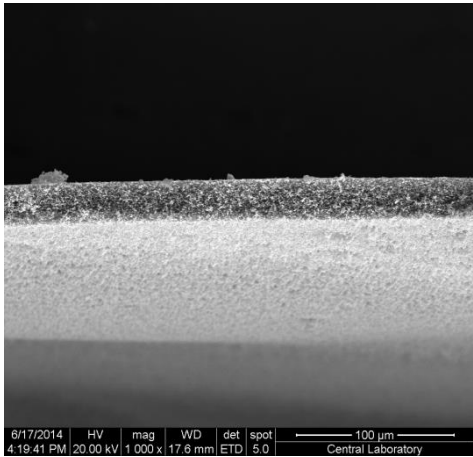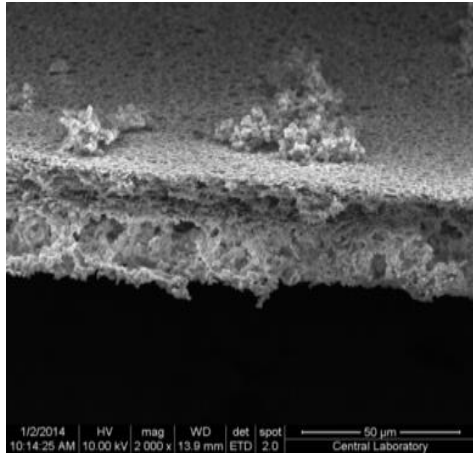
Table 4. 2(cont'd) Comparison of the membranes with symmetric morphology.

PES 10 PEG6k 30 NMP 60	Humid Air Exposure for 10 minutes	3.7±0.4 µm	
PES 10 PEG6k 30 H₂O 8 NMP 52	NMP/water Bath for 2 minutes	0.15±0.7 µm	
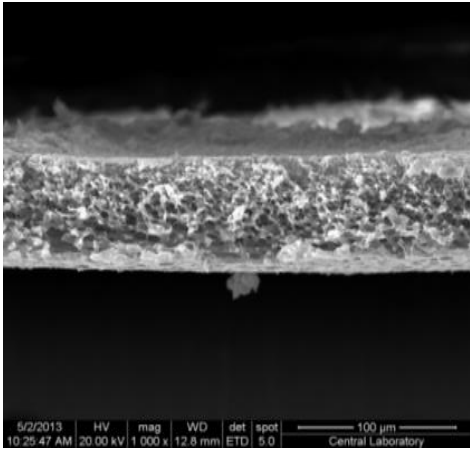
Table 4. 2(cont'd) Comparison of the membranes with symmetric morphology.

PES 10 PEG400 30 H$_2$O 8 NMP 52	NMP/water Bath for 2 minutes	0.25±0.1 µm	
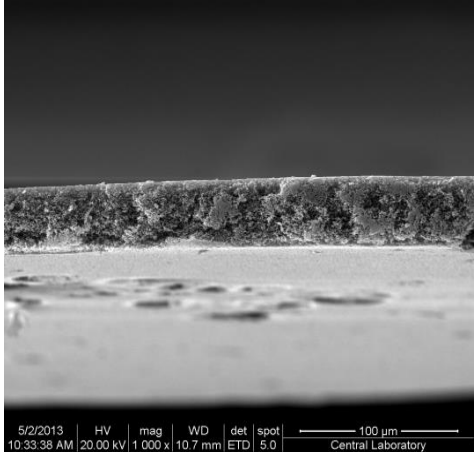
The symmetric membranes that were prepared in this work can be seen in Table 4.2. The chosen recipe was 10 wt% PES, 60 wt% PEG 400, 5 wt% water and 25 wt% NMP with 10 minutes humid air exposure which resulted in an average pore diameter of 1.3±0.3 µm. Membrane with 60% PEG 400 addition and 15 minutes humid air exposure had the closest structure to the chosen one with 1.2±0.4 µm average pore size. However, increase in humid air exposure time was not preferred it increases shrinkage. Membrane that have 30% PEG 6k and again 10 minutes of humid air exposure had slight asymmetry with nearly 2.8 µm pores on solution - non-solvent interface and 4.8 µm pores on the mold side which was undesired. Symmetric membranes with NMP/water pre-coagulation bath had smaller pore sizes than others. Moreover, since solutions with both PEG 6k and water addition needed to heat up before casting which causes evaporation of water to some extent, these solutions were not preferable.

4.5 Corrugated (Patterned) Membranes

Corrugated membranes were started to be cast on a silicon wafer with chosen polymer solution (10% PES, 60% PEG 400, 5% H_2O, 25% NMP), different humid air exposure times and NMP/water solution as pre-coagulation treatment. The morphologies can be observed from SEM images in Table 4.3 and 4.4.

Table 4. 3 Cross section and surface morphologies of corrugated membranes

PreCoagulation Treatment	Cross Section Image
Humid Air Exposure for 5 Minutes	
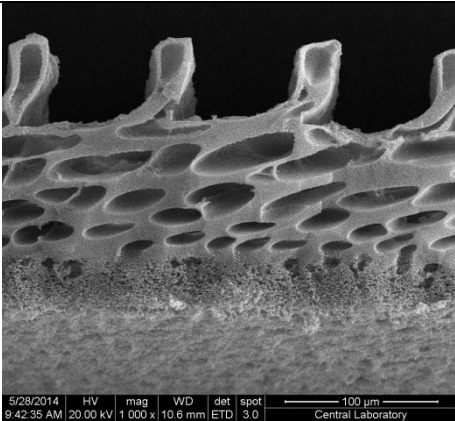
Table 4. 3(cont'd) Cross section and surface morphologies of corrugated membranes
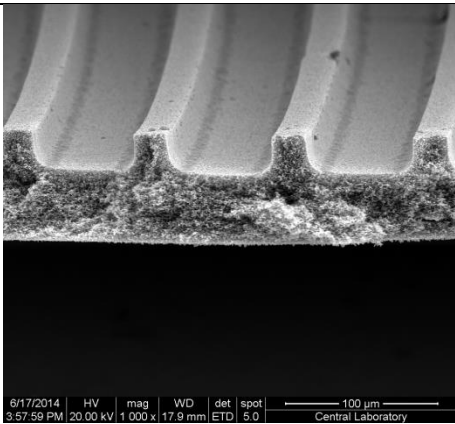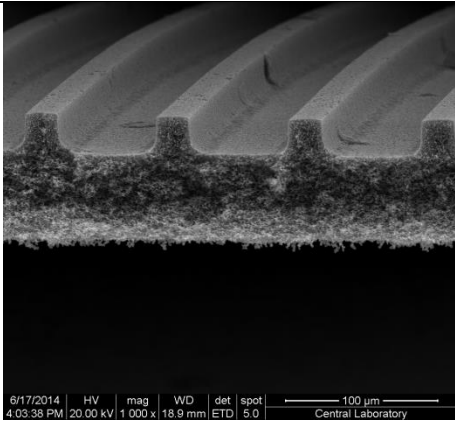
Humid Air Exposure for 10 Minutes	
Humid Air Exposure for 15 Minutes	
NMP/Water Bath Immersion for 2 Minutes	
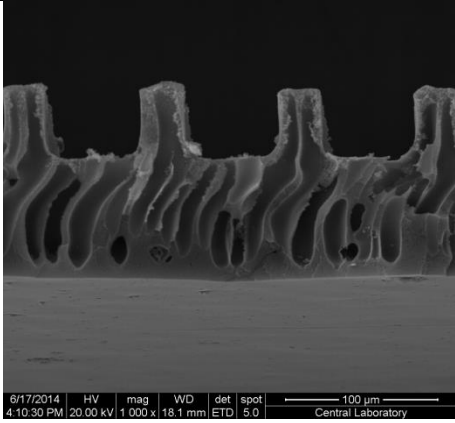
Table 4. 4 SEM images of membrane corrugations and membrane surfaces near corrugations.

PreCoagulation Treatment	Corrugated Surface Image	Non-Corrugated Surface Image
Humid Air Exposure for 5 Minutes		
Humid Air Exposure for 10 Minutes		
Humid Air Exposure for 15 Minutes		
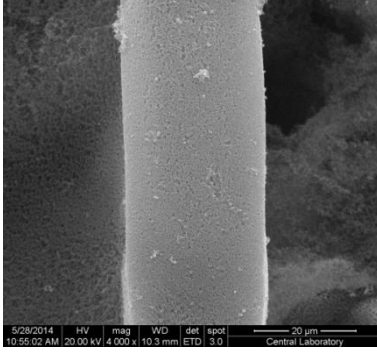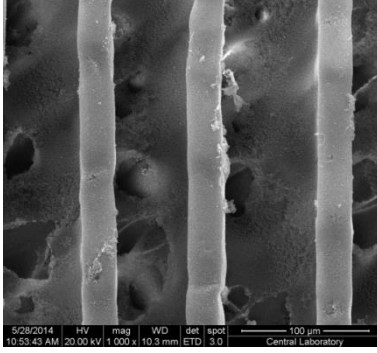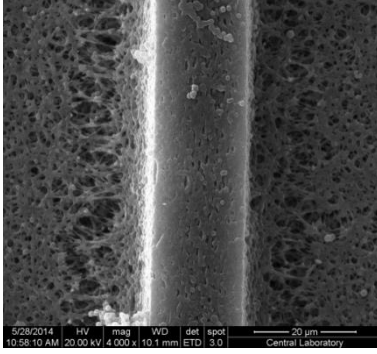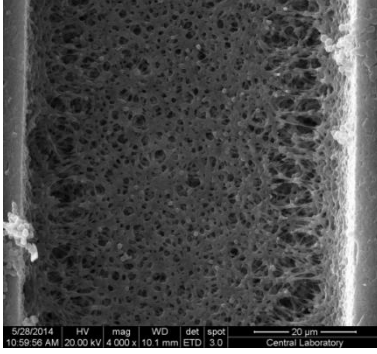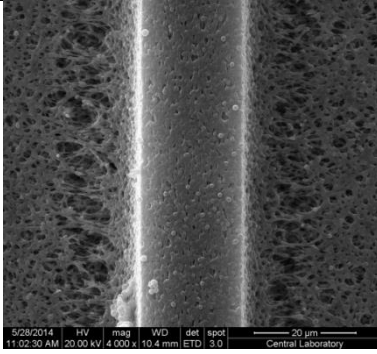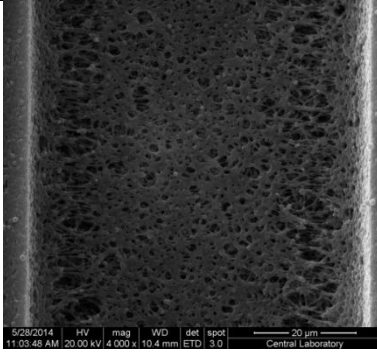
Table 4. 4(cont'd) SEM images of membrane corrugations and membrane surfaces near corrugations.

NMP/Water Bath Immersion for 2 Minutes		

Table 4. 5 Cross section and surface morphologies of flat membranes made with the same recipe as corrugated membranes in Tables 4.3 and 4.4.

PreCoagulation Treatment	Cross Section Image	Surface Image
Humid Air Exposure for 5 Minutes		
Humid Air Exposure for 10 Minutes		

Table 4. 5(cont'd) Cross section and surface morphologies of flat membranes made with the same recipe as corrugated membranes in Tables 4.3.and 4.4.
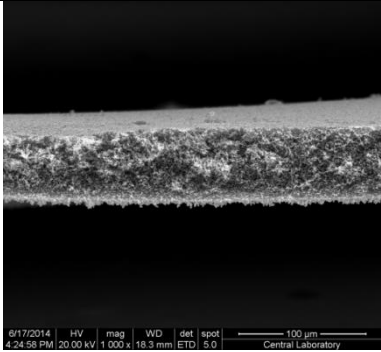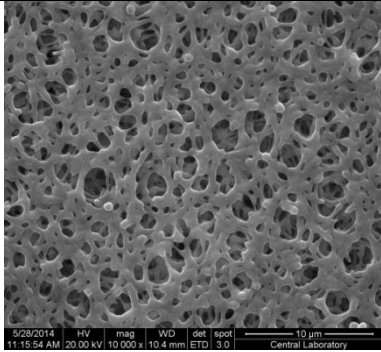
Humid Air Exposure for 15 Minutes		
NMP/Water Bath Immersion for 2 Minutes		
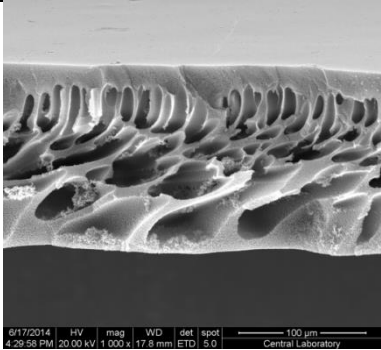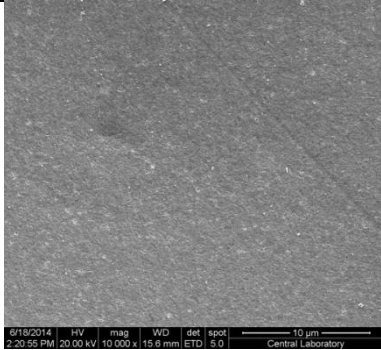
From the SEM images in Table 4.3 and 4.4, it is seen that there is nearly no difference between the morphologies of membranes exposed to humid air for 10 and 15 minutes. These membranes have symmetric structures as the flat ones with same conditions and solution which can be seen in the Table 4.5.

On the other hand, 5 minutes humid air exposed corrugated membrane had an exceptional asymmetric morphology. Typically, an asymmetric membrane has smaller pores at the solution, non-solvent interface and pores become larger by moving away from it. However from the Table 4.3 it is seen that, this membrane had somewhat smaller pores (nearly 1 µm) at the mold side and larger pores (nearly 1.8 µm) at the interface which made it applicable for filtration.

Table 4.3 shows NMP/water bath immersion made an asymmetric corrugated membrane with macro voids and large cavities on the sides of corrugations. Since this morphology was like typical asymmetric membrane morphology with smaller pores on the mold side, it was not used in the filtration process.

Figure 4.22 and Table 4.6 show the dimensions of corrugated membranes.
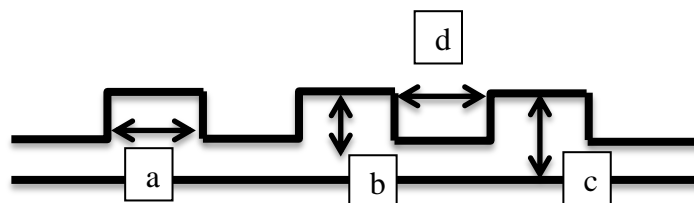
Figure 4. 22 Schematic of corrugated membrane dimensions. a) Corrugation width b)Corrugation height c) Total thickness d) Distance between corrugations

Table 4. 6 Corrugated membrane dimensions.

PreCoagulation Treatment	Corrugation Width (a) µm	Corrugation Height (b) µm	Total Thickness (c) µm	Distance Between Corrugations (d) µm
Humid Air Exposure for 5 Minutes	25	47	170	71
Humid Air Exposure for 10 Minutes	20	21	72	71
Humid Air Exposure for 15 Minutes	20	21	74	66

Table 4. 6(cont'd) Corrugated membrane dimensions.

NMP/Water Bath Immersion for 2 Minutes	27	49	123	61

Table 4.6 shows that humid air exposure time directly affects the membrane thickness. Increasing humid air exposure time from 5 minutes to 15 minutes made membrane thinner. While membrane with 5 minutes humid air exposure was 170 µm, thickness of the membrane ,which was exposed to humid air for 15 minutes, was 74 µm. Both membranes with higher thickness values (2 minutes NMP/water immersed and 5 minutes humid air exposed) had macrovoids on their morphology. In the literature, it was observed that decreasing membrane thickness supresses macro void formation [29,30]. Height fidelity for corrugations was much higher for 5 minutes humid air exposure and 2 minutes NMP/water immersion pre coagulation treatments. Corrugation width and distance between corrugations were similar irrespective of the precoagulation treatment type.

To sum up, recipes chosen from flat membrane experiments could be successfully applied on corrugated molds. The only exception was the membrane with 5 minutes humid air exposure. For the flat one there was a symmetric morphology without macrovoids while the corrugated one had an asymmetric morphology and macrovoids. However the asymmetric membrane had somewhat smaller pores on the mold side and therefore could be used in yeast filtrations. Other recipes gave the same results for both flat and corrugated membranes. For 10 minutes and 15 minutes of humid air exposed ones gave symmetric morphology while NMP/water bath made asymmetric membranes with macrovoids for both flat and corrugated membranes.

4.6 Membrane Fouling Measurements

In this work, cross-flow filtration of 1g/L yeast suspension was done in order to observe fouling characteristics of flat and corrugated membranes. Before yeast suspension, ultrapure water was permeated and intrinsic resistance of the membrane and pure water permeance were calculated. These flux-stepping experiments were made with 20, 40 and 60 L/h.m^2 fluxes and 0.1 and 0.2 m/s cross-flow velocities.
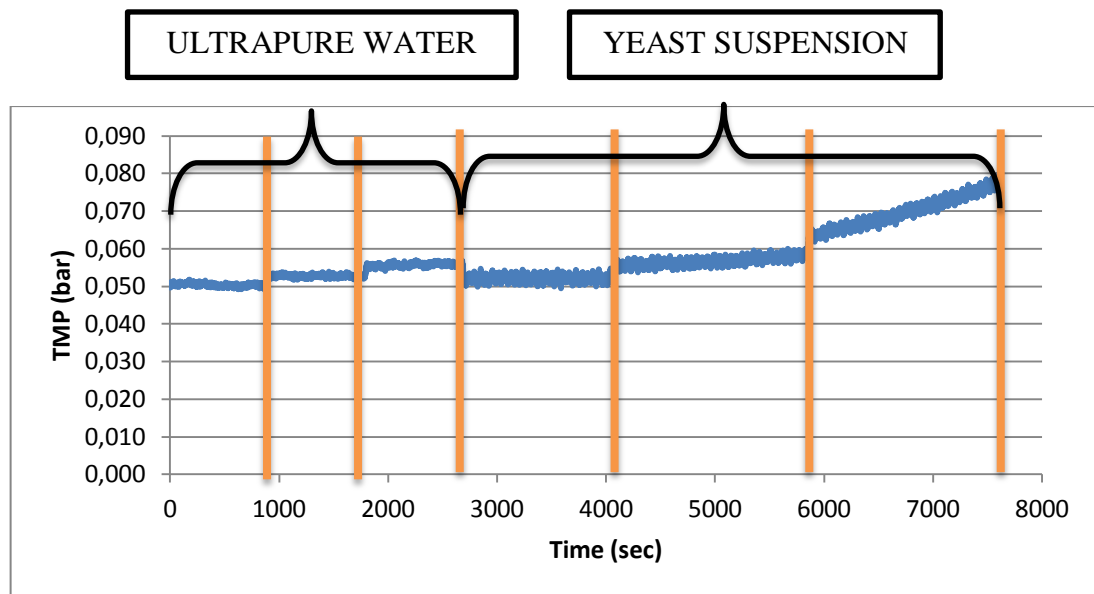
Figure 4. 23 Example of flux-stepping experiment with ultrapure water and yeast suspension cross-flow filtration

In Figure 4.23, one of the flux stepping experiments, is shown. The first three parts of the graph show the ultrapure water permeance results. These parts represent 20, 40 and 60 L/h.m^2 ultrapure water fluxes respectively. Since there is no expected fouling behavior in pure water permeance experiments, constant pressure is expected which means no fouling or compaction of pores in the same flux. After that, 1g/L yeast suspension is started to be filtered with the same fluxes, 20, 40 and 60 L/h.m^2 and

fouling increases the pressure. During the yeast cell filtrations, as the flux increased the fouling rate was also increased.

4.6.1 Pure Water Permeances

Pure water permeances of the membranes were measured as explained in experimental methods part. From TMP versus flux values (calculated using corrugated membrane area for the corrugated membranes), it was seen that corrugated membranes had higher pure water permeances even after effective membrane area enhancement effect was eliminated.
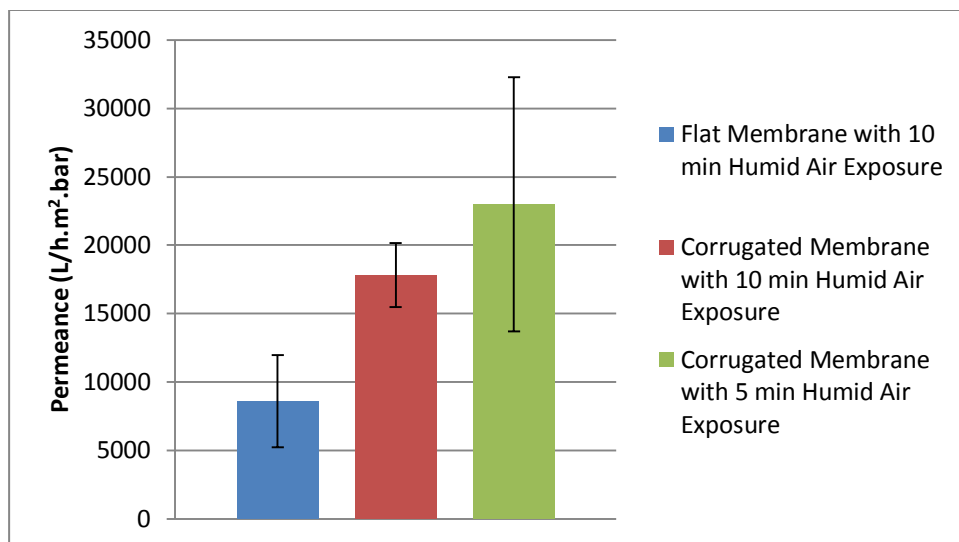
Figure 4. 24 Pure water permeance values of flat and corrugated membranes. For corrugated membranes actual membrane area was used.
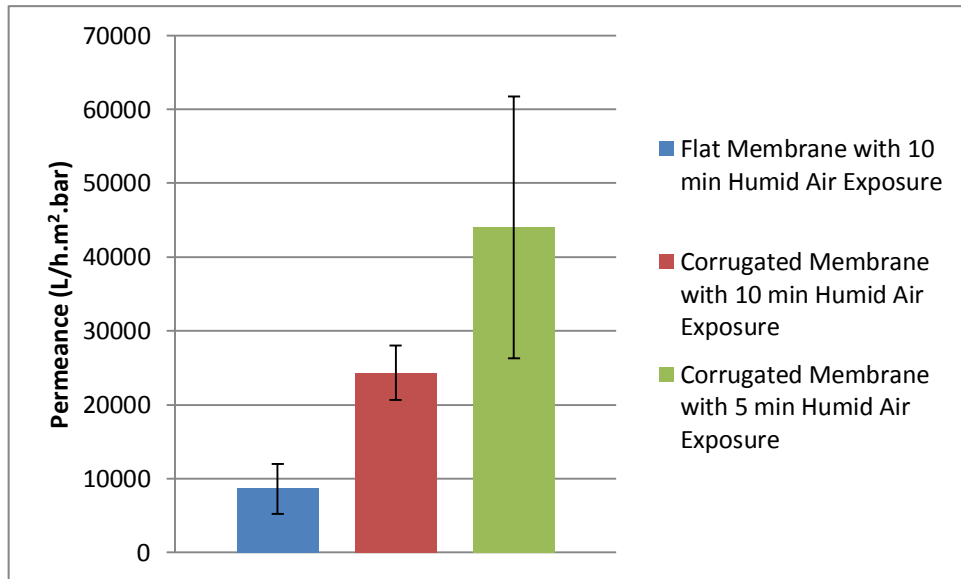
Figure 4. 25 Pure water permeance values of flat and corrugated membranes. For corrugated membranes projected membrane area was used.

Since, 10 minutes humid air exposure made lower corrugation height fidelity then 5 minutes humid air exposure, membranes exposed to humid air for 10 minutes had lower membrane area. Because of this, pure water flux increase from surface area to projected area was higher for membranes with 5 minutes of humid air exposure. While pure water permeance increased from 18000 L/h.m^2.bar to 24000 L/h.m^2.bar for corrugated membranes with 10 minutes humid air exposure, it increased from 23000 L/h.m^2.bar to 44000 L/h.m^2.bar for 5 minutes ones.

In order to see the reason behind the difference between pure water permeance values, average pore diameters and surface morphology were illustrated in Table 4.7.

Table 4. 7 PWP, average pore diameters and surface SEM images of membranes

Membrane	Average Pore Diameter, dp (µm)	Pure Water Permeance, PWP (L/m^2.h.bar)	Pure Water Permeability, (L.µm /m^2.h.bar)	SEM Images of Membranes
Flat Membrane with 10 min Humid Air Exposure	1.3±0.3	9000	2.2x10^5	
Corrugated Membrane with 10 min Humid Air Exposure	1.6±0.3	24000	1.2x10^6	
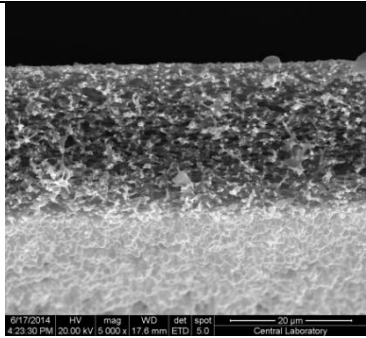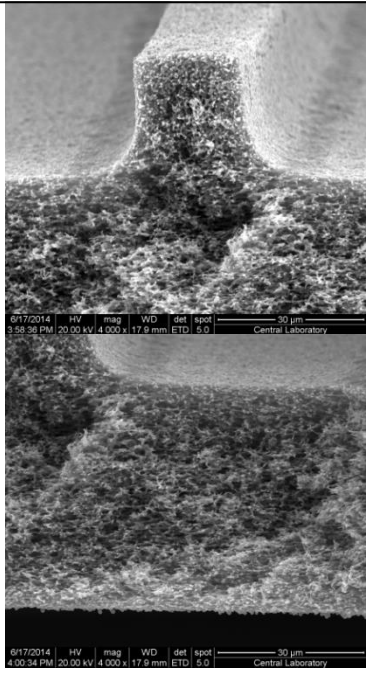
Table 4. 7(cont'd) PWP, average pore diameters and surface SEM images of membranes

Corrugated Membrane with 5 min Humid Air Exposure	1.0±0.1 at the corrugated layer and 1.8±0.3 at the lower part	44000	Asymmetric Structure	
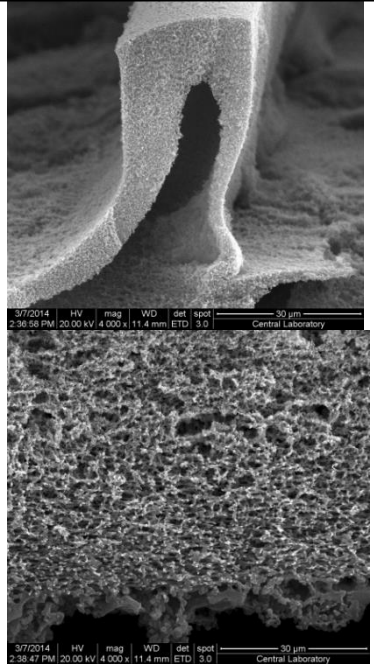
The permeability of corrugated membrane, calculated from effective thickness data and permeance value which can be seen in App. B, was 6 times higher than flat membrane's permeability for 10 minutes humid air exposed membranes. This difference can be explained by larger pore diameter of corrugated membrane. Average pore diameter of corrugated membrane was nearly 1.6±0.3 µm while flat one had nearly 1.3±0.3 µm pores. This 25% increase in average pore diameter meant corrugated membrane had nearly twofold increase in pore volume. However, pore volume difference was not enough to explain sixfold increase in permeability. The another reason to this permeability enhancement could be the pores in the edges of corrugations which were even larger. These large pores in the edges of the corrugations can be seen in Figure 4.26.
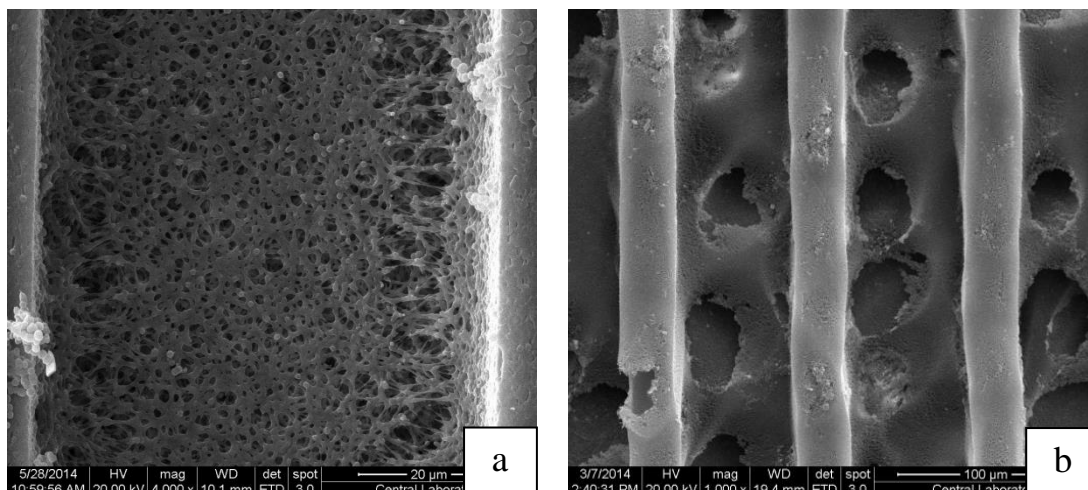
Figure 4. 26 SEM images of membrane corrugations. a) Corrugated Membrane with 10 min Humid Air Exposure b) Corrugated Membrane with 5 min Humid Air Exposure

The highest permeance value was observed at the corrugated membrane with 5 minutes humid air exposure. The increase in permeance value from 10 minutes humid exposed corrugated membrane to 5 minutes humid air exposed corrugated one can be explained by the pore diameters and macrovoids on the morphology. Membrane with 5 minutes humid air exposure had large macrovoids and 1.0 ± 0.1 µm on the corrugations and 1.8 ± 0.3 µm at the lower part of the membrane while 10 minutes humid air exposed corrugated membranes had a homogeneous pore distribution on the morphology with an average pore size of 1.6 ± 0.3 µm without any macrovoids.

4.6.2 Membrane and Fouling Resistances
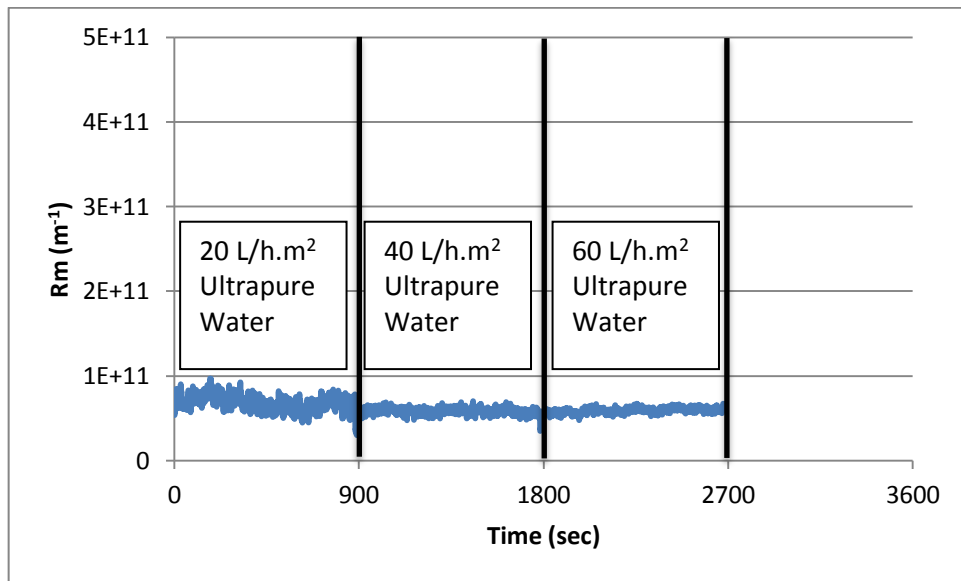
Figure 4. 27 Intrinsic membrane resistance variation graph for the same experiment in Figure 4.23

This figure above is from the experiment of flat membrane with 10 minutes humid air exposure and 0.1 m/s cross-flow velocity. In the first 2700 seconds of the experiment just ultrapure water was permeated with 900 second intervals and 20,40 and 60 $L/h.m^2$ fluxes respectively. Since fouling is not expected in the permeation of ultrapure water, increase in total resistance was not observed. The purpose of ultrapure water permeation was calculation of pure water permeance and intrinsic membrane resistances. The total resistance values of pure water permeation part directly give the membrane intrinsic resistance for each flux.

After that, 0.1 g/L yeast suspension was started to be filtered with the same fluxes and by substracting the intrinsic membrane resistance from total resistance, the fouling resistances caused by yeast particles were calculated. Since the pore sizes of membranes (1.3-1.6 μm) were much smaller than yeast particles (ca. 5 μm), retention

values were accepted as 100% which was also verified by the clear apperreance of the permeate.
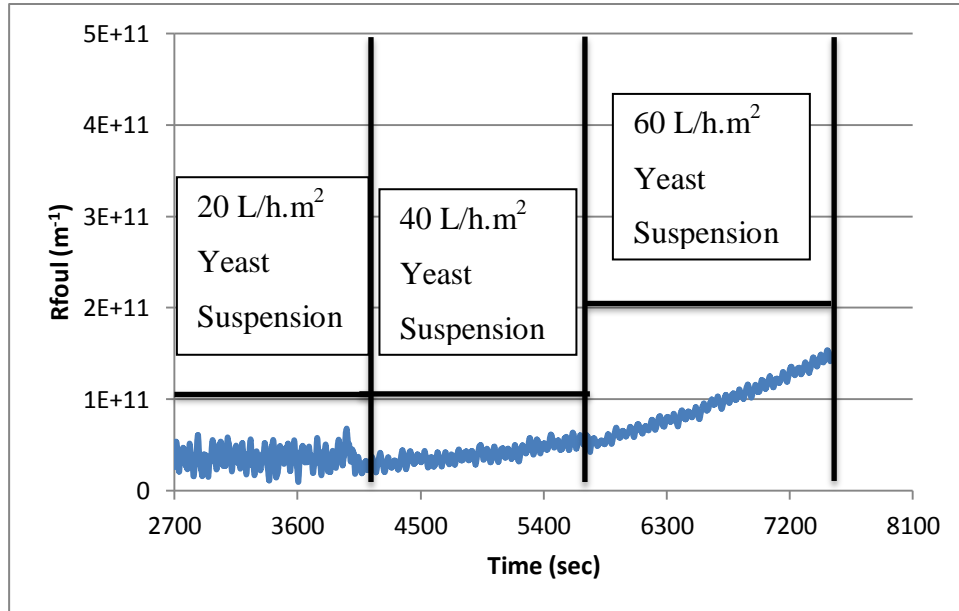
Figure 4. 28 Fouling resistance variation graph for the same experiment in Figure 4.23

Fouling resistance for 20 L/h.m^2 yeast suspension permeate flux did not show any increase while 40 L/h.m^2 gradually increased the resistance and 60 L/h.m^2 flux caused a rapid fouling. The 20 L/h.m^2 flux caused a steady state fouling resistance values which may be because flux was too low which made degree of fouling to be too slow or non at all. The plateau of nearly 4E+10 m^{-1} was obtained with some oscillations and it was obtained immediately upon start-up. The part of the experiment which was run with 40 L/h.m^2 had gradually increase in resistance values. For the constant flux, increase in TMP thereby resistance means occurrence of fouling. The resistance started at 3.3E+10 m^{-1} and after 1800 seconds it reached to almost 5.4E+10 m^{-1}. The final part of yeast filtration experiments was with 60 L/h.m^2

permeate flux which caused sharper fouling rates with higher increase in fouling resistance values. For the illustrated filtration in Figure 4.23, resistance was increased from 5E+10 m^{-1} to 1.4E+11 m^{-1} in 1800 seconds.

After that, fouling rates were calculated for each flux and fouling rates versus flux graph for both cross-flow velocities are given in Figures 4.29, 4.30 and 4.31.
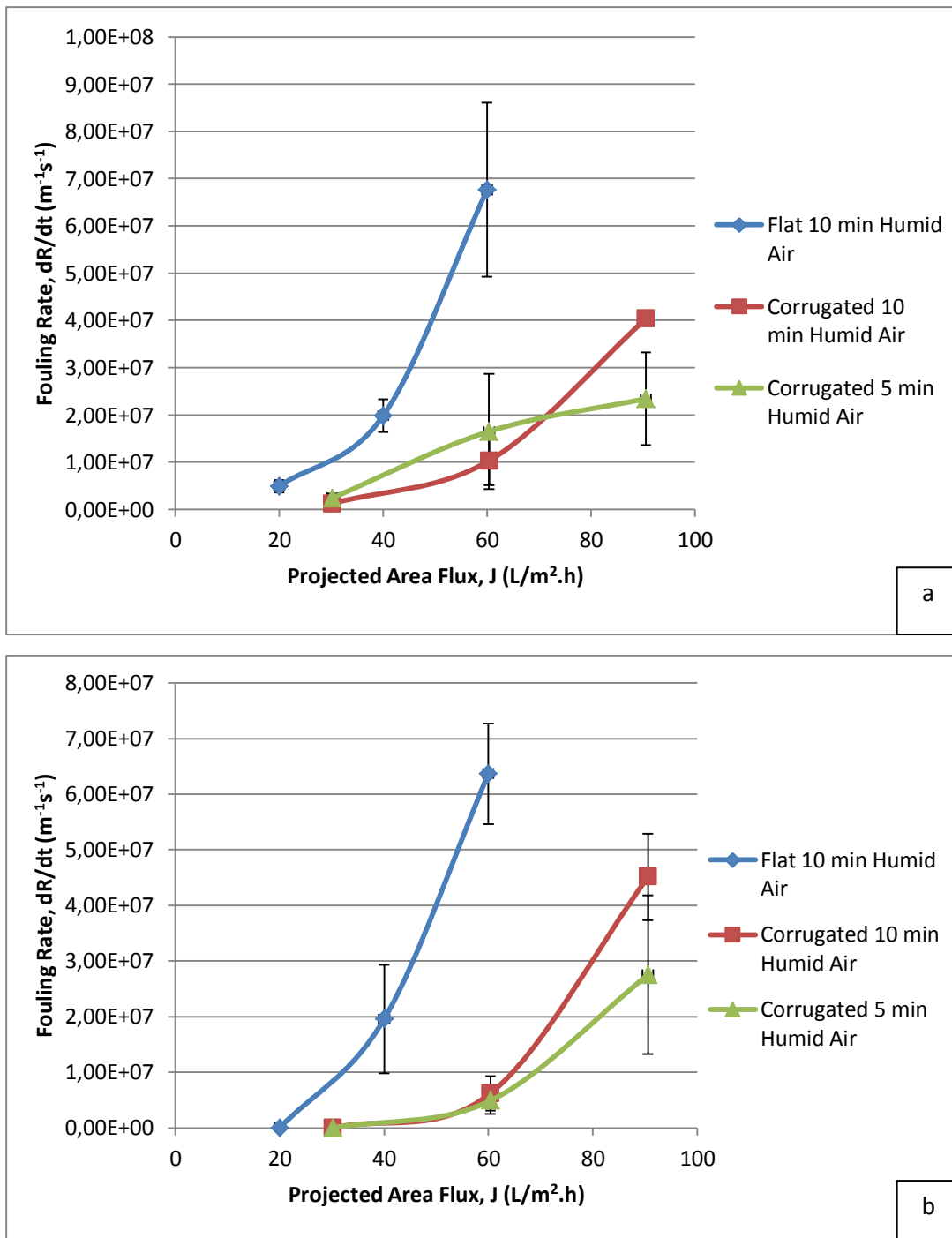
Figure 4. 29 The change in fouling rate versus projected area flux values. a) 0.1 m/s cross-flow velocity b) 0.2 m/s cross-flow velocity
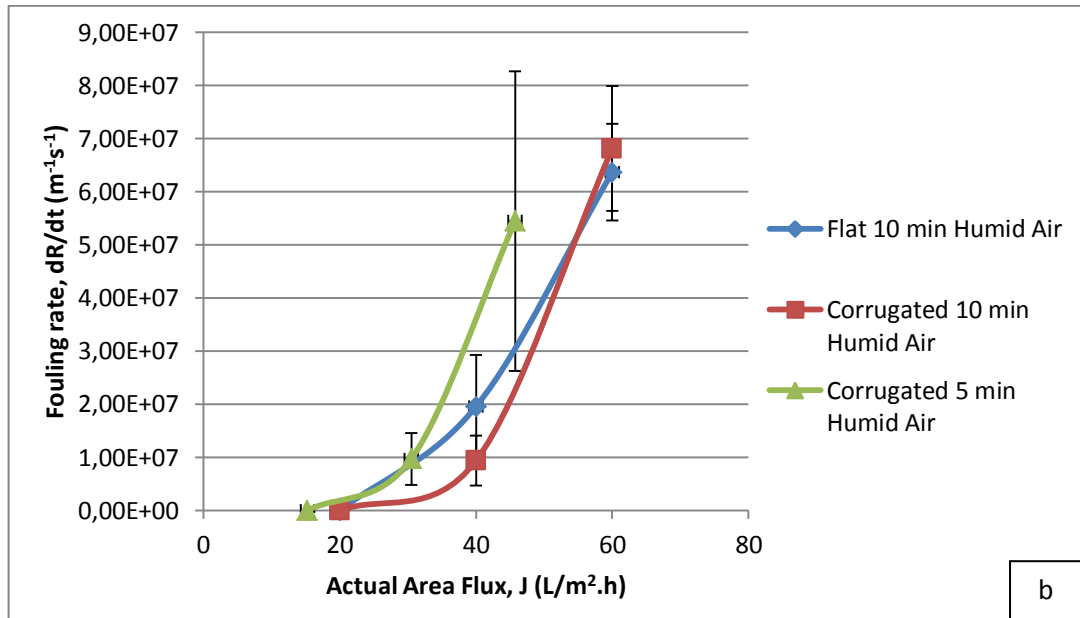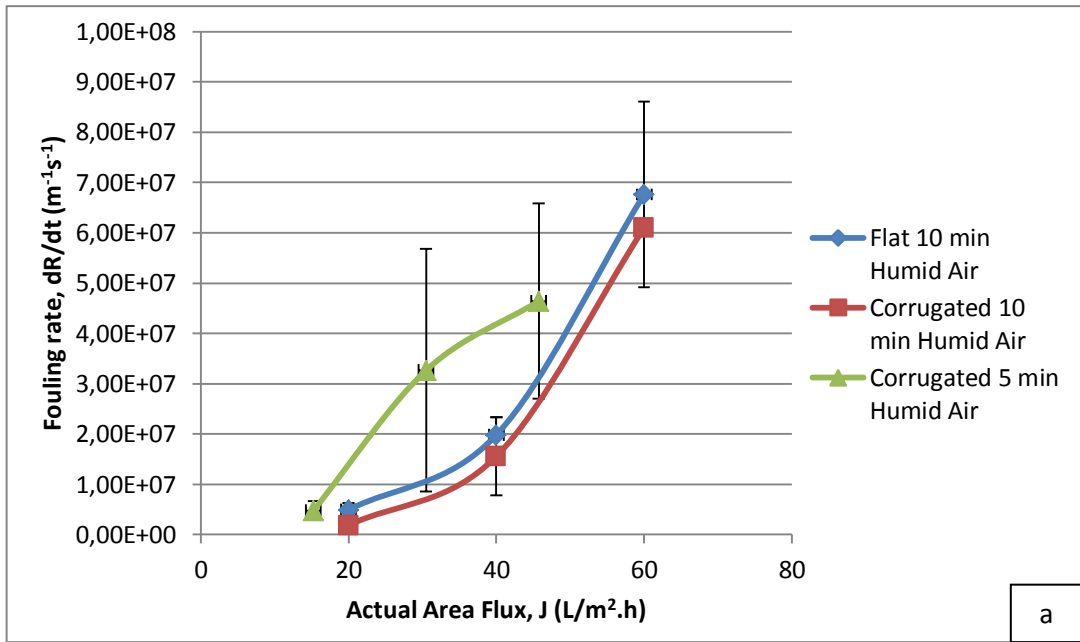
Figure 4. 30 The change in fouling rate versus actual area flux values. a) 0.1 m/s cross-flow velocity b) 0.2 m/s cross-flow velocity

From the first graph in Figure 4.29 and Figure 4.30, fouling rates versus flux values can be seen for flat and corrugated membranes at 0.1 m/s velocity and the b part of these figures, the experiments were done with 0.2 m/s cross-flow velocity. It was observed from Figure 4.29 that corrugated membranes were fouled much slower than flat membranes when fluxes were calculated from projected area values. Also, at the lowest permeate fluxes membranes had 0 $m^{-1}s^{-1}$ fouling rates for the 0.2 m/s cross-flow velocity. However, when the velocity was 0.1 m/s membranes were fouled at even lowest permeate fluxes. When the fluxes were calculated with actual areas of the membranes, which were larger for corrugated ones, the fouling rate differences that can be seen in Figure 4.29 were not observed. So, it can be concluded that, area enhancement made membrane fouling slower for the corrugated membranes.
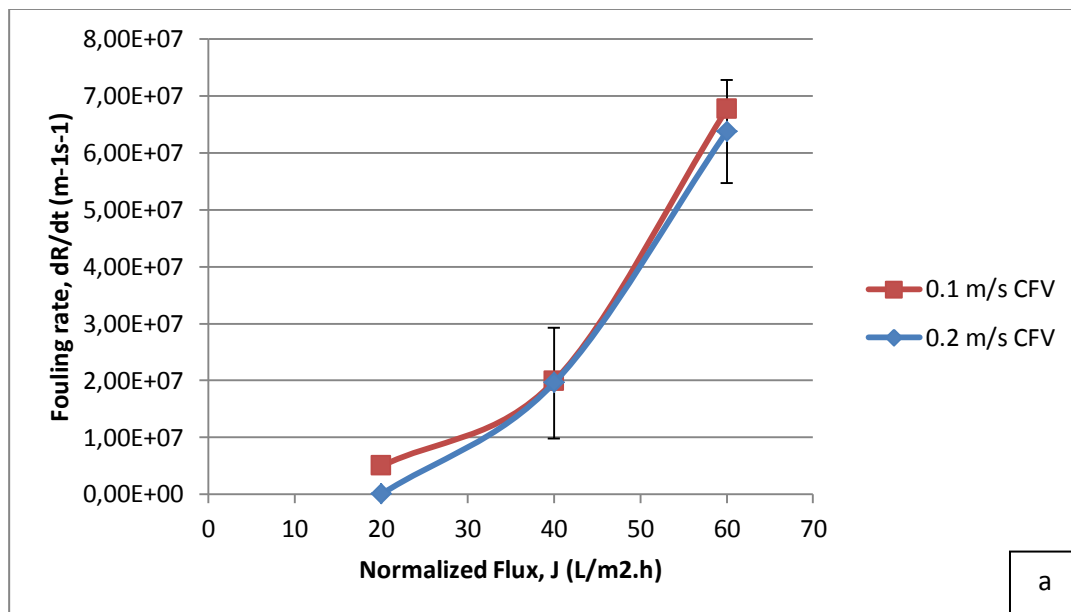
Figure 4. 31 The change in fouling rate values with different cross-flow velocities for same membrane.a) Flat membrane with 10 min humid air b) Corugated membrane with 10 min humid air c) Corrugated membrane with 5 min humid air
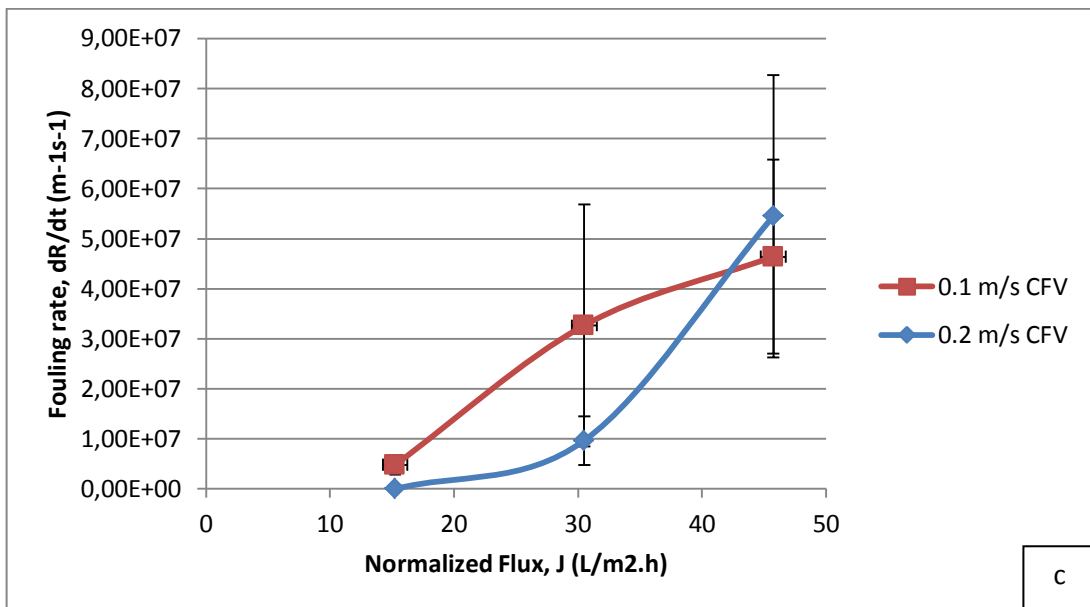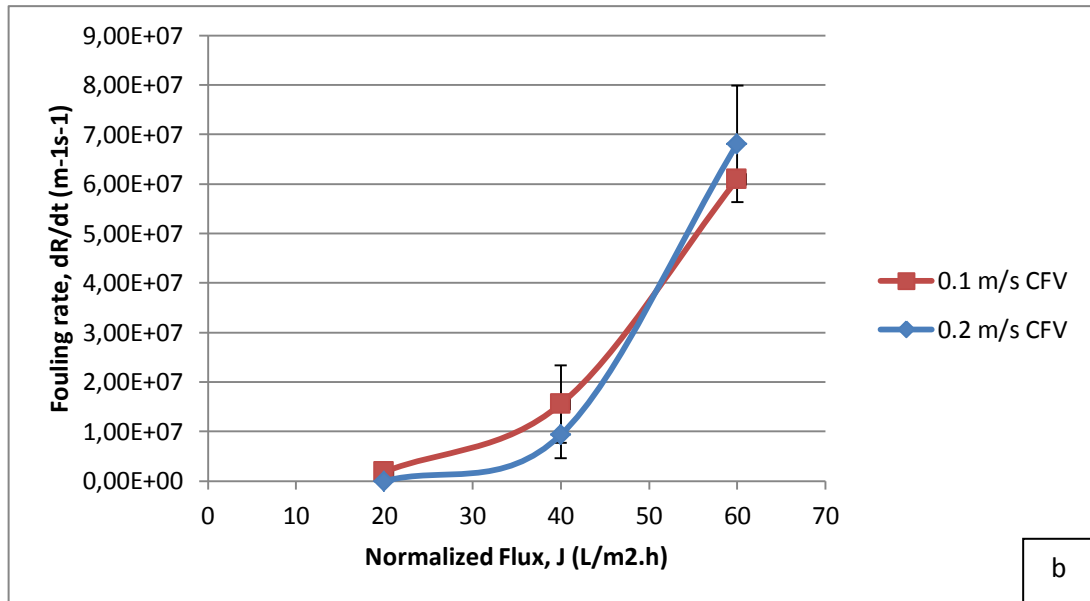
Figure 4. 31 (cont'd) The change in fouling rate values with different cross-flow velocities for same membrane.a) Flat membrane with 10 min humid air b) Corugated membrane with 10 min humid air c) Corrugated membrane with 5 min humid air

In the graphs above, 0.1 and 0.2 m/s cross flow velocities of same filtration processes were compared according to fouling rates. Sherwood number ($D_h k / D_{AB}$), where D_h is the hydraulic diameter, k is the mass transfer coefficient and D_{AB} is the binary diffusion coefficient, is a constant for laminar flow inside a channel. [32] Although the increasing Reynolds number with increasing velocity will increase the mass transfer coefficient in the entry length and may also cause higher back diffusion within the corrugations, this effect was negligible for both flat and corrugated membranes.

CHAPTER 5

CONCLUSIONS

In this study, fabrication of corrugated membranes and comparison of their and flat membrane performances were examined. Polyethersulfone(PES) microfiltration membranes were prepared with phase separation condition and polymer concentration modifications and membrane morphologies were examined by scanning electron microscopy (SEM) images. Under cross-flow filtration water permeabilities and fouling characteristics of membranes were investigated. The following conclusions were obtained;

1. From the fabrication of flat membranes it was observed that, membranes with humid air exposure and NMP/water bath immersion as pre-coagulation treatments gave more symmetric morphologies then directly coagulated membranes. PEG 400, PEG 6k and water additions to the polymer solution have a positive effect on membrane symmetry and suppressing macrovoid formation. Desired symmetric morphology was achieved with 10wt%PES, 60wt%PEG400, 25wt%NMP, 5wt%water solution and 10 minutes humid air exposure.

2. Same recipe was applied on corrugated mold and prepared symmetric corrugated membranes. Moreover, different humid air exposure times (5 min and 15 min) were performed. While 15 minutes humid air exposure did not change the membrane morphology, 5 minutes humid air exposure changed that morphology totally. This membrane had larger pores on the non-corrugated side with an average of 1.8μm and

smaller pores on the mold side and also have some macrovoids which is usable for filtration also.

3. After effective membrane area enhancement eliminated from permeate flux values corrugated membrane still had nearly twofold higher pure water permeance values than flat membranes. This was considered by calculating the permeabilities of the symmetric membranes. The permeability of corrugated membrane was 6 times higher than flat membrane's permeability for 10 minutes humid air exposed membranes. This difference was explained by larger pore diameter of corrugated membranes and even larger pores in the edges of corrugations

4. During saccharomyces cerevisiae suspension filtration, there was no obvious difference between flat and corrugated membranes performances. Fouling resistance rates of membranes were close to each other at the same flux.

5. Increase in cross-flow velocity (CFV) affected fouling especially at the 20 L/h.m^2 permeate flux. The membranes did not show any fouling sign at the 0.2 m/s CFV while they started to be fouled at 0.1m/s CFV and 20 L/h.m^2 permeate flux.

6. As recommendation, this methodology is very simple to make corrugations on membrane walls, however in order to see the effect of decreasing concentration polarization on membrane fouling, Reynolds Number can be increased by increasing cross flow velocity and shape and size of corrugations or mutual distances between corrugations can be changed.

REFERENCES

[1]. Baker, R.W., Membrane Technology and Applications, 2004, John Wiley and Sons.

[2]. Bikel, M., Pünt, I. G. M., Lammertink, R. G. H., & Wessling, M. (2009). Micropatterned polymer films by vapor-induced phase separation using permeable molds. *ACS Applied Materials & Interfaces*, *1*(12), 2856–61.

[3]. Strathmann, H., Scheible, P., & Baker, R. W. (1971). A rationale for the preparation of Loeb-Sourirajan-type cellulose acetate membranes. *Journal of Applied Polymer Science, 15*(4), 811-828.

[4]. Scott, K., Mahmood, A. J., Jachuck, R. J., & Hu, B. (2000). Intensified membrane filtration with corrugated membranes, *173*(January), 1–16.

[5]. Van der Waal & Racz, I. G. (1989). Mass transfer in corrugated-plate membrane modules. I. Hypherfiltration experiments. *Journal of Membrane Science*, *40*,.243-260.

[6]. Miller, D. J., Kasemset, S., Wang, L., Paul, D. R., & Freeman, B. D. (2014). Constant flux crossflow filtration evaluation of surface-modified fouling-resistant membranes. *Journal of Membrane Science*, *452*, 171–183.

[7]. Mulder, M., Basic Principles of Membrane Tehcnology, 1996, Kluwer Publications.

[8]. Le Clech, P., Jefferson, B., Chang, I. S., & Judd, S. J. (2003). Critical flux determination by the flux-step method in a submerged membrane bioreactor. *Journal of Membrane Science*, *227*(1-2), 81–93.

[9]. Kingdom, U. (1995). Sub-critical flux operation of microfiltration, *107*, 165–171.

[10]. Stoller, M., Bravi, M., & Chianese, A. (2013). Threshold flux measurements of a nano filtration membrane module by critical flux data conversio. *Desalination*, *315*, 142–148.

[11]. Miller, D. J., Kasemset, S., Paul, D. R., & Freeman, B. D. (2014). Comparison of membrane fouling at constant flux and constant transmembrane pressure conditions. *Journal of Membrane Science*, *454*, 505–515. **[12].** Zhao, C., Xue, J., Ran, F., & Sun, S. (2013). Modification of polyethersulfone membranes - A review of methods. *Progress in Materials Science*, *58*(1), 76–150.

[13]. Chakrabarty, B., Ghoshal, a. K., & Purkait, M. K. (2008). Effect of molecular weight of PEG on membrane morphology and transport properties. *Journal of Membrane Science*, *309*(1-2), 209–221.

[14]. Susanto, H., Ulbricht, M., Characteristics, performance and stability of polyethersulfone ultrafiltration membranes prepared by phase separation method using different macromolecular additives, 2009, *Journal of Membrane Science*, 125-135.

[15]. Pagidi, A., Saranya, R., Arthanareeswaran, G., Ismail, a. F., & Matsuura, T. (2014). Enhanced oil–water separation using polysulfone membranes modified with polymeric additives. *Desalination*, *344*, 280–288.

[16]. Susanto, H., Stahra, N., & Ulbricht, M. (2009). High performance polyethersulfone microfiltration membranes having high flux and stable hydrophilic property. *Journal of Membrane Science*, *342*(1-2), 153–164.

[17]. Rajal, B., Castro, E. F., Calvo, I., Mercedes, L. M., Romero, I., Palacio, L., … Valladolid, U. De. (2014). Properties of Polyethersulfone Ultrafiltration Membranes Modified With Polyethylene Glycols.

[18]. Ulbricht, M., Matuschewski, H., Oechel, A., & Hicke, H. (1996). Photo-induced graft polymerization surface modifications for the preparation of hydrophilic and low-protein-adsorbing ultrafiltration membranes, *115*, 31–47.

[19]. Sagle, A. C., Van Wagner, E. M., Ju, H., McCloskey, B. D., Freeman, B. D., & Sharma, M. M. (2009). PEG-coated reverse osmosis membranes: Desalination properties and fouling resistance. *Journal of Membrane Science*, *340*(1-2), 92–108.

[20]. Van der Waal, M. J., Stevanovic, S., & Racz, I. G. (1989). Mass transfer in corrugated-plate membrane modules. II. Ultrafiltration experiments. *Journal of Membrane Science*, *40*(2), 261–275.

[21]. Won, Y.-J., Lee, J., Choi, D.-C., Chae, H. R., Kim, I., Lee, C.-H., & Kim, I.-C. (2012). Preparation and application of patterned membranes for wastewater treatment. *Environmental Science & Technology*, *46*(20), 11021–7.

[22]. Maruf, S. H., Wang, L., Greenberg, A. R., Pellegrino, J., & Ding, Y. (2013). Use of nanoimprinted surface patterns to mitigate colloidal deposition on ultrafiltration membranes. *Journal of Membrane Science*, *428*, 598–607.

[23]. Lee, Y. K., Won, Y.-J., Yoo, J. H., Ahn, K. H., & Lee, C.-H. (2013). Flow analysis and fouling on the patterned membrane surface. *Journal of Membrane Science*, *427*, 320–325.

[24]. Jamshidi Gohari, R., Lau, W. J., Matsuura, T., & Ismail, a. F. (2013). Effect of surface pattern formation on membrane fouling and its control in phase inversion process. *Journal of Membrane Science*, *446*, 326–331.

[25]. Won, Y.-J., Choi, D.-C., Jang, J. H., Lee, J.-W., Chae, H. R., Kim, I., … Kim, I.-C. (2014). Factors affecting pattern fidelity and performance of a patterned membrane. *Journal of Membrane Science*, *462*, 1–8.

[26]. Chae Park, H., Po Kim, Y., Yong Kim, H., & Soo Kang, Y. (1999). Membrane formation by water vapor induced phase inversion. *Journal of Membrane Science*, *156*(2), 169–178.

[27]. Yeow, M. L., Liu, Y. T., & Li, K. (2004). Morphological study of poly(vinylidene fluoride) asymmetric membranes: Effects of the solvent, additive, and dope temperature. *Journal of Applied Polymer Science*, *92*(3), 1782–1789.

[28]. Çulfaz, P. Z., Rolevink, E., van Rijn, C., Lammertink, R. G. H., & Wessling, M. (2010). Microstructured hollow fibers for ultrafiltration. *Journal of Membrane Science*, *347*(1-2), 32–41.

[29]. Musil, V., & Brumen, M. (2002). The wet phase separation : the effect of cast solution thickness on the appearance of macrovoids in the membrane forming ternary cellulose acetate / acetone / water system , *207*, 139–141.

[30]. Ahmad, a. L., Low, S. C., & Shukor, S. R. A. (2007). Effects of membrane cast thickness on controlling the macrovoid structure in lateral flow nitrocellulose membrane and determination of its characteristics. *Scripta Materialia*, *57*(8), 743–746.

[31]. Field, R. W., Wu, D., Howell, J. a., & Gupta, B. B. (1995). Critical flux concept for microfiltration fouling. *Journal of Membrane Science*, *100*(3), 259–272.

[32]. Incropera, F. P. (2007). Internal Flow. *Fundamentals of heat and mass transfer* (pp. 465-531). John Wiley.

APPENDIX A

PURE WATER PERMEANCE AND YEAST SUSPENSION FILTRATION RAW DATA
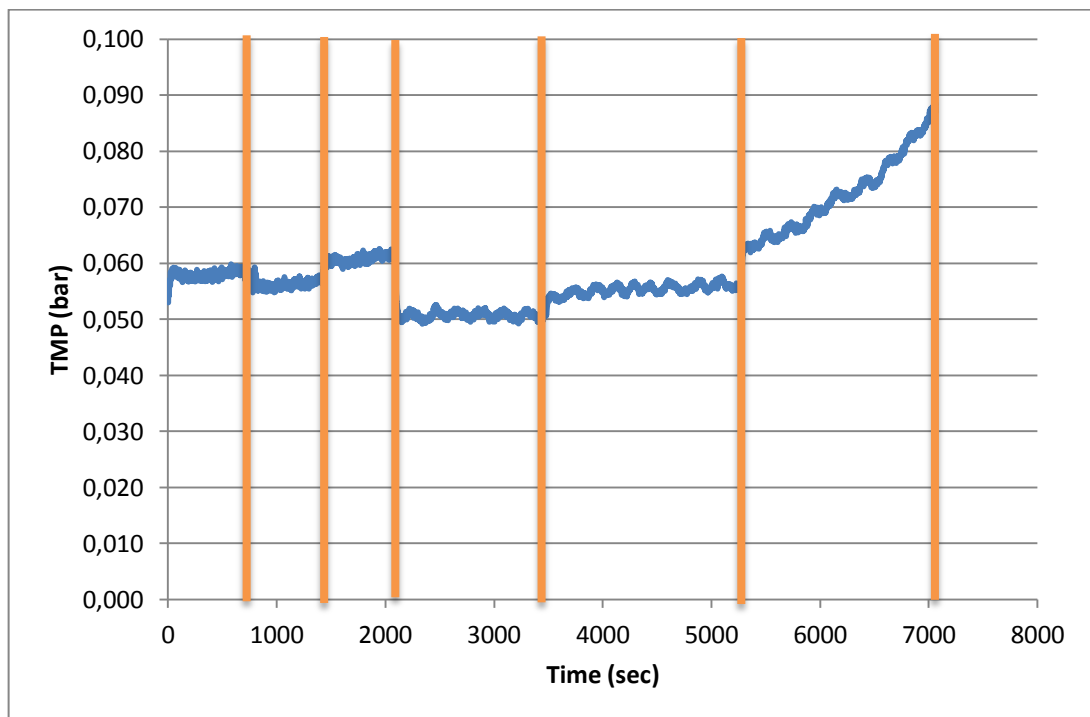
Figure A. 1 Flux-stepping experiment for flat membrane with 10 minutes humid air exposure and 0.1 m/s cross-flow velocity
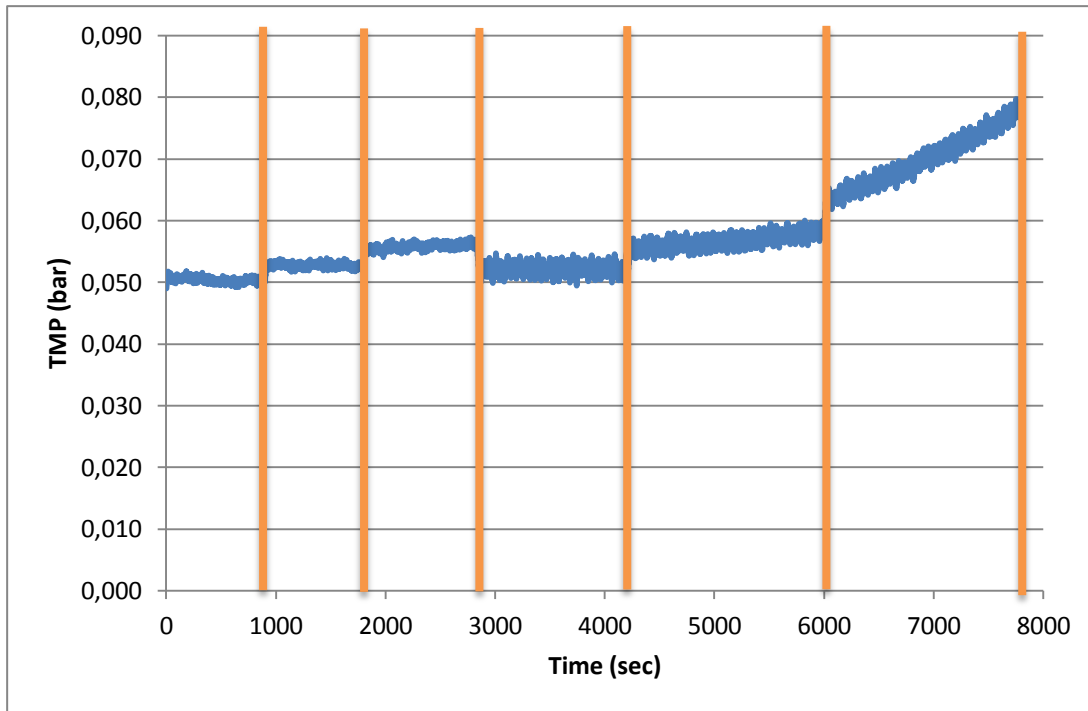
Figure A. 2 Flux-stepping experiment for flat membrane with 10 minutes humid air exposure and 0.1 m/s cross-flow velocity
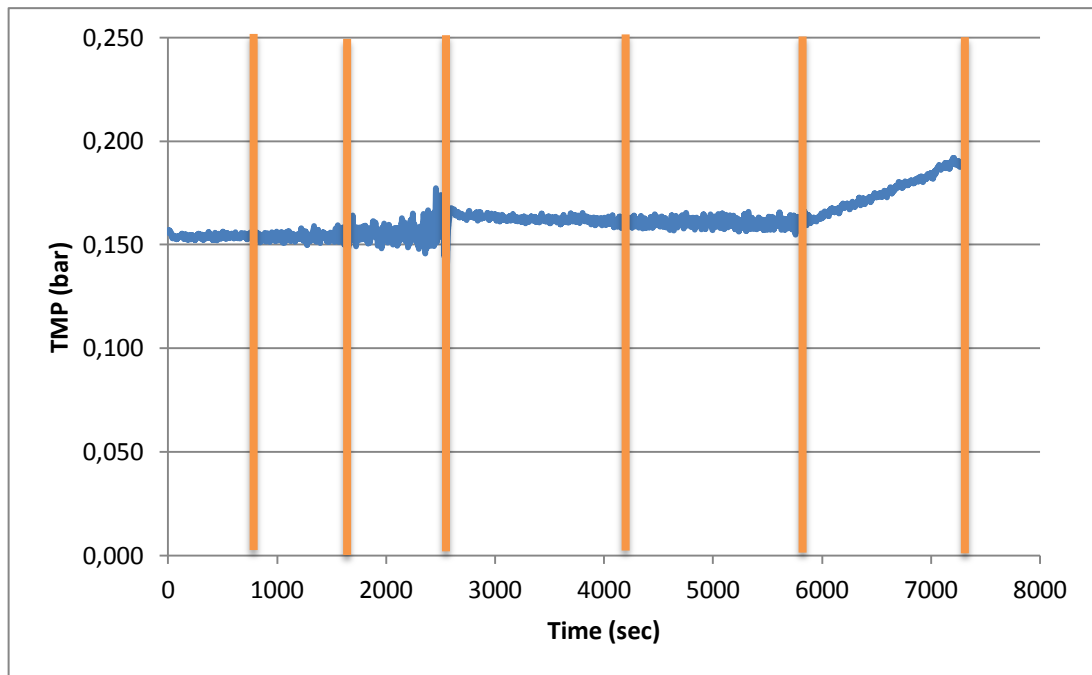
Figure A. 3 Flux-stepping experiment for flat membrane with 10 minutes humid air exposure and 0.2 m/s cross-flow velocity
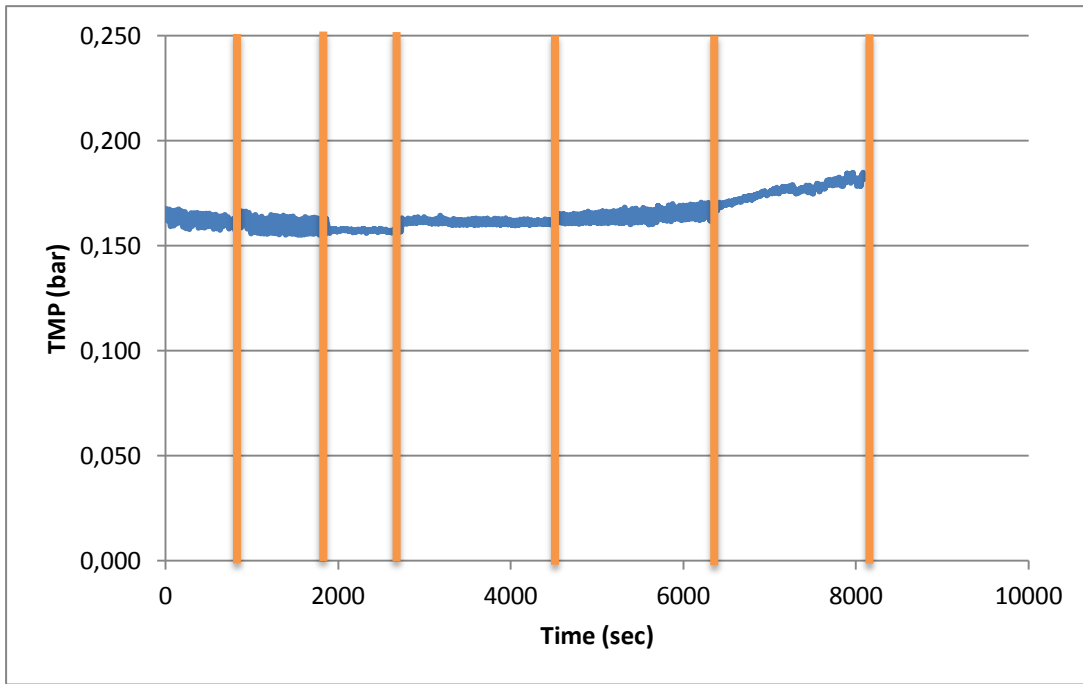
Figure A. 4 Flux-stepping experiment for flat membrane with 10 minutes humid air exposure and 0.2 m/s cross-flow velocity
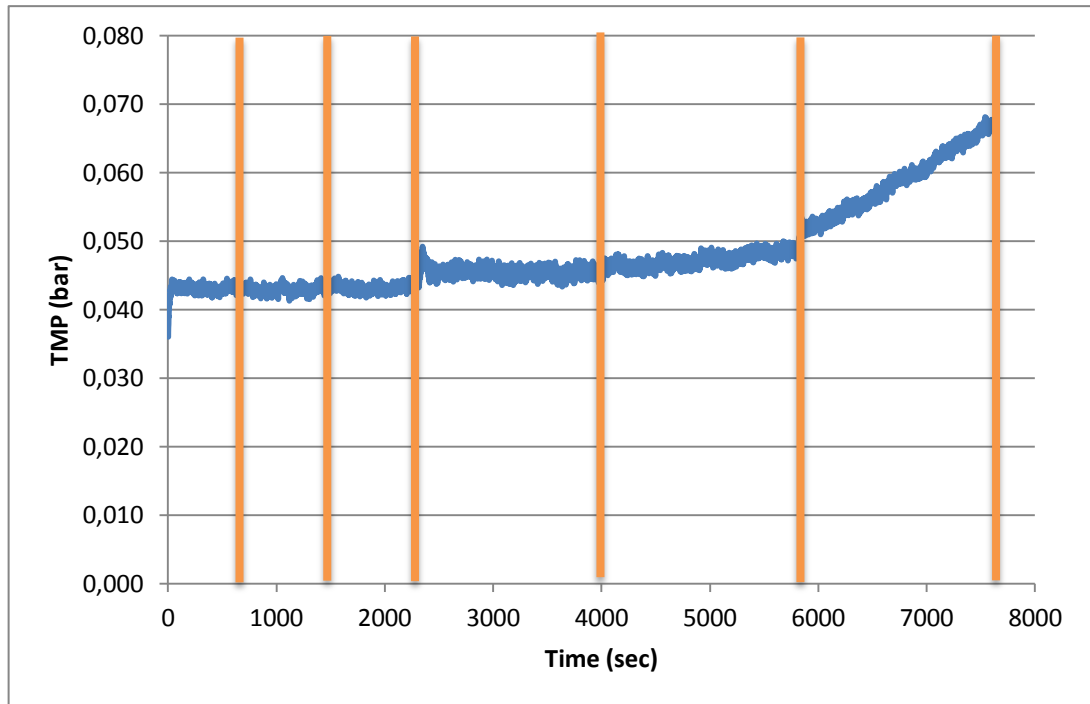
Figure A. 5 Flux-stepping experiment for corrugated membrane with 10 minutes humid air exposure and 0.1 m/s cross-flow velocity
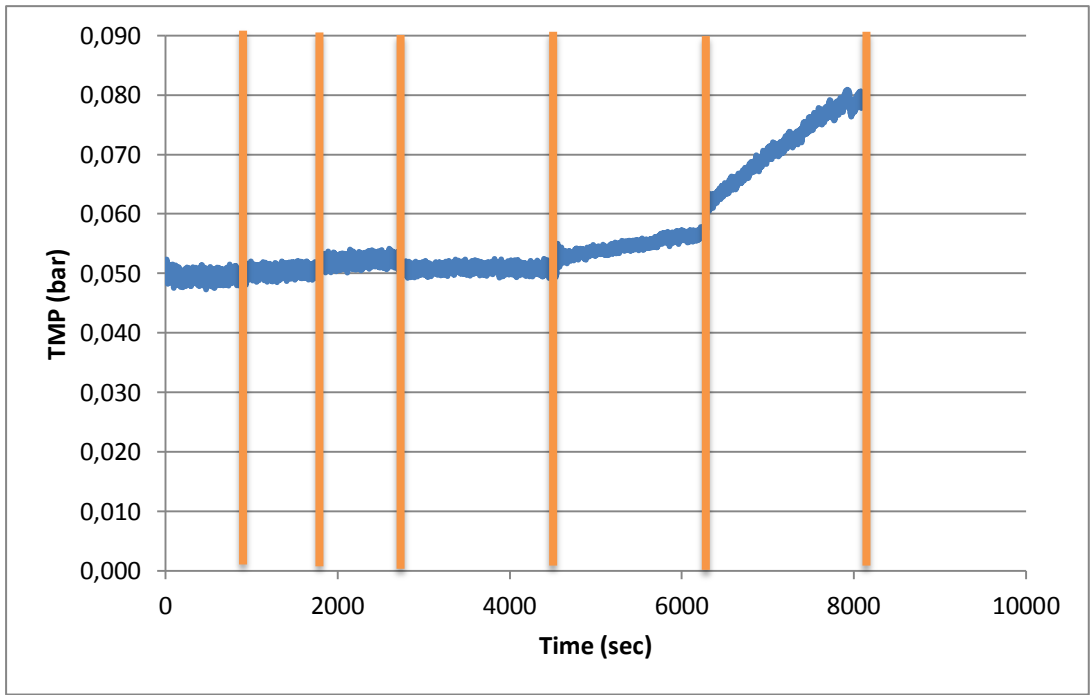
Figure A. 6 Flux-stepping experiment for corrugated membrane with 10 minutes humid air exposure and 0.1 m/s cross-flow velocity
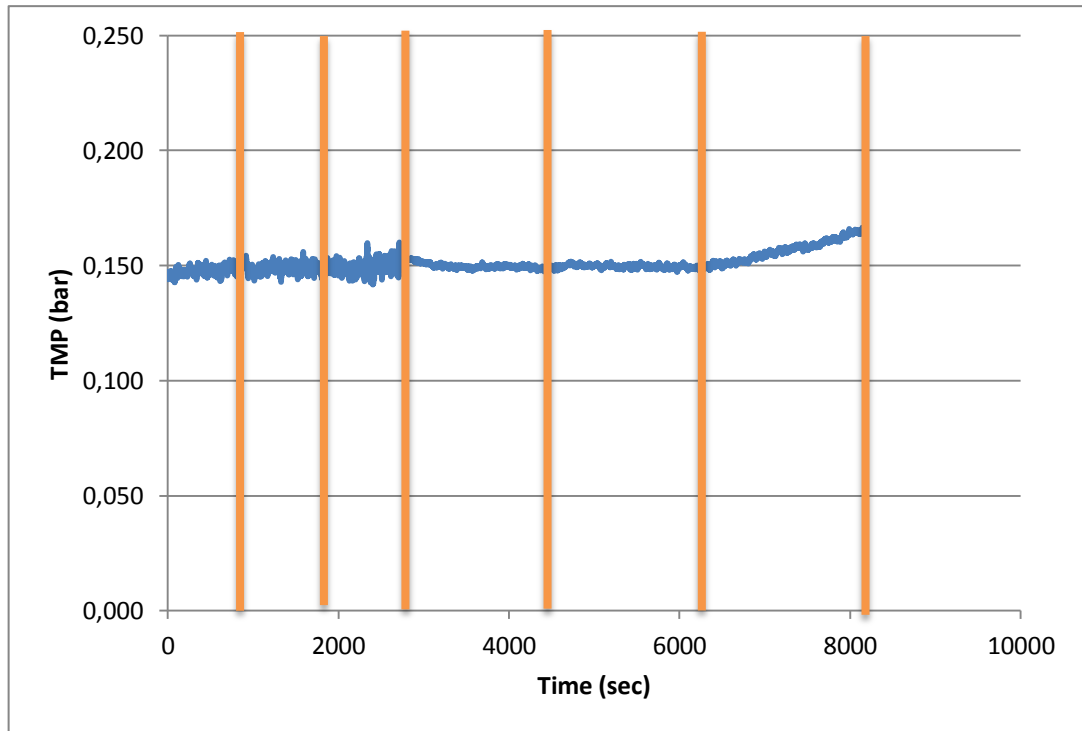
Figure A. 7 Flux-stepping experiment for corrugated membrane with 10 minutes humid air exposure and 0.2 m/s cross-flow velocity
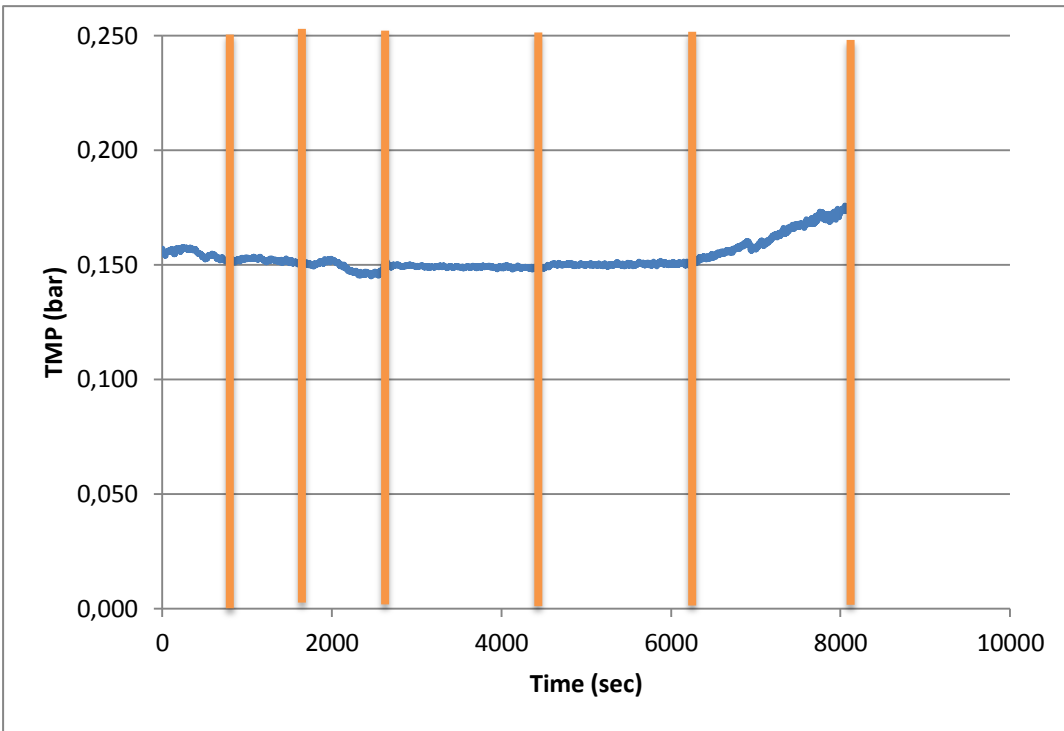
Figure A. 8 Flux-stepping experiment for corrugated membrane with 10 minutes humid air exposure and 0.2 m/s cross-flow velocity
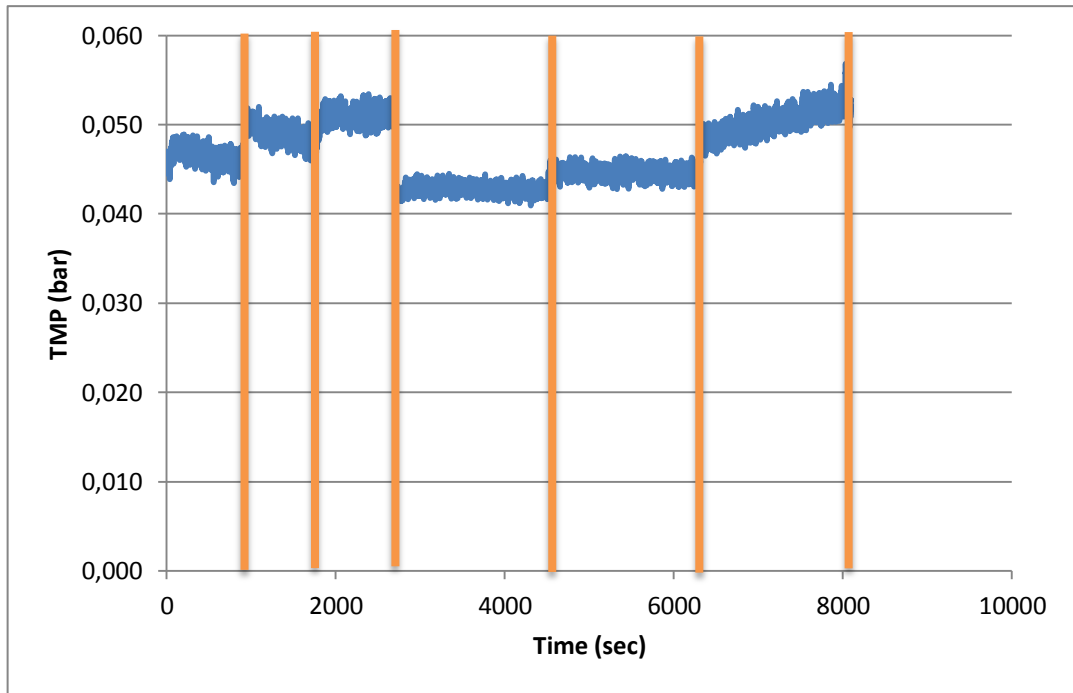
Figure A. 9 Flux-stepping experiment for corrugated membrane with 5 minutes humid air exposure and 0.1 m/s cross-flow velocity
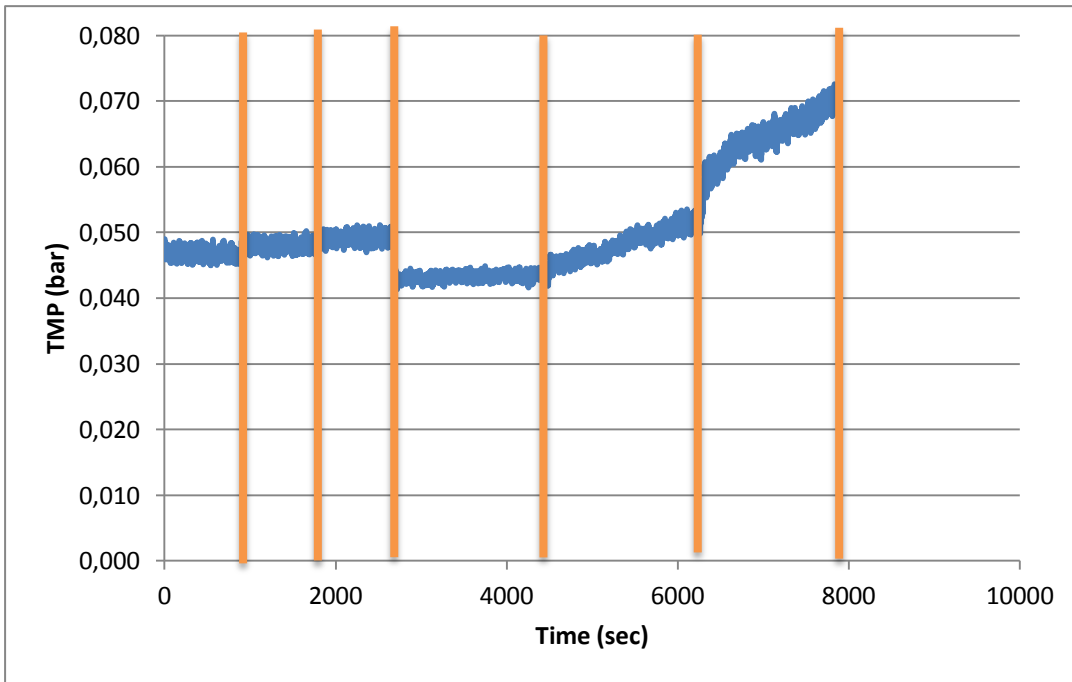
Figure A. 10 Flux-stepping experiment for corrugated membrane with 5 minutes humid air exposure and 0.1 m/s cross-flow velocity
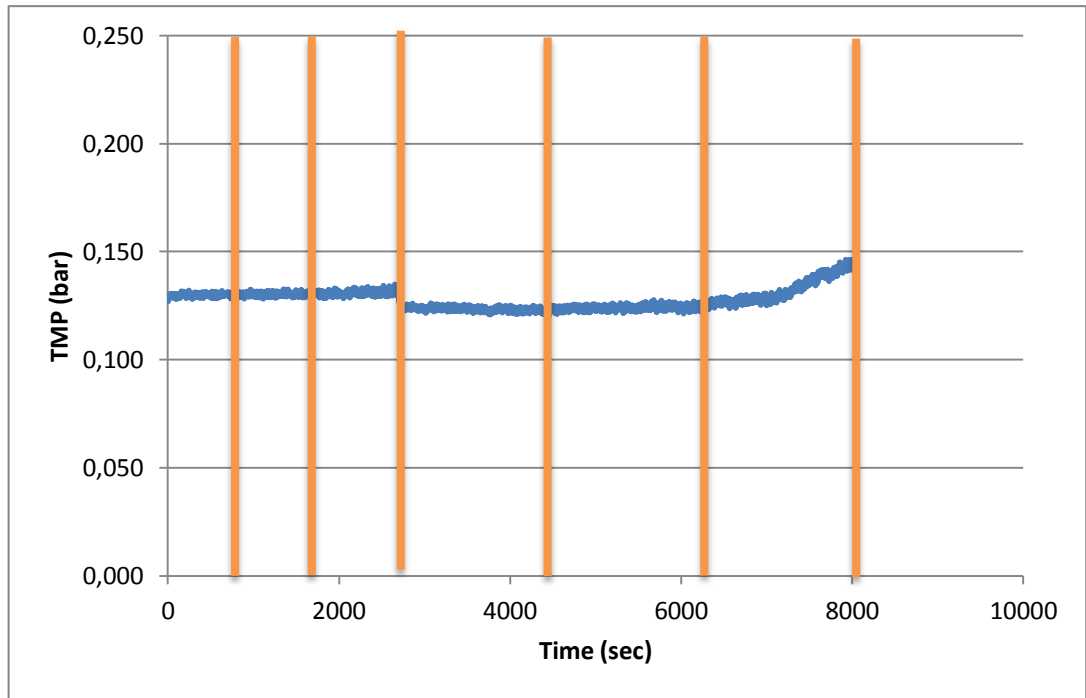
Figure A. 11 Flux-stepping experiment for corrugated membrane with 5 minutes humid air exposure and 0.2 m/s cross-flow velocity
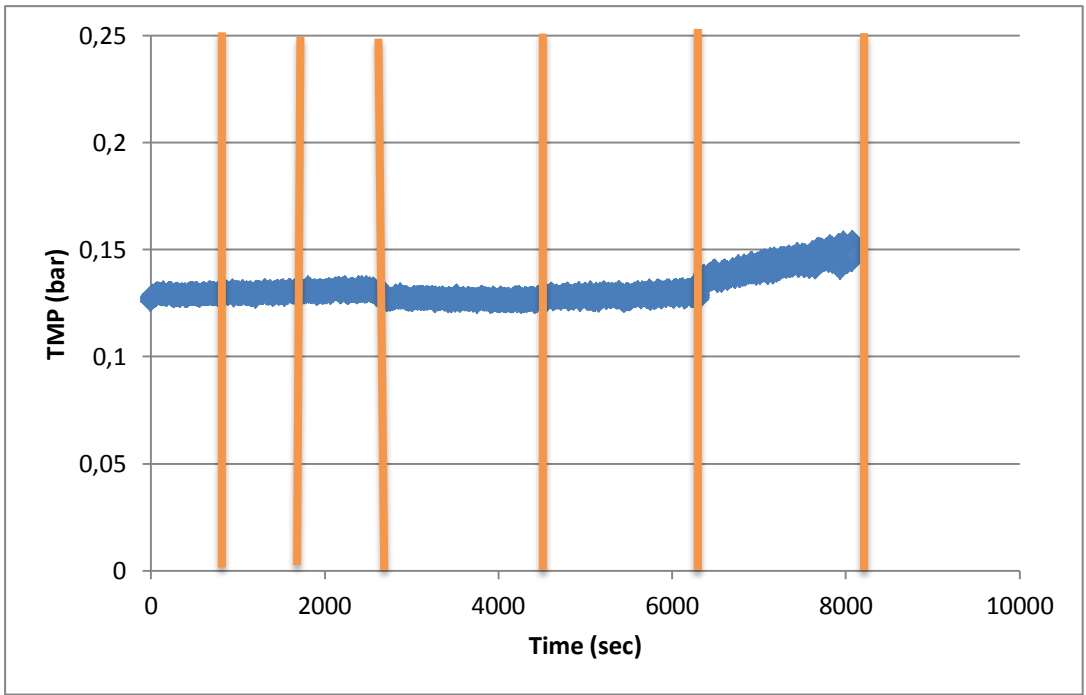
Figure A. 12 Flux-stepping experiment for corrugated membrane with 5 minutes humid air exposure and 0.2 m/s cross-flow velocity

APPENDIX B

CALCULATION OF PURE WATER PERMEANCES AND PERMEABILITIES

Pure water permeance,

$$PWP = \frac{J}{TMP}$$

where,

J is the permeate flux

TMP is the trans-membrane pressure.

Before calculating ultrapure water permeances from trans-membrane pressure and permeate flux values, the offset pressure (when there is no permeate flux) due to cross-flow velocity was eliminated.

$$TMP = \Delta P_m - \Delta P_o$$

Where,

ΔP_m is the measured pressure difference

ΔP_o is the offset pressure difference when permeate flux is 0.

After pure water permeance values were calculated, via multiplying by thickness of symmetric membranes permeability values were calculated.

$$Permeability = Permeance \times Effective\ Thickness$$

Sample calculation for flat membrane with 10 minutes humid air exposure;
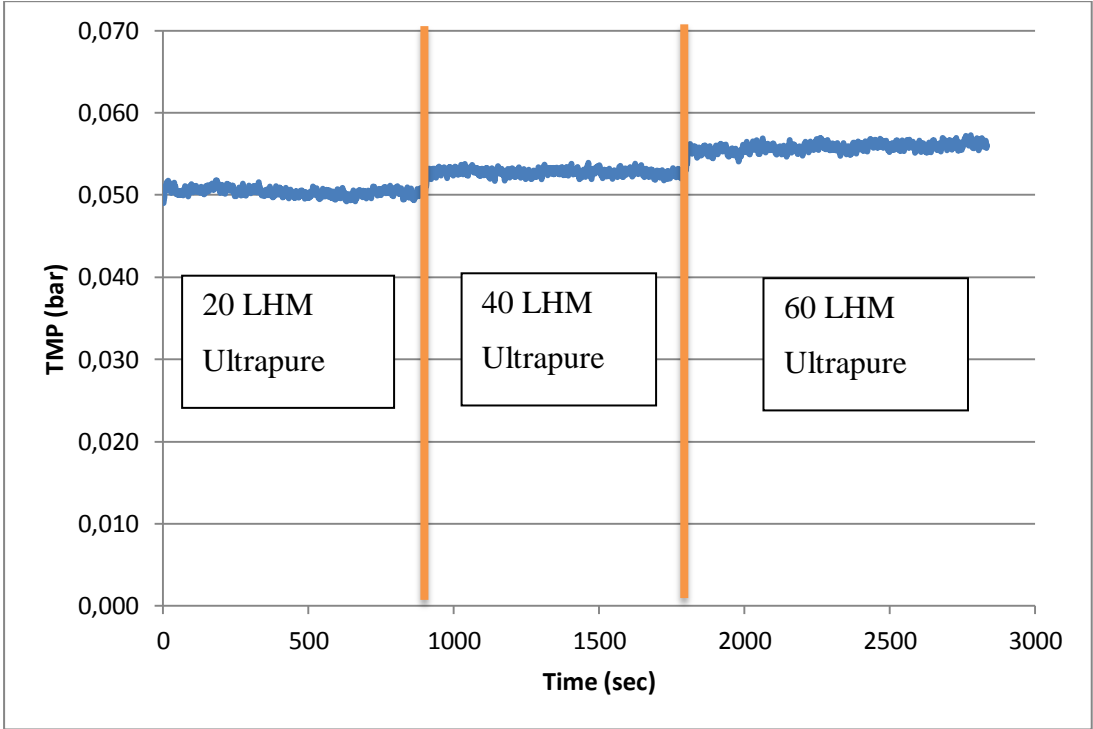
Figure B. 1 Ultra pure water permeanbility experiments for flat membrane with 10 minutes humid air exposure and 0.1 m/s cross-flow velocity

Ultrapure water was filtered for 900 seconds in each different flux which means 900 different pressure measurements since pressure transmitters measure the pressure in every second. In order to get more accurate measurements, average of these 900 measurements was taken. Moreover, there was some offset pressure in our cross-flow filtration set-up even if there was no permeance stream which was 0.047 bar for this experiment and we need to eliminate it.After averages were taken the result was;

Table B. 1 Ultrapure water filtration measurements for flat membrane at 0.1 m/s cross-flow velocity

Ultrapure Water Flux J (L/h.m^2)	Average Trans-Membrane Pressure TMP (bar)	Average Trans-Membrane Pressure TMP (bar) (Offset Eliminated)
20	0.050	0.003
40	0.053	0.006
60	0.056	0.009

In order to calculate pure water permeabilities a graph of J vs TMP was drawn.
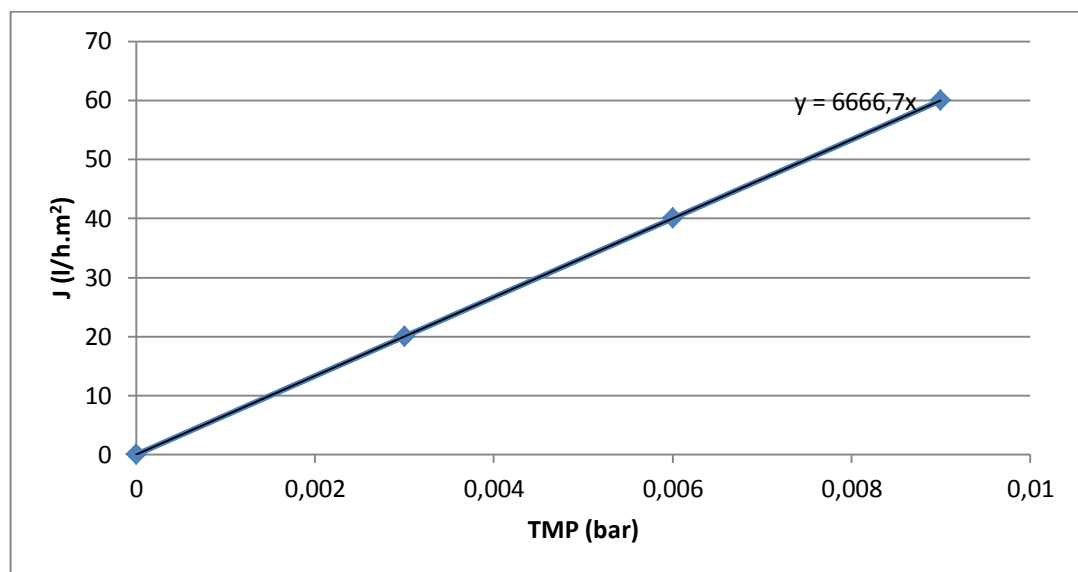
Figure B. 2 Pure water flux versus trans-membrane pressure for flat membrane with 10 minutes humid air exposure at 0.1 m/s cross-flow velocity

The slope of pure water flux versus trans-membrane pressure graph gives the pure water permeance of the membrane which was nearly 6670 L/h.m^2.bar for illustrated membrane.

After extracting offset pressure from average pressure values, via Darcy's Law intrinsic membrane resistances were also calculated for three different permeate fluxes;

<div align="center">@20 LHM TMP was 0.003</div>

$$R_m = \frac{TMP}{\mu \times J} = \frac{0.003 \times 10^5 Pa}{0.89 x 10^{-3} Pa.s \times 20 \frac{1h}{3600 sec} \times \frac{1m^3}{1000L} L/hm^2} = 6.1 \times 10^{10} \ m^{-1}$$

<div align="center">@40 LHM TMP was 0.006</div>

$$R_m = \frac{TMP}{\mu \times J} = \frac{0.006 \times 10^5 Pa}{0.89 x 10^{-3} Pa.s \times 40 \frac{1h}{3600 sec} \times \frac{1m^3}{1000L} L/hm^2} = 6.1 \times 10^{10} \ m^{-1}$$

<div align="center">@60 LHM TMP was 0.009</div>

$$R_m = \frac{TMP}{\mu \times J} = \frac{0.009 \times 10^5 Pa}{0.89 x 10^{-3} Pa.s \times 60 \frac{1h}{3600 sec} \times \frac{1m^3}{1000L} L/hm^2} = 6.1 \times 10^{10} \ m^{-1}$$

To calculate permeability value, effective membrane thickness was found from SEM images via ImageJ software. Firstly, we set the scale according to SEM image and measure the pore sizes and membrane thicknesses.
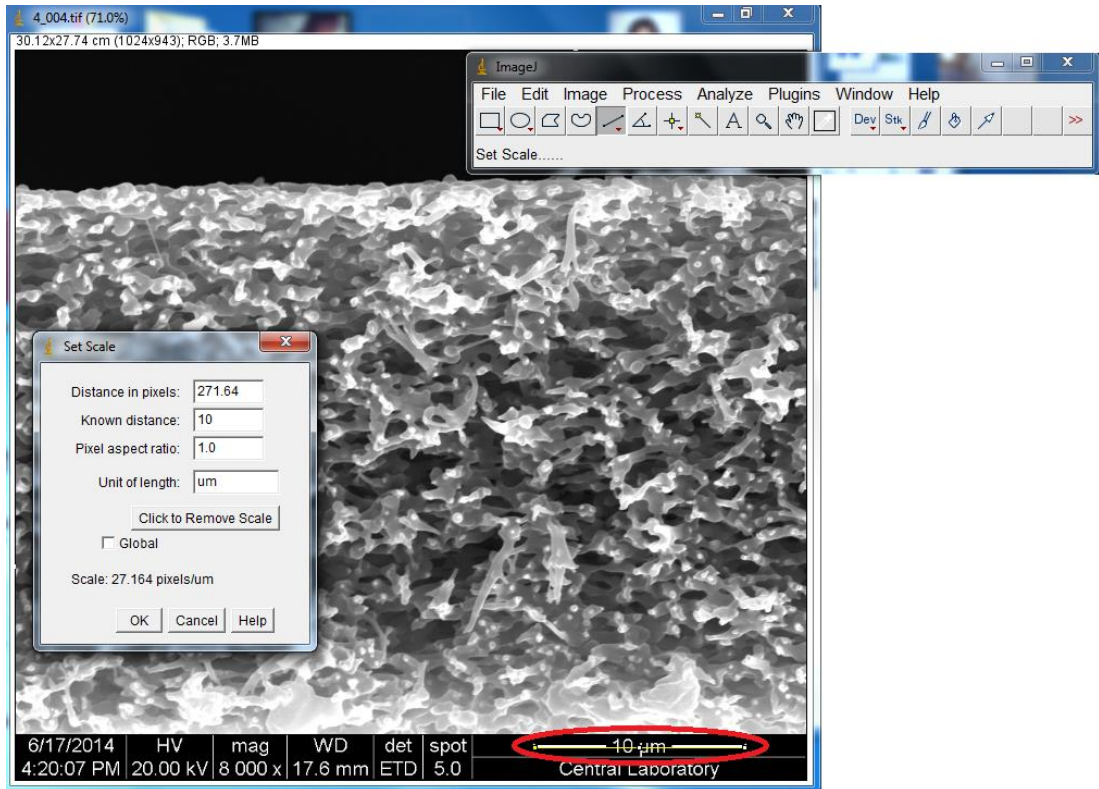
Figure B. 3 Setting the scale in ImageJ.
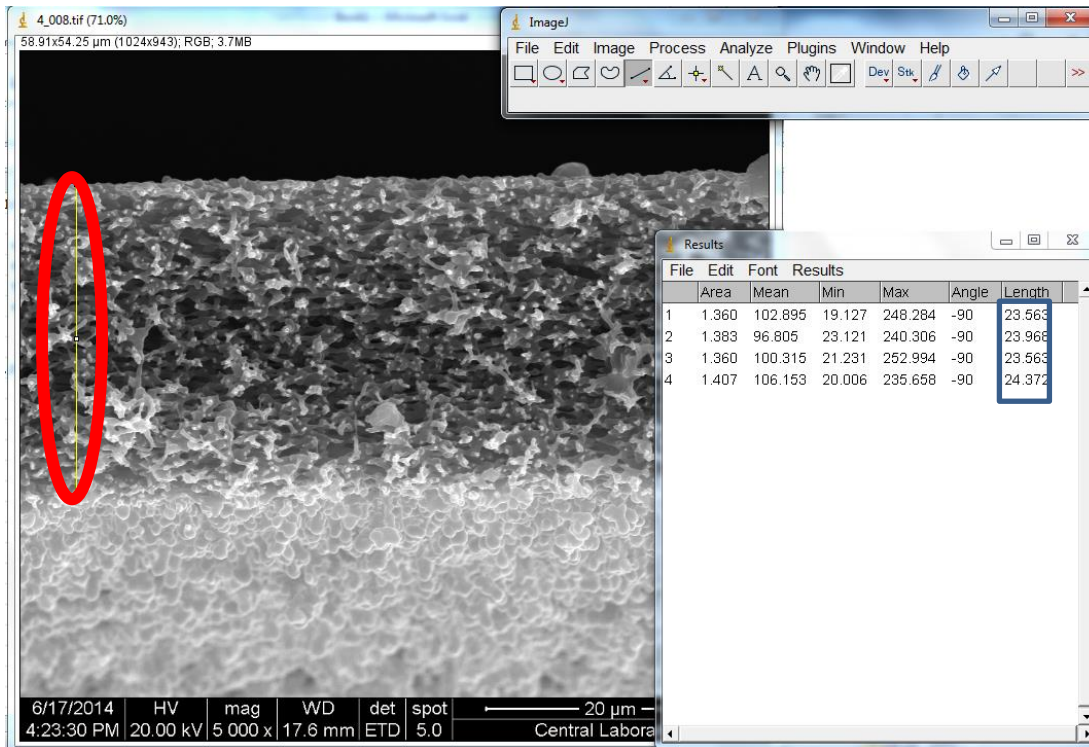
Figure B. 4 Measuring Effective Membrane Thickness in ImageJ.
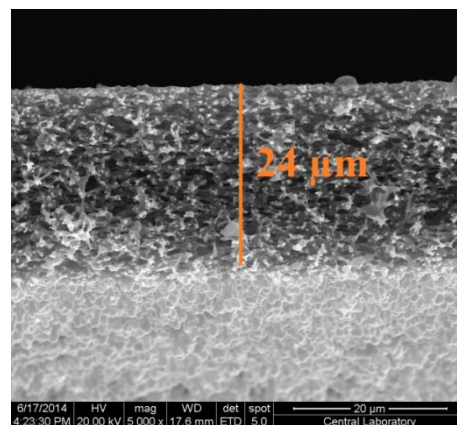
Figure B. 5 SEM image of flat membrane with 10 minutes humid air exposure

On the other hand, the effective thickness of corrugated membrane was calculated differently. Effective thicknesses of the corrugated membranes were calculated from dividing cross sectional area to width of that area.
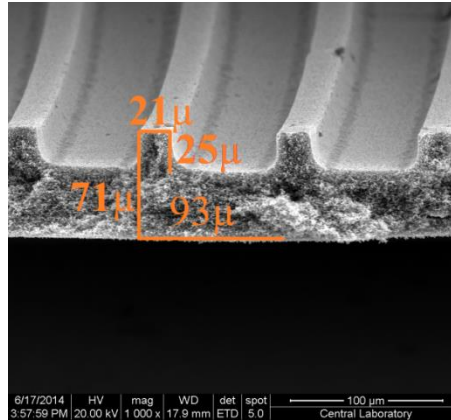
Figure B. 6 SEM image of corrugated membrane with 10 minutes humid air exposure

$$Thickness = \frac{Cross-sectional\ area}{Width}$$

$$Thickness = \frac{(21 \times 25) + ((71 - 25) \times 93)}{93} = 51\mu m$$

After measuring the effective membrane thickness for flat and corrugated membranes with 10% PES 60% PEG400, 5% water, 25% NMP and 10 minutes humid air exposure, pure water permeabilities of these membranes were calculated.

Flat membrane;
Thickness 24μm (Figure 3.9)

$$Permeability = 9000\frac{L}{h}.\,m2.\,bar\ \times 24\mu m$$

$$= 2.2 \times 10^5 \frac{L.\,\mu m}{h}.\,m2.\,bar$$

Corrugated membrane;
Thickness 51 μm (Figure 3.10)

$$Permeability = 24000\frac{L}{h}.\,m2.\,bar\ \times 51\mu m$$

$$= 1.2 \times 10^6 \frac{L.\,\mu m}{h}.\,m2.\,bar$$

We also measured the pore sizes with the same procedure. As it can be seen in the Figure B.5, pores were measured from different locations and the average values of pore diameters were calculated with standard deviations.
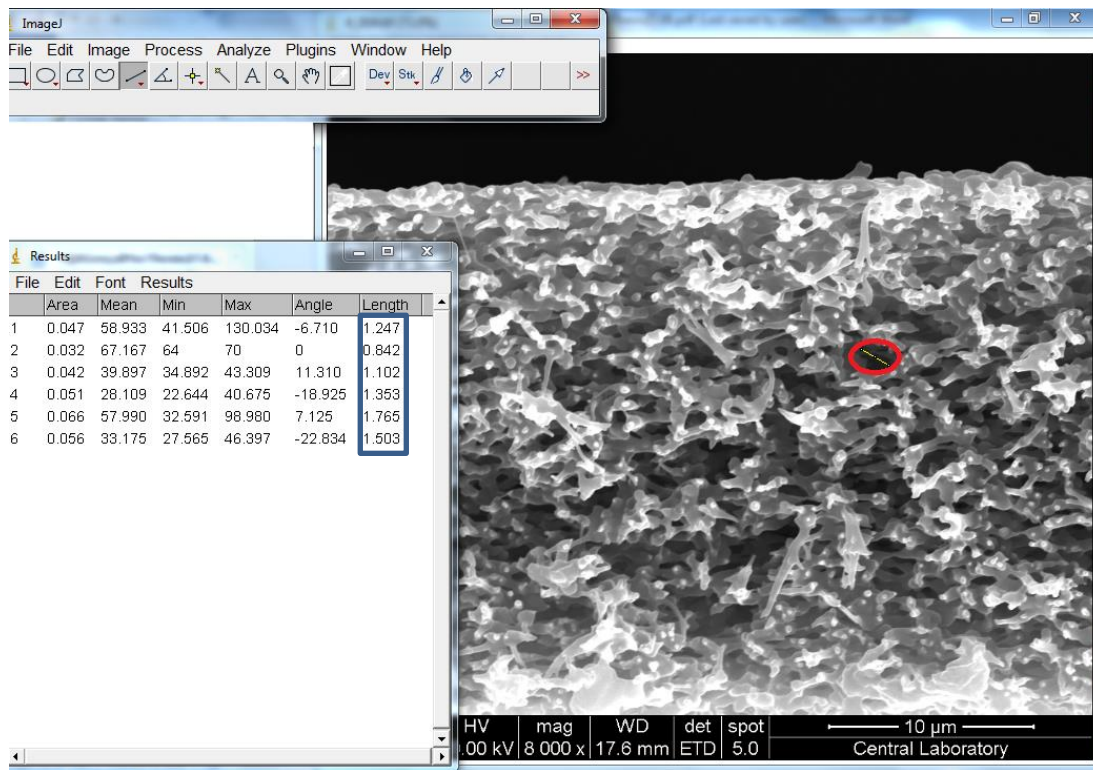
Figure B. 7 Measuring Pore Sizes in ImageJ.

YEAST FILTRATION AND CALCULATION OF FOULING RESISTANCES AND FOULING RATES

In Figure C.1 flux-stepping yeast filtration experiment data for flat membrane with 10 minutes humid air exposure was given.
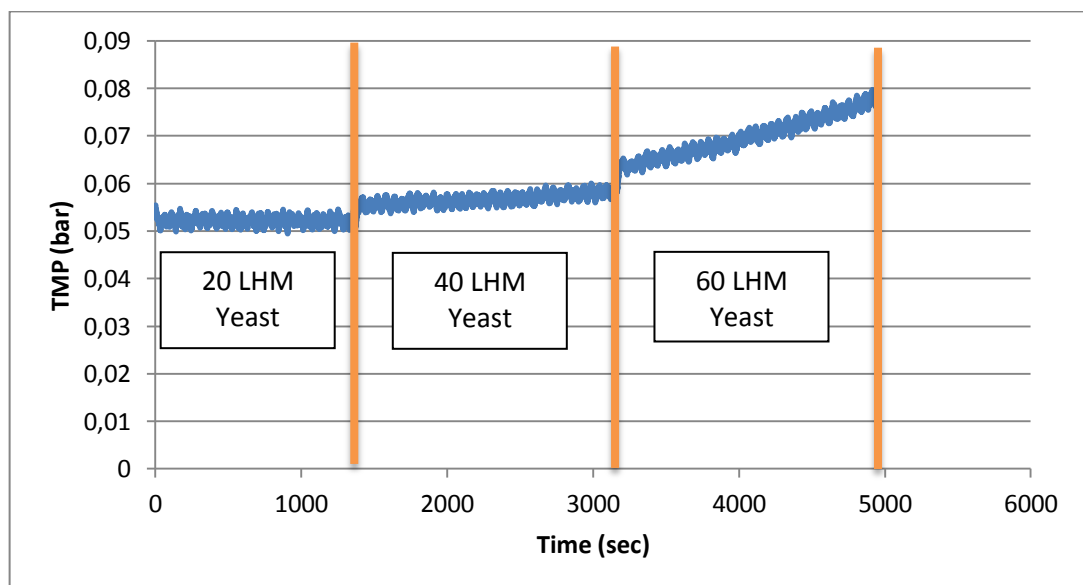
Figure C. 1 Yeast filtration experiments for flat membrane with 10 minutes humid air exposure and 0.1 m/s cross-flow velocity

Since yeast filtration changed the total resistance by increasing fouling resistance, unlike pure water permeability calculation, average of all pressure values at the same flux could not be used. However, due to oscillatory behaviour average of first and last 100 data at the same permeate flux were taken and used to calculate fouling resistances and rates.

Table C. 1 Yeast filtration experiment for flat membrane with 10 minutes humid air exposure and 0.1 m/s cross-flow velocity

60 LHM YEAST FILTRATION PRESSURE VALUES					
	First	Last		First	Last
1st	0.061583	0.075955	16th	0.064056	0.077564
2nd	0.061325	0.075459	17th	0.06385	0.076908
3rd	0.061592	0.075013	18th	0.064365	0.077017
4th	0.062633	0.075712	19th	0.064629	0.077815
5th	0.06307	0.075841	20th	0.063966	0.077734
6th	0.062463	0.075057	21st	0.063669	0.077461
7th	0.063417	0.076151	22nd	0.064302	0.078214
8th	0.063875	0.076536	23rd	0.064272	0.078493
9th	0.063587	0.076582	24th	0.063445	0.077444
10th	0.062929	0.075824	25th	0.0635	0.077399
11th	0.063736	0.076742	26th	0.06425	0.078159
12th	0.063962	0.077168	27th	0.064125	0.078243
13th	0.063166	0.076651	28th	0.063813	0.077719
14th	0.063649	0.076586	29th	0.064332	0.078147
15th	0.064284	0.077627	30th	0.064898	0.078832

Table C. 1(cont'd) Yeast filtration experiment for flat membrane with 10 minutes humid air exposure and 0.1 m/s cross-flow velocity

31st	0.064709	0.077849	57th	0.062344	0.076849
32nd	0.064538	0.077564	58th	0.062309	0.076464
33rd	0.065084	0.078208	59th	0.062878	0.077517
34th	0.065276	0.078787	60th	0.06239	0.077466
35th	0.064248	0.077708	61st	0.061851	0.076519
36th	0.064223	0.077638	62nd	0.062966	0.077367
37th	0.065001	0.078074	63rd	0.06307	0.07753
38th	0.064101	0.077566	64th	0.062563	0.077177
39th	0.063791	0.07681	65th	0.063006	0.07716
40th	0.063912	0.076629	66th	0.063806	0.078044
41st	0.06472	0.076966	67th	0.063925	0.078339
42nd	0.063748	0.076369	68th	0.063233	0.078005
43rd	0.063474	0.076132	69th	0.062809	0.078205
44th	0.064226	0.076419	70th	0.063528	0.079084
45th	0.063904	0.076477	71st	0.063576	0.078976
46th	0.063113	0.07573	72nd	0.062718	0.077978
47th	0.063202	0.075657	73rd	0.063646	0.078381
48th	0.063482	0.076191	74th	0.063982	0.079142
49th	0.063134	0.076172	75th	0.063583	0.079128
50th	0.06282	0.075455	76th	0.063525	0.078815
51st	0.063638	0.076409	77th	0.064273	0.079434
52nd	0.063874	0.076768	78th	0.064445	0.07969
53rd	0.062987	0.076091	79th	0.063701	0.078721
54th	0.062888	0.076382	80th	0.063731	0.078549
55th	0063399	0.077344	81st	0.064458	0.079294
56th	0.063159	0.07761	82nd	0.063612	0.078665

Table C. 1(cont'd) Yeast filtration experiment for flat membrane with 10 minutes humid air exposure and 0.1 m/s cross-flow velocity

83rd	0.063451	0.077798	93rd	0.063941	0.077969
84th	0.064106	0.077919	94th	0.063747	0.077472
85th	0.064395	0.078627	95th	0.063872	0.077425
86th	0.063556	0.077764	96th	0.063985	0.077582
87th	0.0634	0.077488	97th	0.063187	0.076724
88th	0.06426	0.078139	98th	0.063068	0.076251
89th	0.064534	0.078725	99th	0.063861	0.076826
90th	0.063781	0.077752	100th	0.063475	0.076944
91st	0.063903	0.077677	Average	0.063	0.077
92nd	0.064712	0.07841			

@60 LHM average value of first 100 pressure data was 0.063 bar

$$TMP = \Delta P_m - \Delta P_o = 0.063 - 0.047 = 0.016 \text{ bar}$$

After extracting offset pressure values, resistances were calculated via Darcy's Law;

$$R_{tot} = \frac{TMP}{\mu \times J}$$

$$R_{tot} = \frac{TMP}{\mu \times J} = \frac{0.016 \times 10^5 Pa}{0.89 x 10^{-3} Pa.s \times 60 \frac{1h}{3600sec} \times \frac{1m^3}{1000L} \frac{L}{hm^2}} = 1 \times 10^{11} \ m^{-1}$$

$$R_{fi} = R_{tot} - R_{mem} = 1 \times 10^{11} - 6.1 \times 10^{10} = 3.9 \times 10^{10} m^{-1}$$

R_{fi} means the fouling resistance of the first 100 data of the same permeate flux.

@60 LHM average value of last 100 pressure data was 0.077 bar

$$TMP = \Delta P_m - \Delta P_o = 0.077 - 0.047 = 0.03 \text{ bar}$$

$$R_{tot} = \frac{TMP}{\mu \times J} = \frac{0.03 \times 10^5 \, Pa}{0.89 x 10^{-3} \, Pa.s \times 60 \, \frac{1h}{3600 sec} \times \frac{1m^3}{1000L} \frac{L}{hm^2}} = 1.9 \times 10^{11} \, m^{-1}$$

$$R_{ff} = R_{tot} - R_{mem} = 1.9 \times 10^{11} - 6.1 \times 10^{10} = 12.9 \times 10^{10} m^{-1}$$

R_{ff} means the fouling resistance of the last 100 data of the same permeate flux.

Fouling rates calculated via following equation;

$$\frac{dR_f}{dt} = \frac{R_{ff} - R_{fi}}{\Delta t} = \frac{(12.9 \times 10^{10} - 3.9 \times 10^{10})m^{-1}}{1708 \, sec} = 5.2 \times 10^7 m^{-1} s^{-1}$$